NAVAL POSTGRADUATE SCHOOL
Monterey, California

THESIS

ESTIMATION OF ROTOR BLADE TORSIONAL DEFORMATIONS FROM MEASURED BLADE TORSION MOMENTS

by

Ronald S. Volkin

March 2002

Thesis Co-Advisors: E. Roberts Wood
William Bousman

Approved for public release; distribution is unlimited

THIS PAGE INTENTIONALLY LEFT BLANK

REPORT DOCUMENTATION PAGE			Form Approved OMB No. 0704-0188
Public reporting burden for this collection of information is estimated to average 1 hour per response, including the time for reviewing instruction, searching existing data sources, gathering and maintaining the data needed, and completing and reviewing the collection of information. Send comments regarding this burden estimate or any other aspect of this collection of information, including suggestions for reducing this burden, to Washington headquarters Services, Directorate for Information Operations and Reports, 1215 Jefferson Davis Highway, Suite 1204, Arlington, VA 22202-4302, and to the Office of Management and Budget, Paperwork Reduction Project (0704-0188) Washington DC 20503.			
1. AGENCY USE ONLY ***(Leave blank)***	**2. REPORT DATE** March 2002	**3. REPORT TYPE AND DATES COVERED** Master's Thesis	
4. TITLE AND SUBTITLE: Title (Mix case letters) **Estimation Of Rotor Blade Torsional Deformations From Measured Blade Torsion Moments**			**5. FUNDING NUMBERS** **RAA9B**
6. AUTHOR(S) Ronald S. Volkin			
7. PERFORMING ORGANIZATION NAME(S) AND ADDRESS(ES) Naval Postgraduate School Monterey, CA 93943-5000			**8. PERFORMING ORGANIZATION REPORT NUMBER**
9. SPONSORING /MONITORING AGENCY NAME(S) AND ADDRESS(ES) Aeromechanics Branch, Army/NASA Rotorcraft Division NASA Ames Research Center, MS 215-1 Moffett Field, CA 94035-1000			**10. SPONSORING/MONITORING AGENCY REPORT NUMBER**
11. SUPPLEMENTARY NOTES The views expressed in this thesis are those of the author and do not reflect the official policy or position of the Department of Defense or the U.S. Government.			
12a. DISTRIBUTION / AVAILABILITY STATEMENT Approved for public release; distribution is unlimited			**12b. DISTRIBUTION CODE** A

13. ABSTRACT ***(maximum 200 words)***

The strain pattern analysis (SPA) method is applied to estimate rotor blade torsional deflections. The SPA technique requires calculated mode shapes for the tested rotor blade and strain measurements from the rotor's wind tunnel or flight test. The Holzer method is developed to calculate the required mode shapes from rotor blade stiffness and mass properties and the torsional equation of motion. The Holzer method is tested with numerous theoretical and experimental cases and is proven accurate. The strain measurements are from wind tunnel tests conducted by the Army, NASA, United Technologies Research Center (UTRC) and Sikorsky at DNW with a (1:5.73) model-scale UH-60A rotor blade with an advance ratio of 0.301, an advancing tip Mach number of 0.8224 and an average Reynolds number of 1,278,729. The SPA method predicts slightly larger torsional deflections that compare well with the overall trend and range of UTRC static method integrated deflections. The SPA method was evaluated to determine the tolerance to change in the number of measurements and the modes applied, errors in the measurements, and errors in rotor blade stiffness and mass properties. The method is tolerant to all effects except a decrease in the number of measurements and modes.

14. SUBJECT TERMS Rotor Wing Structural Dynamics, Torsional Deflection, Rotor Blade Aeroelasticity, Holzer's Method, Strain Pattern Analysis, Helicopter Dynamics.			**15. NUMBER OF PAGES** 157
			16. PRICE CODE
17. SECURITY CLASSIFICATION OF REPORT Unclassified	**18. SECURITY CLASSIFICATION OF THIS PAGE** Unclassified	**19. SECURITY CLASSIFICATION OF ABSTRACT** Unclassified	**20. LIMITATION OF ABSTRACT** UL

NSN 7540-01-280-5500 Standard Form 298 (Rev. 2-89)
Prescribed by ANSI Std. 239-18

THIS PAGE INTENTIONALLY LEFT BLANK

Approved for public release; distribution is unlimited

ESTIMATION OF ROTOR BLADE TORSIONAL DEFORMATIONS FROM MEASURED BLADE TORSION MOMENTS

Ronald S. Volkin
Captain, U.S. Army
B.S., Embry-Riddle Aeronautical University, 1991

Submitted in partial fulfillment of the
requirements for the degree of

MASTER OF SCIENCE IN AERONAUTICAL ENGINEERING

from the

NAVAL POSTGRADUATE SCHOOL
March 2002

Author: Ronald S. Volkin

Approved by: E. Roberts Wood, Thesis Co-Advisor

William Bousman, Thesis Co-Advisor

Max Platzer, Chairman
Department of Aeronautics and Astronautics

THIS PAGE INTENTIONALLY LEFT BLANK

ABSTRACT

The strain pattern analysis (SPA) method is applied to estimate rotor blade torsional deflections. The SPA technique requires calculated mode shapes for the tested rotor blade and strain measurements from the rotor's wind tunnel or flight test. The Holzer method is developed to calculate the required mode shapes from rotor blade stiffness and mass properties and the torsional equation of motion. The Holzer method is tested with numerous theoretical and experimental cases and is proven accurate. The strain measurements are from wind tunnel tests conducted by the Army, NASA, United Technologies Research Center (UTRC) and Sikorsky at DNW with a (1:5.73) model-scale UH-60A rotor blade with an advance ratio of 0.301, an advancing tip Mach number of 0.8224 and an average Reynolds number of 1,278,729. The SPA method predicts slightly larger torsional deflections that compare well with the overall trend and range of UTRC static method integrated deflections. The SPA method was evaluated to determine the tolerance to change in the number of measurements and the modes applied, errors in the measurements, and errors in rotor blade stiffness and mass properties. The method is tolerant to all effects except a decrease in the number of measurements and modes.

THIS PAGE INTENTIONALLY LEFT BLANK

TABLE OF CONTENTS

LIST OF FIGURES

LIST OF TABLES

THIS PAGE INTENTIONALLY LEFT BLANK

LIST OF SYMBOLS

Symbols presented are shown in order of appearance with their units of measure appearing after their description. If a symbol has numerous commonly used units of measure they will be listed. The following abbreviations are used: inches (in), feet (ft), degrees (deg), radians (rad), second (sec), revolution-per-minute (RPM), Hertz (Hz), and pounds force (lb or lbf), kilogram (kg), meter (m), and Newton (N).

w	Flapwise Coordinate
v	Chordwise Coordinate
θ	Feathering Coordinate
Ω	Rotor Rotational Speed (rad/sec, also seen as RPM or Hz)
ϕ	Elastic Torsional Deformation (rad or deg)
α	Blade Section Angle of Attack (rad or deg)
Φ	Blade Section Inflow Angle (rad or deg)
Θ	Geometric Pitch Angle (rad or deg)
θ_0	Collective (Steady) Pitch Angle (rad or deg)
θ_{1c}	Lateral Cyclic Pitch Angle (rad or deg)
θ_{1s}	Longitudinal Cyclic Pitch Angle (rad or deg)
θ_B	Built-in Twist (rad or deg)
x	Non-Dimensional Rotor Spanwise Coordinate, x = r/R
r	Rotor Spanwise Coordinate (in, ft or m)
R	Rotor Radius (in, ft or m)
t	time (sec)

β Feathering blade angle prior to any deformation (rad or deg)

ψ rotor azimuth (0 to 2π rad), $\psi = \Omega t$

M Torsion Moment (ft-lb or N-m)

GJ Effective Cross-Section Torsion Stiffness (lbf-ft^2 or N-m^2)

e radial axis pitch link offset (inches)

e_f feathering axis pitch link offset (inches)

$\{\ \}$ Denotes a Vector

$[\ ]$ Denotes a Matrix

{q} (m x1) vector of SPA Least Squares Best Fit Solutions (non-dimensional)

m mode number

[T] (g x m) matrix of Holzer Calculated Torsion Moments (ft-lb or N-m)

g measurement station number

{M} (g x 1) vector of Measured Torsion Moments (in-lb or ft-lb)

$\{\phi\}$ (n x1) vector of SPA Calculated Torsional Deformation (rad or deg)

n calculation station number

[D] (n x m) matrix of Holzer Calculated Torsional Deformation (rad or deg)

I Torsional Mass Moment of Inertia about the elastic axis;
(slug-ft^2 or lbf-ft-sec^2 or kg-m^2)

ω frequency of harmonic motion (rad/sec or Hz)

k_{Root} Root Spring Constant (in-lb/rad)

C Tension (lbf or N); $C = \frac{1}{2}\frac{(mass)}{(\Delta r)}(\Omega^2)(R^2 - r^2)$

k_A Radius of Gyration of blade cross sectional area (in or m)

ω_{NR} Non-Rotating Natural Frequency (rad/sec or Hz)

ω_{ROT} Rotating Natural Frequency (rad/sec or Hz)

h harmonic number

THIS PAGE INTENTIONALLY LEFT BLANK

ACKNOWLEDGEMENTS

I would like to thank the following people who were critical to my successfully completing this thesis. Mr. William Bousman suggested the thesis topic, served as co-advisor, provided office space at NASA-Ames, and assisted me throughout the research process. Professor E. Roberts Wood served as co-advisor and provided extensive insight into rotor blade dynamics, solution methods, techniques to solve Fourier series, and references to his journal papers. Dr. Joon Lim was critical as project lead in coordinating for the funding transfer between NASA and the Naval Postgraduate School and he provided support and advice on solution methods and helicopter dynamics theory. Dr. William Warmbrodt, Aeromechanics Branch Chief at the Army/NASA Rotorcraft Division and LTC Bob Schulz, both coordinated for my initial meetings within their organizations to assist in selecting a research topic. Dr. Peter Lorber at the United Technology Research Center (UTRC) was especially helpful in my efforts to understand and recreate the results presented in the UTRC report he authored in 1991. Mr. Robert Goodman at Sikorsky Aircraft Company coordinated for the authorized release of data pertaining to their natural frequency calculations and helped explain rotor blade coupling effects. Thanks to my wife and daughter who have provided the needed moral support, and understanding during the last year.

I. INTRODUCTION

A. ROTOR BLADE TORSIONAL DEFORMATION

Helicopter rotor blades have high aspect ratios and are highly flexible and therefore the effects of aeroelasticity are larger and therefore more important than found in more rigid structures. The aeroelastic response of rotor blades includes elastic deformation in the flapwise, *w*, chordwise, *v*, and feathering, θ, planes of motion. The coordinate system for rotor blade deformation in the positive direction is shown below in Figure 1. The airfoil shown in Figure 1 is representative of any segment along the rotor blade span at rotational speed, Ω. [Ref. 1]

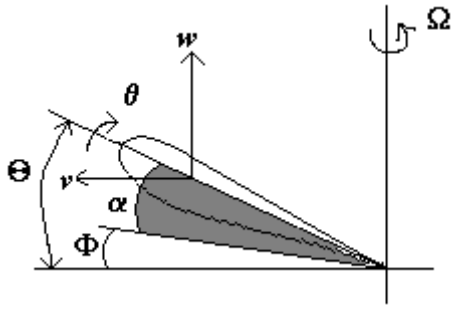

Figure 1. Rotor Blade Coordinate System.

Aeroelastic deformations of the rotor blade affect helicopter performance, air loads, and vibration. Deformation in the feathering plane is known as torsional deformation, ϕ. The torsional deformation has the most immediate influence on aerodynamics since it contributes to the angle of attack, α, for the rotor blade. The angle of attack is the most important factor in the production of lift along the span of the rotor blade. Equation 1.1 shows how the inflow angle, Φ, and the geometric pitch angle, Θ, contribute to the angle of attack. These angles are also shown above in Figure 1, with the angle of attack shown in gray shading. [Ref. 1]

$$\alpha = \Theta - \Phi \tag{1.1}$$

Torsional deformation contributes to the angle of attack as a significant term in the geometric pitch angle, Equation 1.2, where θ_0, θ_{1c}, and θ_{1s} are the collective and cyclic pitch control angles, and θ_B is the built-in twist. For all terms in Equation 1.2, a

positive angle denotes the nose up or leading edge up direction in the feathering plane. [Ref. 2]

$$\Theta(x,t) = \theta_B(x) + \phi(x,t) + \theta_o + \theta_{1c}\cos\omega t + \theta_{1s}\sin\omega t \tag{1.2}$$

where

x = spanwise coordinate
t = time coordinate

A subgroup to the geometric pitch angle is the feathering blade angle without deformation, β, shown in Equation 1.3. The feathering blade angle includes all of the terms in Equation 1.2 minus the torsional deformation. [Ref. 2]

$$\beta(x,t) = \theta_B(x) + \theta_o + \theta_{1c}\cos\omega t + \theta_{1s}\sin\omega t \tag{1.3}$$

B. MEASUREMENT OF TORSIONAL DEFORMATION

Given the importance of torsional deformation, a method to measure elastic twist during wind tunnel experiments and flight test programs is desired. Unfortunately, torsional deformation of a rotating blade is not easily measured during wind tunnel experiments or flight-tests [Ref. 3]. The methods to measure or estimate torsional deflections during high-speed rotation include the optical projected grid and target attitude in real time methods, and the strain-measurement based static and strain pattern analysis (SPA) methods. [Ref. 4]

The projected grid method (PGM) and the target attitude in real time method (TART) are both optical methods of measuring deflection. These optical methods are only applicable to wind tunnel tests. The projected grid method was developed at the German-Dutch wind tunnel (Deutsch-Niederlandischer Windkanal or DNW). With PGM, a grid is projected optically onto the surface of the blade and images of the grids from the deformed and undeformed blades are compared. Both flapwise and torsional deformations can be measured. The method is generally applied over a limited azimuth range, ψ, and extensive video equipment is required. The TART method was developed by France's Office National D'Etudes et Recherches Aerospatiales (ONERA). The TART method measures flapwise and torsional deformations for the blade tip at selected azimuths. The TART method requires adhesive material embedded with reflective micro

spheres be applied to the rotor blade. Pulsing light at selected azimuths illuminates the micro spheres and the reflected light is recorded by video equipment. Both PGM and TART were shown to provide accurate results when compared to the SPA method for torsional deformations. [Ref. 4]

An alternative to optical methods is to use blade strain measurements. Detailed strain measurements, if accurate and of sufficient quantity, can be used to estimate deformations. One approach, referred to here as the static method, is based on simple beam theory and estimates the torsional deformation directly from the measured torsion moments, M, and the torsional stiffness term, GJ, as shown in Equation 1.4. [Ref. 5]

$$\frac{d\phi(x)}{dx} = \frac{M(x)}{GJ(x)} \tag{1.4}$$

Solving Equation 1.4 for the torsional deformation, ϕ, yields an integral form of the static equation shown in Equation 1.5. The non-dimensional radial term, x, increases from zero to one at the tip, as shown in Figure 2. The rotor blade extends from the pitch link offset, e, to the tip. Integration is done in steps from the tip to the pitch link offset. If necessary the torsion moments and torsional stiffness values may be interpolated to span locations that coincide with the chosen integral step size.

$$\Delta\phi\,(\mathrm{x}) = \int_{e}^{1} \frac{M(x)}{GJ(x)}\,dx \tag{1.5}$$

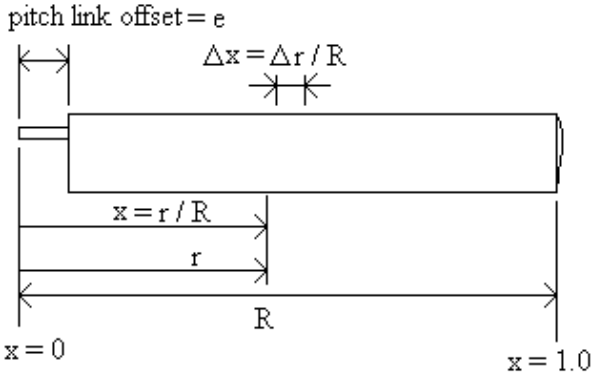

Figure 2. Rotor Blade Radial Coordinates.

The torsion moment and torsional stiffness values are piecewise uniform terms at each individual segment, which provides the descritized Equation 1.6.

$$\Delta\phi(\mathrm{x}) = \sum_{e}^{1} \frac{M(x)\Delta x}{GJ(x)} \tag{1.6}$$

A second approach to estimate deformations from strain measurements is the Strain Pattern Analysis (SPA) method, which will be discussed in detail in section C. The SPA method uses a least squares estimator derived from fitting calculated torsion moment mode shapes to measured torsion moments to estimate the actual deflections from calculated deflection mode shapes. [Ref. 6]

Strain measurements provide an alternative to optical techniques, but have their own problems and limitations. To avoid coupling effects, care must be taken to use strain gages exclusively for measuring either flapwise or torsional strain [Ref. 7]. The coupling between torsional and flapwise deformations occurs when centrifugal forces change blade stiffness and mode shapes during rotation [Ref. 7]. When the strain gages successfully isolate torsion and flapwise bending mode shapes the results of SPA compared to optical methods are shown to be very accurate [Ref. 7].

C. STRAIN PATTERN ANALYSIS

C.J.W. Hassal and D.R. Gaukroger developed the SPA method during the 1970's at the Royal Aircraft Establishment in England. Strain Pattern Analysis was developed to confirm mode calculations and to estimate the flap, lag, and torsional deflections of a rotating helicopter rotor blade given a set of non-rotating calibration modes and corresponding patterns of strain gage measurements from a wind tunnel or flight test. The original SPA technique required that calibration modes be determined by loading a non-rotating blade and measuring deflections and the corresponding strain gage responses [Ref. 6]. William Bousman investigated an extension to the original SPA method substituting calculated flapwise mode shapes for the calibration modes [Ref. 3]. This thesis applies Bousman's extension of SPA to the torsional mode shapes.

The first step in the SPA method is to calculate the least squares estimating vector, {q} of size *mx1* where *m* is the number of mode shapes calculated. Equation 1.7 gives the solution for {q} based on the matrix of calculated torsion moment mode shapes,

[T], and the vector of strain measurements for one harmonic, {M} [Ref. 8]. The [T] matrix is size *g x m* where *g* is the number of measurement station locations that must be greater than the number of modes calculated, *m*. The {M} vector is size *g x 1*. [Ref. 6]

$$\{q\} = ([T]^T[T])^{-1}[T]^T\{M\} \tag{1.7}$$

The second step of the SPA method is to confirm the least-squares accuracy of the SPA vector. Equation 1.8 solves the least-squares approximation to {M}. [Ref. 8]

$$\{M\} \cong [T]\{q\} \tag{1.8}$$

The final step of the SPA method is to calculate the estimated deflection vector, $\{\phi\}$, from the SPA vector and the matrix of calculated torsional deformation mode shapes, [D] as shown in Equation 1.9. The [D] matrix is size *n x m*, where *n* is the number of calculation stations. The estimated deflection vector is size *n x 1* and is an estimate of the actual deflection by harmonic. [Ref. 6]

$$\{\phi\} = [D]\{q\} \tag{1.9}$$

Both [T] and [D] are obtained analytically, based on blade structural and inertial properties. This thesis will focus on developing the application of the SPA method to estimate torsional deformation. The accuracy and robustness of the technique will be evaluated. The goal of this thesis is to provide the Army/NASA Rotorcraft Division a computational program to use in applying SPA to current full-scale and model-scale wind tunnel and flight test strain measurements to estimate torsional deformation.

D. TORSIONAL MODE SHAPE CALCULATIONS

To apply the SPA method to strain measurements a set of calculated torsion moment mode shapes, [T], and a set of calculated torsional deformation mode shapes, [D] are required. There are numerous dynamic methods to calculate these mode shapes.

Modal methods of calculating torsional deformation are accomplished by solving the differential equations of motion of the rotor blade [Ref. 9]. The differential equations are developed in Chapter II. Exact solutions are available for the differential equations of motion representing the non-rotating, uniform blade. For the non-rotating, non-uniform or for the rotating case there is no exact solution to the equations of motion. The solution can only be approximated, even for the simplest case of a rotating, uniform beam [Ref.

10]. The solution obtained with a modal method accounts for the harmonic motion that the rotor undergoes in the time domain, as well as the variations that occur spanwise. Many methods are available to solve the equation of motion including the Rayleigh method, the Rayleigh-Ritz method, the Holzer method, the Myklestad method, and finite element analysis. [Ref. 9]

The Rayleigh method assumes a deflection curve for the first mode. The first mode approximation is used to solve the ordinary differential equation for the maximum kinetic energy that is set equal to the potential energy. The Rayleigh method achieves good approximations for the natural frequencies. The Rayleigh-Ritz method makes the first assumed mode a sum of several functions. The functions used to define the first mode must collectively satisfy the boundary conditions. The Rayleigh-Ritz method provides a more accurate estimate for the natural frequency than the original Rayleigh method. [Ref. 9]

Solution methods known as lumped-mass parameter methods include the Holzer method, and the Myklestad method. A lumped-mass model refers to the technique of representing a continuous blade as a number of discrete segments connected by massless shafts. Each radial location where structural properties are known is considered a segment [Ref. 10]. A seven-segment example of a lumped-mass model is shown in Figure 3. Each individual segment is located at a discrete span location and can have unique values for its mass properties, stiffness properties, and built-in twist angle. A uniform lumped-mass model would have identical values for all segments.

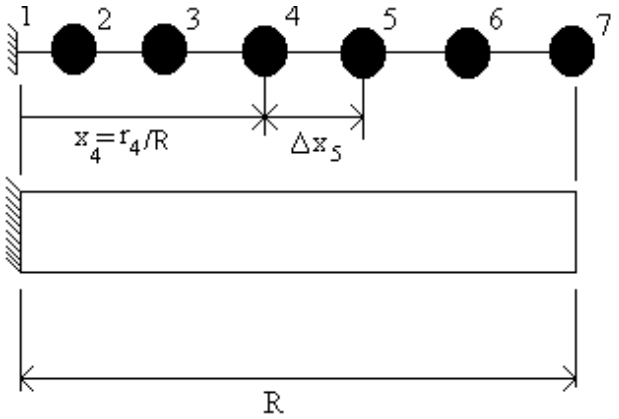

Figure 3. Lumped-Mass Model of a Cantilevered Beam.

The lumped-mass model allows for a partial differential equation of motion to be replaced by a set of ordinary differential equations. The Holzer method is used to calculate torsional oscillations using a second order differential equation. Myklestad extended Holzer's method to solve for the bending frequencies and modes using a fourth order differential equation. The Myklestad method is developed in Professor E. Roberts Wood and W. Gerstenberger's paper titled, "Analysis of Helicopter Aeroelastic Characteristics in High-Speed Flight". [Ref. 9]

The Holzer method was chosen for calculating the torsional moment mode shapes and torsional deformation mode shapes required for this thesis. The Holzer method is valid for uncoupled torsion and is directly applicable to my research of uncoupled, torsional deformation. A few modifications were required to apply Holzer's method to the rotor blade equations of motion as described in Chapter II. The Holzer method is easily used in tabular form with programs like EXCEL^{TM} when solving for a specific, narrowly defined case. A MATLAB^{TM} program was written to compute mode shapes for the broadest set of boundary conditions and beam types using the Holzer method. The Holzer method is developed more thoroughly in Chapter II. The purpose of this thesis is to develop and test SPA for the ability to estimate torsional deformation of a rotor blade using calculated, rotating torsional mode shapes and experimentally measured torsion moments.

THIS PAGE INTENTIONALLY LEFT BLANK

II. THE HOLZER METHOD

A. NATURAL FREQUENCY DEFINITION

A natural frequency occurs where an undamped system vibrates freely and continuously with no external force. Equation 2.1 represents the eigenvalue (or characteristic value) form of the equation associated with matrices [m] and [k]. [Ref. 5]

$$[k]\{u\} = \omega^2 [m]\{u\} \tag{2.1}$$

Equation 2.1 possesses a nontrivial solution when the determinant of the coefficients of u_j vanish. The nontrivial solution is expressed in Equation 2.2 known as the characteristic or frequency equation. [Ref. 5]

$$\Delta(\omega^2) = \left| k_{ij} - \omega^2 m_{ij} \right| = 0 \tag{2.2}$$

where

$\Delta(\omega^2)$ is the characteristic determinant

The characteristic equation is of degree p in ω^2, and possesses in general p distinct roots that are called characteristic roots or eigenvalues. The p roots are denoted ω_1^2, $\omega_2^2, \ldots \omega_p^2$ and the square roots of these quantities are the system natural frequencies ω_m (m=1,2,…p). The natural frequencies can be arranged in order of increasing magnitude where $\omega_1 \le \omega_2 \le \ldots \le \omega_p$. The lowest frequency ω_1 is referred to as the fundamental frequency, and for many practical problems it is the most important natural frequency. [Ref. 5]

Associated with every one of the natural frequencies ω_m is a certain nontrivial vector $\{u\}_m$ (m=1,2,…p) of real numbers u_{im} where $\{u\}_m$ is a solution of the eigenvalue such that Equation 2.3 is valid. [Ref. 5]

$$[k]\{u\}_m = \omega_m^2 [m]\{u\}_m \tag{2.3}$$

where

m=1,2,….p

The vectors $\{u\}_m$ are known as characteristic vectors or eigenvectors. These vectors are unique only in the sense that the ratio between any two elements u_{im} and u_{jm} is constant. The value of the elements themselves is arbitrary. We say that the shape of the natural modes is unique, but the amplitude is not. [Ref. 5]

B. THE ORIGINAL HOLZER METHOD

For the Holzer's method, calculations are initiated by assuming a value for the frequency and applying a unit deformation to the blade tip with zero value for tip torsional moment. Then proceeding from tip to root, the torsion moments and torsional deformations of each segment are calculated. [Ref. 5]

The partial differential equation (PDE) of motion for torsional inertia is shown in Equation 2.4 for a simple, non-rotating blade modeled as a non-uniform beam. [Ref. 5]

$$\frac{\partial M(x,t)}{\partial x} = I(x)\frac{\partial^2 \phi(x,t)}{\partial t^2} \tag{2.4}$$

The torsional mass moment of inertia term, I, is a function of mass and geometry. The Torsion Moment, M, in Equation 2.4 is replaced with the time domain equivalent of Equation 1.4. For the lumped-mass model the torsional stiffness and the mass moment of inertia terms are piecewise uniform at each segment. The result of applying the above terms to Equation 2.4 is seen in Equation 2.5. [Ref. 5]

$$GJ\frac{\partial^2 \phi(x,t)}{\partial x^2} = I\frac{\partial^2 \phi(x,t)}{\partial t^2} \tag{2.5}$$

For free vibration the motion is simple harmonic and substitution for the torsional deformation term can be done to separate the time and space variables. Separation of variables for torsional deformation with simple harmonic motion of frequency, ω, is shown in Equation 2.6. [Ref. 1]

$$\phi(x,t) = e^{i\omega t}\phi(x) \tag{2.6}$$

The variable, e, in Equation 2.3 is the base-e exponential and is not to be confused with the pitch link offset term. Substituting for the torsional deformation in Equation 2.5 with Equation 2.6 and carrying out the differentiating and canceling out the imaginary

terms we solve for the ordinary differential equation (ODE) shown in Equation 2.7. [Ref. 5]

$$GJ\frac{\partial^2\phi(x)}{\partial x^2} = -I\omega^2\phi(x) \tag{2.7}$$

The right side of Equation 2.7 represents the torsional inertia at any segment. The negative sign in front of the torsional inertial term represents a negative direction. In Figure 4 the torsional inertia term is shown in the negative direction according to the right hand rule

An analysis of a single lumped-mass segment develops the incremental solution to the total torsion moment at any segment. The free body diagram for the single segment in Figure 4 helps derive the total torsion moment solution. [Ref. 11]

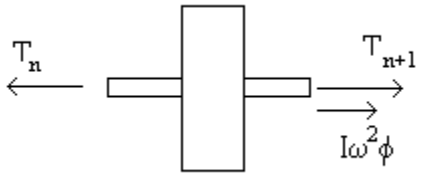

Figure 4. Free Body Diagram of a Lumped-Mass Segment.

Figure 4 shows the total torsion moment of a segment will equal the segment's torsional inertia plus the torsion moment from the right of the segment as represented in Equation 2.8. The segment number is represented by the variable, n. [Ref. 9]

$$T_n = T_{n+1} + I_n\omega^2\phi_n \tag{2.8}$$

Equation 2.9 represents the torsional deformation at a single segment and Equation 1.6 is substituted for the term, $\Delta\phi_{n+1}$. The term Δx_{n+1} in Equation 2.9 is equal to the difference between the span location of segments, n+1 and n. [Ref. 5]

$$\phi_n = \phi_{n+1} - \Delta\phi_{n+1} = \phi_{n+1} - \frac{T_{n+1}\Delta x_{n+1}}{GJ_{n+1}} \tag{2.9}$$

Equations 2.8 and 2.9 combined with the boundary conditions for the lumped-mass system establishes the solution equations for Holzer's method.

The presented example of the Holzer method is a twenty segment lumped-mass system. The first step to obtain a solution using the Holzer method is to set the torsional deformation at the last segment equal to one. Segments will always be numbered from one at the root and will ascend in order to the last segment for all lumped-mass model applications in this thesis. Equation 2.10 represents the first step of the Holzer method. [Ref. 12]

$$\phi_{20} = 1 \text{ radian} \tag{2.10}$$

The second step of the Holzer method is to solve for the total torsion moment at the last segment by substituting zero for the free end torsion moment and one radian for the last segment's torsional deformation into Equation 2.8. Equation 2.11 represents the result of the second step of the Holzer method. [Ref. 12]

$$T_{20} = I_{20}\omega^2 \tag{2.11}$$

The third step of the Holzer method is to solve for the next to last segment's torsional deformation using Equation 2.9. The result of step three for a twenty-segment system is shown in Equation 2.12. [Ref. 12]

$$\phi_{19} = 1 - \frac{T_{20}\Delta x_{20}}{GJ_{20}} \tag{2.12}$$

The fourth step of the Holzer method is to solve for the total torsion moment at the next to the last segment using Equation 2.8. The result of step four is shown in Equation 2.13. [Ref. 12]

$$T_{19} = T_{20} + I_{19}\omega^2\phi_{19} \tag{2.13}$$

The fifth step of the Holzer method requires that steps three and four be repeated for each segment in descending order until the solution for segment one at the root is obtained. It is important to note that the entire iteration from tip to root is done once for each test frequency. The sixth and final step of the Holzer method is to check the root solution against the root boundary conditions. The natural frequencies exist where the root solution and root boundary conditions match. [Ref. 12]

The set of each segment's torsion moment solution can be plotted versus span to give the torsion moment mode shape. Each natural frequency will have an independent set of mode shapes. [Ref. 5]

Three possible root boundary conditions are used for the applications described in this thesis. The first condition is for a Free-Free beam. If no external torsion moment is applied the torsion moments at both the right and left ends of the beam are zero. Additionally, the torsional deformation at the right end is set at one radian. The second condition is for a Fixed-Free cantilevered beam where the left end of the beam is clamped and therefore has a torsional deformation equal to zero. The right end of the beam is free and has a torsion moment of zero and a torsional deformation set at one radian. The third condition will be called Flex-Free, where the left end is supported by a flexible root restraint that is represented as a spring of stiffness, k_{Root}. The right end is free and has a moment of zero and a torsional deformation set at one radian. [Ref.5] The left end boundary condition is represented by Equation 2.14 [Ref. 10].

$$\phi_{Root} = k_{Root}\theta_o e_f / GJ_{Root} \tag{2.14}$$

The natural frequency solutions can be seen graphically by plotting the root boundary condition term of torsion moment or torsional deformation against the range of test frequencies. The natural frequencies for the Free-Free case are where the root torsion moment equals zero. The natural frequencies for the Fixed-Free case without a flexible root are where the root torsional deformation equals zero. The natural frequencies for the Fixed-Free case with a flexible root are where the root torsional deformation equals a positive value of, ϕ_{Root}, for odd numbered modes (i.e., the first, third, and fifth natural frequencies) or a negative value of, ϕ_{Root}, for even numbered modes (i.e., the second, fourth, and sixth natural frequencies). [Ref. 2]

The Holzer method can be represented in transfer matrix form as shown in Equation 2.15. To utilize the transfer matrix method the torsional deformation and total torsion moment at the last segment must be solved for prior to using the matrix. [Ref. 2]

$$\begin{Bmatrix} \phi \\ T \end{Bmatrix}_n = \begin{bmatrix} 1 & -\Delta x_{n+1} / GJ_{n+1} \\ I_n\omega^2 & [(-\Delta x_{n+1} / GJ_{n+1})(I_n\omega^2) + 1] \end{bmatrix} \begin{Bmatrix} \phi \\ T \end{Bmatrix}_{n+1} \tag{2.15}$$

C. ROTOR BLADE TORSIONAL EQUATION OF MOTION

To obtain accurate natural frequencies and mode shapes with Holzer's method, the torsional equation of motion for the system must be specific for rotating blades. The development of coupled, non-uniform, rotating blade equations of motion for flapwise, chordwise and torsion are based on the work of Hodges and Dowell [Ref. 13]. The ordering scheme eliminated all of the third order terms except terms involving rotation and torsional deformation. To obtain the uncoupled torsion equation the applied moment equals zero for the modal application, the flapwise and chordwise deformations were set at zero, the tension term and torsional mass moment of inertia terms were substituted according to Hodges and Dowell, and third order terms were eliminated. The torsional partial differential equation of motion is shown in Equation 2.16. [Ref. 2,13]

$$(GJ + Ck_A^{\,2})\frac{\partial^2\phi(x,t)}{\partial x^2} - mk_m^{\,2}\frac{\partial^2\phi(x,t)}{\partial t^2} - m(k_{m_2}^{\,2} - k_{m_1}^{\,2})\Omega^2\phi(x,t)\cos 2\beta = 0 \quad (2.16)$$

where

k_m = the polar moment of inertial, $k_m = \sqrt{k_{m_1}^{\,2} + k_{m_2}^{\,2}}$

C = Tension $= \frac{1}{2}\frac{(mass)}{(\Delta r)}(\Omega^2)(R^2 - r^2)$

k_A = Radius of Gyration of blade cross sectional area

The blade cross-section thickness is much less than the chord. Thus, the mass radii of gyration simplify as follows in Equation 2.17. [Ref. 2]

$$k_{m_2}^{\,2} \gg k_{m_1}^{\,2} \rightarrow k_m^{\,2} \approx k_{m_2}^{\,2} \quad (2.17)$$

The torsional mass moment of inertia, I, is equal to $mk_m^{\,2}$ and yields Equation 2.18.

$$(GJ + Ck_A^{\,2})\frac{\partial^2\phi(x,t)}{\partial x^2} - I\frac{\partial^2\phi(x,t)}{\partial t^2} - I\Omega^2\phi(x,t)\cos 2\beta = 0 \quad (2.18)$$

The tension term, radius of gyration, torsional stiffness, torsional mass moment of inertia and feathering blade angle are all piecewise uniform at each segment of the blade when it is modeled as a lumped-mass system. The first term of Equation 2.18, $GJ(\partial^2\phi/\partial x^2)$, is the same as the torsional stiffness term in Equation 2.5. The second term of Equation 2.18, $Ck_A^{\,2}(\partial^2\phi/\partial x^2)$ is called the tension-torsion term and tends to

untwist a pre-twisted blade due to centrifugal force. The third term in Equation 2.18, $I(\partial^2\phi/\partial t^2)$, is the same as the torsional inertia term in Equation 2.5. The fourth term in Equation 2.18, $I\Omega^2\phi\cos 2\beta$, is called the "tennis racket" term and also tends to untwist a pre-twisted blade. The untwisting effect from the tension-torsion term and the "tennis racquet" term stiffens the rotating blade as a function of Ω^2. Separation of variables is done by substituting for the torsional deformation in Equation 2.18 with Equation 2.6. Differentiating ϕ and canceling the imaginary terms produces the simplified equation. Equation 2.19 shows the resulting torsional ordinary differential equation (ODE) of motion for rotating blades. [Ref. 13]

$$(GJ + Ck_A^{\,2})\frac{\partial^2\phi(x)}{\partial x^2} + I\omega^2\phi(x) - I\Omega^2\phi(x)\cos 2\beta = 0 \tag{2.19}$$

Equation 2.19 is rearranged to facilitate use with Holzer's method. Equation 2.20 gives the Holzer form of the rotating blade equation that will be applied in this thesis. The tension-torsion term and the "tennis racket" term are the only differences when compared to Equation 2.7.

$$(GJ + Ck_A^{\,2})\frac{\partial^2\phi}{\partial x^2} = -I\phi(\omega^2 - \Omega^2\cos 2\beta) \tag{2.20}$$

D. THE HOLZER METHOD APPLIED TO ROTOR BLADES

The following modifications are required to apply Holzer's original method using the rotor blade torsional equation of motion shown in Equation 2.20. In place of Equation 2.8 we apply the same theory to the free body diagram in Figure 5 with the added "tennis racket" term from Equation 2.20. The result of this analysis is shown in Equation 2.21.

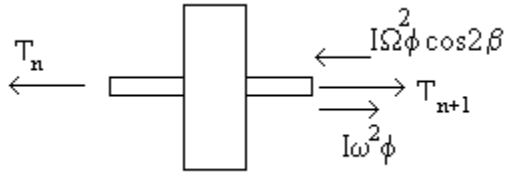

Figure 5. Free Body Diagram of a Lumped-Mass Rotor Segment.

$$T_n = T_{n+1} + I_n \phi_n (\omega^2 - \Omega^2 \cos 2\beta_n) \tag{2.21}$$

Equation 2.22 accounts for the tension-torsion term in the dynamic analysis of rotor blades and is used in place of Equation 1.6.

$$\Delta\phi = \frac{T\Delta x}{(GJ + Ck_A{}^2)} \tag{2.22}$$

Equation 2.23 replaces Equation 2.9 and represents the torsional deformation at a single segment where Equation 2.22 is substituted for the term, $\Delta\phi_{n+1}$.

$$\phi_n = \phi_{n+1} - \Delta\phi_{n+1} = \phi_{n+1} - \frac{T_{n+1}\Delta x_{n+1}}{(GJ_{n+1} + (Ck_A{}^2)_{n+1})} \tag{2.23}$$

Equations 2.21 and 2.23 combined with the boundary conditions for the rotor allow a solution using Holzer's method. The first step of the rotating blade Holzer method is the same as in the original method with the torsional deformation at the last segment equal to one radian as shown in Equation 2.10. The second step of the Holzer method solves for the total torsion moment at the last segment by substituting the boundary condition, $T_{21} = 0$, and Equation 2.10 into Equation 2.21. The result of step two is shown in Equation 2.24. If a twenty segment lumped-mass model of a rotor blade is used, then.

$$T_{20} = I_{20}(\omega^2 - \Omega^2 \cos 2\beta_{20}) \tag{2.24}$$

The third step of the Holzer method for the rotating blade solves for the next to the last segment's torsional deformation using Equation 2.23. The result of step three is shown in Equation 2.25.

$$\phi_{19} = 1 - \frac{T_{20}\Delta x_{20}}{(GJ_{20} + (Ck_A{}^2)_{20})} \tag{2.25}$$

The fourth step of the Holzer method for a rotating blade solves Equation 2.21 for the total torsion moment at the next to last segment. The result of step four is shown in Equation 2.26.

$$T_{19} = T_{20} + I_{19}\phi_{19}(\omega^2 - \Omega^2 \cos 2\beta_{19}) \tag{2.26}$$

The fifth step of the Holzer method for rotating blades repeats steps three and four for each segment in descending order until the root solution is obtained. The sixth step for rotating blades is the same as in the original method and requires that the root solution be compared against the root boundary conditions.

The Holzer method for rotating blades can be represented in transfer matrix form as shown in Equation 2.27. [Ref. 2]

$$\begin{Bmatrix} \phi \\ T \end{Bmatrix}_n = \begin{bmatrix} 1 & -\Delta x_{n+1}/(GJ_{n+1} + (Ck_A{}^2)_{n+1}) \\ I_n(\omega^2 - \Omega^2 \cos 2\beta_n) & \left(-\frac{\Delta x_{n+1} I_n(\omega^2 - \Omega^2 \cos 2\beta_n)}{(GJ_{n+1} + (Ck_A{}^2)_{n+1}} + 1 \right) \end{bmatrix} \begin{Bmatrix} \phi \\ T \end{Bmatrix}_{n+1} \quad (2.27)$$

Steps one through six of the Holzer method as presented for rotor blades is written into a MATLAB™ routine listed in Appendix A.

THIS PAGE INTENTIONALLY LEFT BLANK

III. EVALUATION OF THE HOLZER PROGRAM

A. INTRODUCTION

The Holzer program developed here is validated using a sequence of increasingly more complex test cases. These test cases include a mixture of theoretical and experimental tests. The theoretical test cases start with the simplest case of a uniform beam and increase in complexity until a non-uniform, rotating beam is evaluated. Rotating and non-rotating evaluations are done for both the Fixed-Free and Free-Free boundary conditions to demonstrate that the program is valid for these applications. The theoretical test cases will be presented in the following order:

- Test Case 1a: Uniform, Fixed-Free, Non-Rotating Beam
- Test Case 1b: Uniform, Fixed-Free, Rotating Beam
- Test Case 2a: Free-Free, Non-Rotating, Uniform Beam
- Test Case 2b: Free-Free, Non-Rotating, Non-Uniform Beam
- Test Case 3a: Non-Uniform, Fixed-Free, Non-Rotating Wing
- Test Case 3b: Non-Uniform, Fixed-Free, Rotating Wing

The accuracy of the Holzer program is also demonstrated using a set of realistic, experimental cases. The experimental test cases will be presented in the following order.

- Test Case 1: Non-Uniform, Non-Rotating, Free-Free, Full-Scale Blade
- Test Case 2a: Non-Uniform, Non-Rotating, Flex-Free, Model-Scale Blade
- Test Case 2b: Non-Uniform, Rotating, Flex-Free, Model-Scale Blade

All of the theoretical and experimental test cases are solved with the Holzer program using Equations 2.21 and 2.23. For the non-rotating cases the equations reduce to the form of the original Holzer method's Equations 2.8 and 2.9.

B. THEORETICAL TEST CASES

1. Uniform, Fixed-Free Test Cases

a. Non-Rotating

For the simple case of a uniform, cantilevered beam the Fixed-Free boundary conditions apply. This case can be solved exactly. The approximate solution from the Holzer method will be compared with the exact solution to validate the Holzer code. The Holzer method will be applied to four different, equivalent lumped-mass models of a six-foot long beam. Each model will use a different number of lumped-mass segments to analyze the effects of discretization on the Holzer solution. Equation 3.1 will be used to solve for the exact solution of the non-rotating, uniform rotor blade natural frequency. Equation 3.2 is the equation for the exact solution of the torsional deformation mode shape. [Ref. 1]

$$\omega_{NR}^{m} = (m - \frac{1}{2})\pi\sqrt{\frac{GJ}{IR^2}} \tag{3.1}$$

where

ω_{NR} = the non-rotating natural frequency
m = the mode number

$$\phi_{NR}^{m} = (-1^{m+1})\sin((m - \frac{1}{2})\pi x) \tag{3.2}$$

where

ϕ_{NR} = the non-rotating torsional deformation mode shape

The uniform beam tested for this case is six feet long, has a torsional mass moment of inertia of 40 lb-ft-sec^2 and a torsional stiffness of $3x10^6$ lb-ft^2. To model a uniform beam into an equivalent system of n evenly spaced segments the total length of the beam is divided by (n-1) to get the span length between each segment, Δx_n. The equivalent segment torsional mass moment of inertia equals the original torsional mass moment of inertia multiplied by Δx_n. The torsional stiffness, GJ, remains unchanged in the conversion to an equivalent lumped-mass system. Table 1 shows the properties for four cases using different numbers of elements. For each lumped-mass model (i.e., seven-segment model, 13-segment model, 25-segment model, and 49-segment model) the properties listed are identical for each segment of the same model.

Lumped-Mass Models with "n" Segments			
n	**I** lb-ft-sec^2	**Δr** ft	**GJ** lb-ft^2
7	40.0	1.000	3.0E+06
13	20.0	0.500	3.0E+06
25	10.0	0.250	3.0E+06
49	5.0	0.125	3.0E+06

Table 1. Structural Properties for Uniform, Non-Rotating, Fixed-Free Beam.

The Holzer program was run four separate times, once for each lumped-mass model of the uniform beam and the first three natural frequencies and mode shapes were computed. The calculated natural frequencies are listed in Table 2. Equation 3.1 was used to calculate the exact solution for the first three natural frequencies and is the basis for the error values listed in Table 2.

Model n	**ω_1** rad/sec	**error** %	**ω_2** rad/sec	**error** %	**ω_3** rad/sec	**error** %
7	66.0	-7.9	194.2	-9.7	311.1	-13.2
13	68.8	-4.0	205.3	-4.6	338.5	-5.6
25	70.2	-2.1	210.4	-2.2	349.7	-2.5
49	71.0	-1.0	212.8	-1.1	354.4	-1.1
Exact	**71.7**		**215.1**		**358.5**	

Table 2. Natural Frequency Results for the Uniform, Non-Rotating, Fixed-Free Beam.

As expected, the error decreases as the number of segments increase. Errors are inherent with approximation solutions such as the Holzer method. The errors are greater for the higher natural frequencies. An error of one percent is achieved for the 49-segment case, for the first natural frequency solution.

These calculations are illustrated in Figure 6 that shows the first three exact and Holzer calculated natural frequencies versus the number of segments used. Each exact solution is shown as a horizontal line at its natural frequency. Each natural frequency also has four different attempts to calculate the natural frequency using models with an increasing number of segments. Each calculated natural frequency is marked with a diamond symbol and the number of segments. The lines between calculated solutions simply connect the data points. For all three natural frequencies the calculated values converge towards the exact solution with an increasing number of segments.

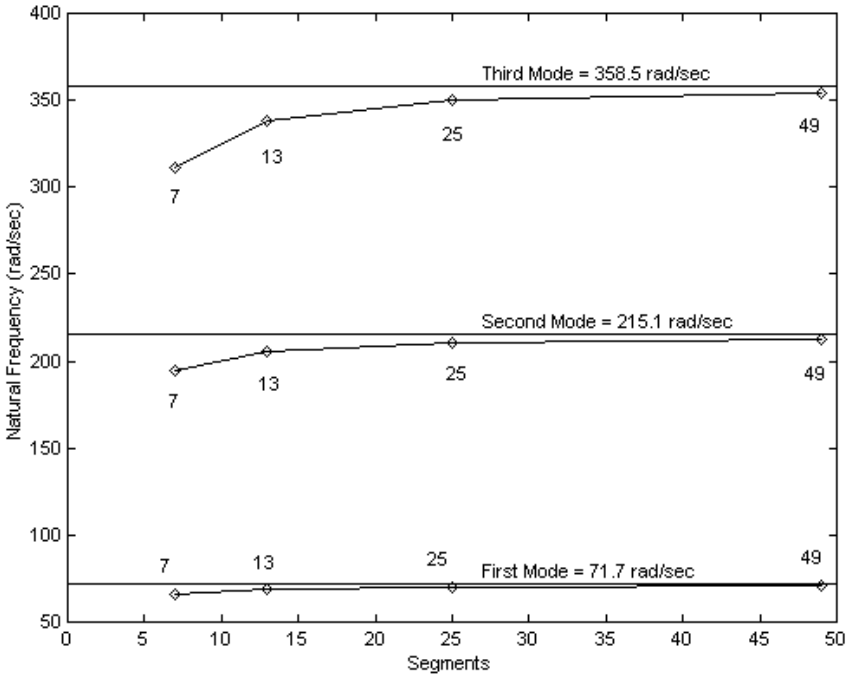

Figure 6. Natural Frequency Accuracy by Segment Number.

Figure 7 displays a plot of the Holzer program natural frequency solutions for the 49-segment model. The y-axis is the root (segment one) torsional deformation. The x-axis is the range of test frequencies attempted. The natural frequencies are where the root boundary condition of zero torsional deformation is met. The natural frequency solution data points are marked with a square. Each root torsional deformation solution is plotted against the respective test frequency at an increment of five (rad/sec). The plotted line connects each data point for test frequencies ranging from zero to 400 (rad/sec) as chosen during program execution.

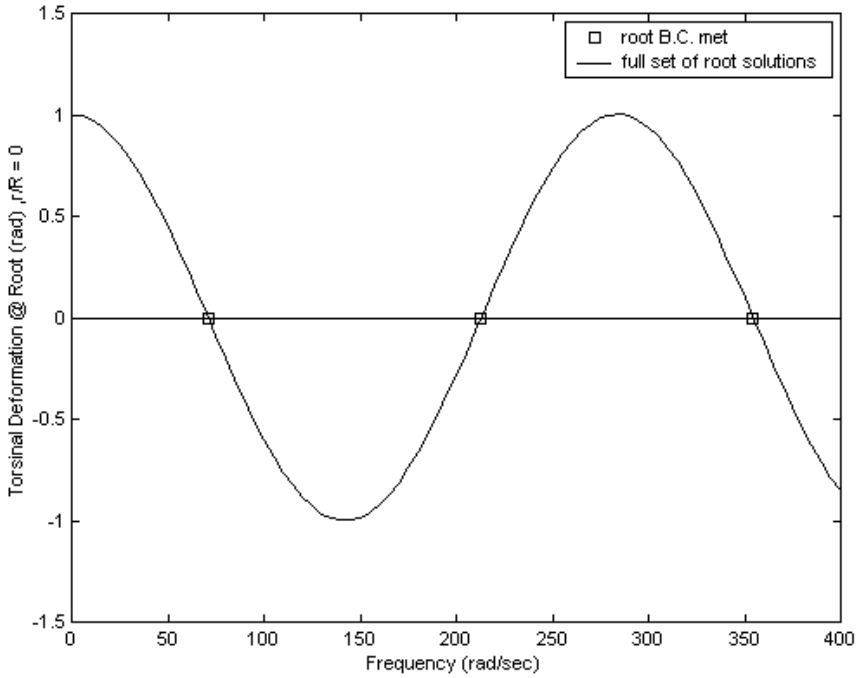

Figure 7. Natural Frequency Graphical Solution to the 49-segment, Uniform, Fixed-Free, Non-Rotating Beam.

Figures 8, 9, and 10 plot the modes shapes for the first, second, and third natural frequencies respectively for the 49-segment Holzer solution. The Holzer calculated torsional deformation is plotted against span location. Each of the 49-segments has its own torsional deformation value marked by a square. The solid line is the exact solution plotted using Equation 3.2.

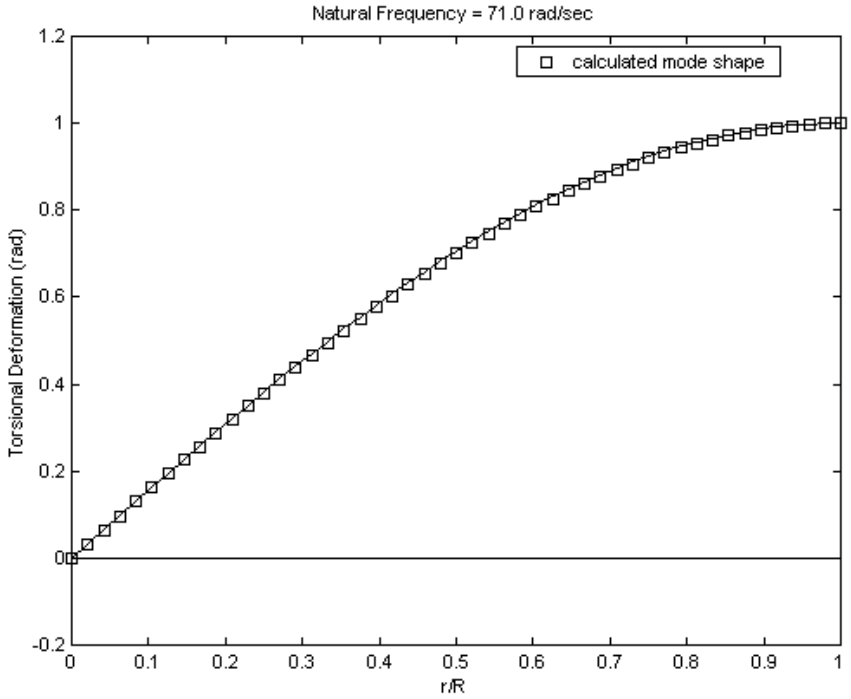

Figure 8. 49-Segment First Mode Shape.

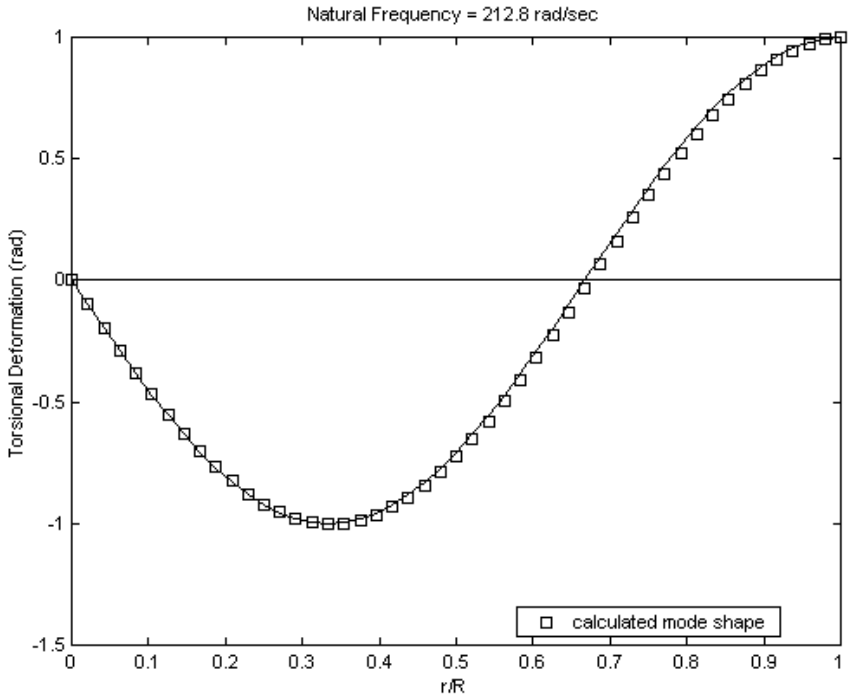

Figure 9. 49-Segment Second Mode Shape.

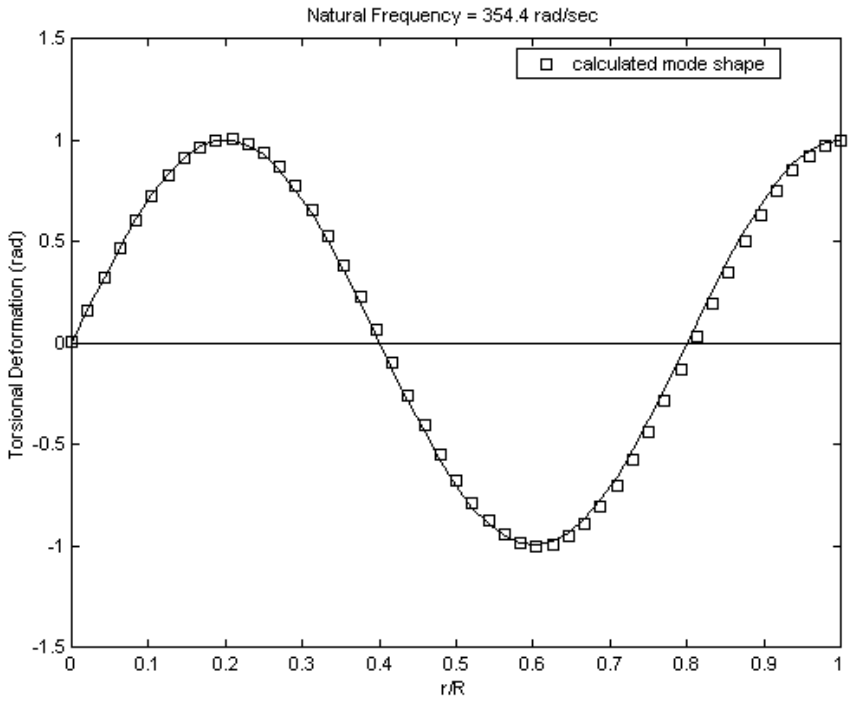

Figure 10. 49-Segment Third Mode Shape.

All three mode shape plots show excellent agreement with the exact solution. Figure 11 shows the deviation of the 49-segment calculated mode shapes with the exact solution mode shapes versus span for the first three modes. Each data point is a single deviation between the exact and calculated torsional deformation by span location. The lines simply connect the data points. The largest error is observed in the third mode on the center portion of the beam, approximately -0.065 (tip deflection is 1.0).

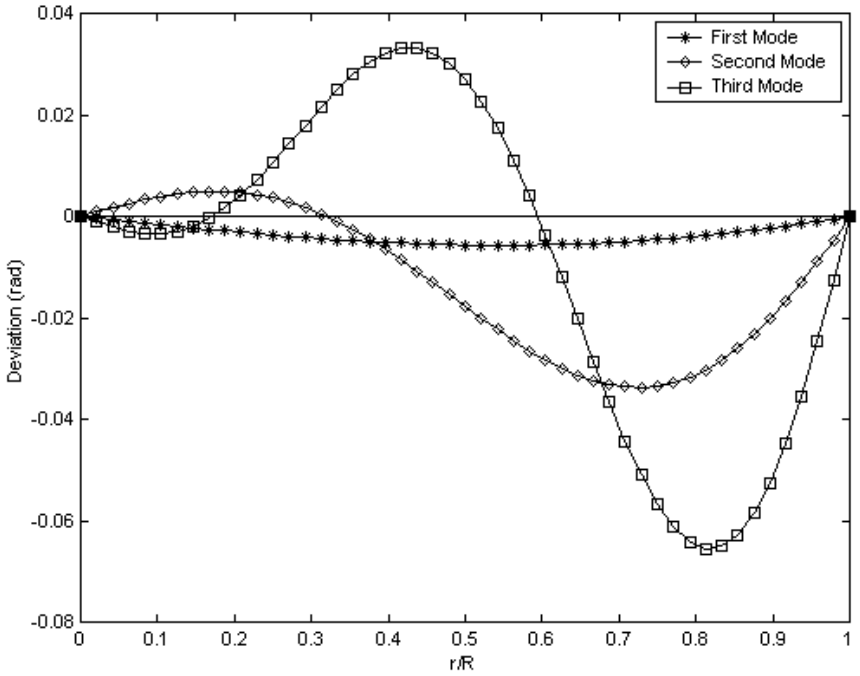

Figure 11. Mode Shape Deviation of the 49-Segment, Calculated versus Exact.

Based on the results presented the Holzer program is valid for the uniform, Fixed-Free, non-rotating test case.

b. Rotating

The exact solution for the Fixed-Free, uniform, rotating natural frequency is represented by Equation 3.3 [Ref. 10].

$$\omega_{ROT} = \sqrt{(\omega_{NR}{}^2 + \Omega^2)} \tag{3.3}$$

This test case is run with the same structural properties used in the previous non-rotating test case listed in Table 1. The rotational speed is 150 (rad/sec) and the natural frequency results from the Holzer program are shown in Table 3.

Model n	**ω_1** rad/sec	**error** %	**ω_2** rad/sec	**error** %	**ω_3** rad/sec	**error** %
7	163.9	-1.4	245.4	-6.4	345.4	-11.1
13	165.0	-0.8	254.2	-3.1	370.3	-4.7
25	165.7	-0.4	258.4	-1.4	380.5	-2.1
49	166.0	-0.2	260.3	-0.7	384.8	-1.0
Exact	**166.3**		**262.2**		**388.6**	

Table 3. Natural Frequency Results for the Uniform, Rotating, Fixed-Free Beam.

The exact rotating natural frequency solutions in Table 3 are found by using the exact non-rotating natural frequency solutions from Table 2 with Equation 3.3. As with the non-rotating case, the most accurate solutions are for the first mode, with the errors increasing with increased mode number. The third mode is still accurate to one percent. It is unknown why the rotating modes are more accurate than their non-rotating counterparts.

The natural frequency error decreases with an increase in segments used. Figure 12 shows the convergence of the Holzer natural frequencies towards their respective exact solutions as the number of segments increase. Each natural frequency solution is marked with a diamond and the number of segments used in the calculation. The lines connect the data points.

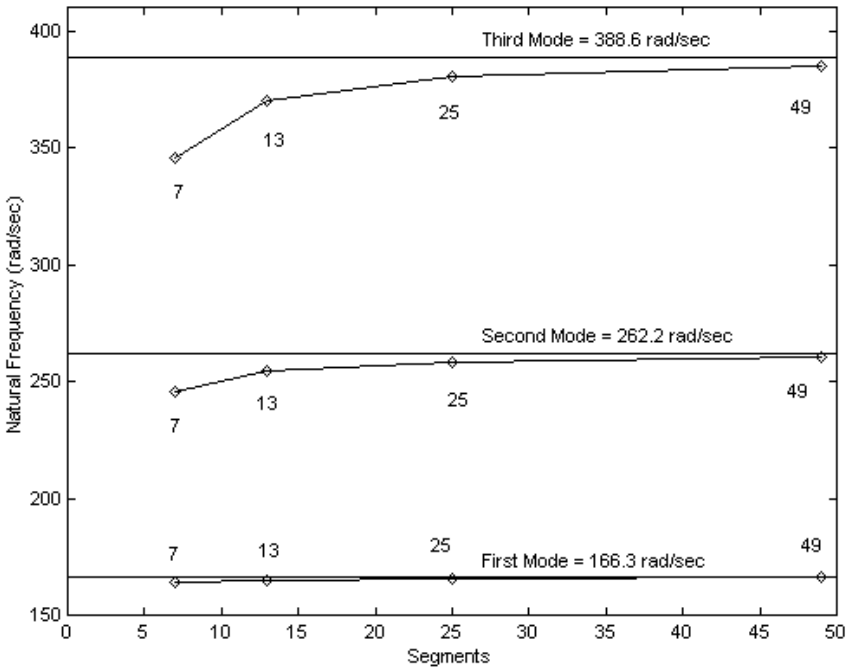

Figure 12. Rotating Natural Frequency Accuracy by Segment Number.

Rotating torsional mode shapes are theoretically identical to the non-rotating mode shapes [Ref. 2]. In reality there is some variance between rotating and non-rotating mode shapes. Figure 13 plots the deviation between the rotating and non-rotating mode shapes versus span for the first three modes. Each data point is the single

point deviation for an individual segment. The lines connect the data points for each mode.

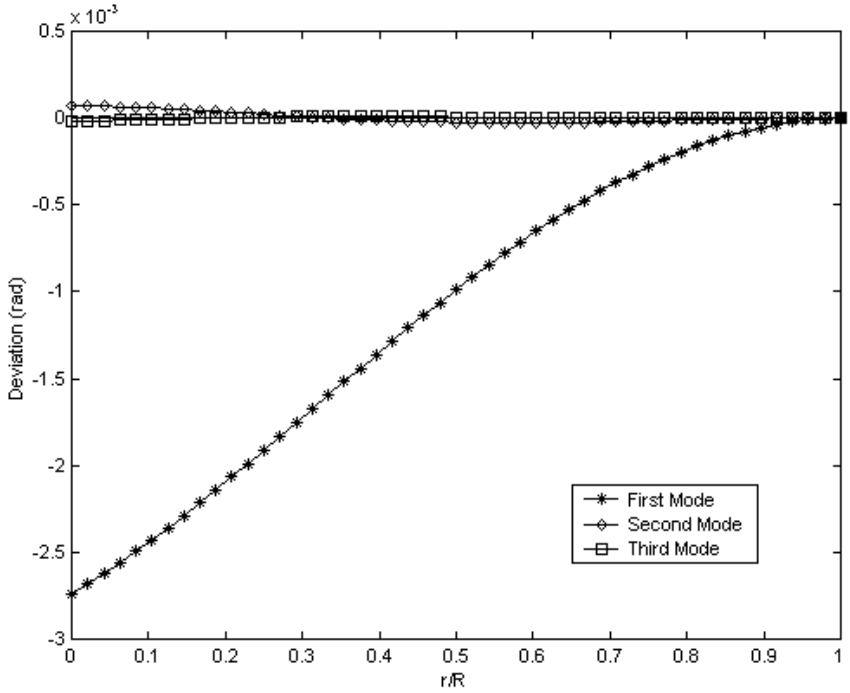

Figure 13. Mode Shape Deviation of the 49 Segment, Rotating versus Non-Rotating.

The deviation for the first mode shape is large in comparison with the second and third mode shape deviations. Despite the relatively large deviation for the first mode, the scale is in the thousandths and the largest deviation is less than -0.003 (tip deflection is 1.0). The Figure 13 mode shape deviations are between Holzer calculated rotating mode shapes and Holzer calculated non-rotating mode shapes. The larger deviations presented in Figure 11 are between the Holzer calculated non-rotating mode shapes and the exact mode shapes. Based on the results presented the Holzer program is valid for the uniform, Fixed-Free, rotating test case.

2. Free-Free, Non-Rotating Test Cases

a. Uniform

A three-segment model of a uniform, Free-Free beam with structural properties listed by segment in Table 4 is tested with the Holzer program. This test case has no exact solution or published solution to compare the calculated results with. This is

a reduced or simplified case from Thomson's non-uniform, Free-Free example 12.4.1 that is discussed in the next section. [Ref. 11]

3-Segment Lumped-Mass Model			
Segment Number	**I** kg-m^2	**Δr** m	**GJ** N-m^2
1	22	0	8.0E+06
2	22	40	8.0E+06
3	22	40	8.0E+06

Table 4. Structural Properties for Uniform, Non-Rotating, Free-Free Beam.

Figures 14 and 15 plot the mode shapes for the first two modes. The data points represent the torsional deformation at each of the three segments. The line simply connects the data points.

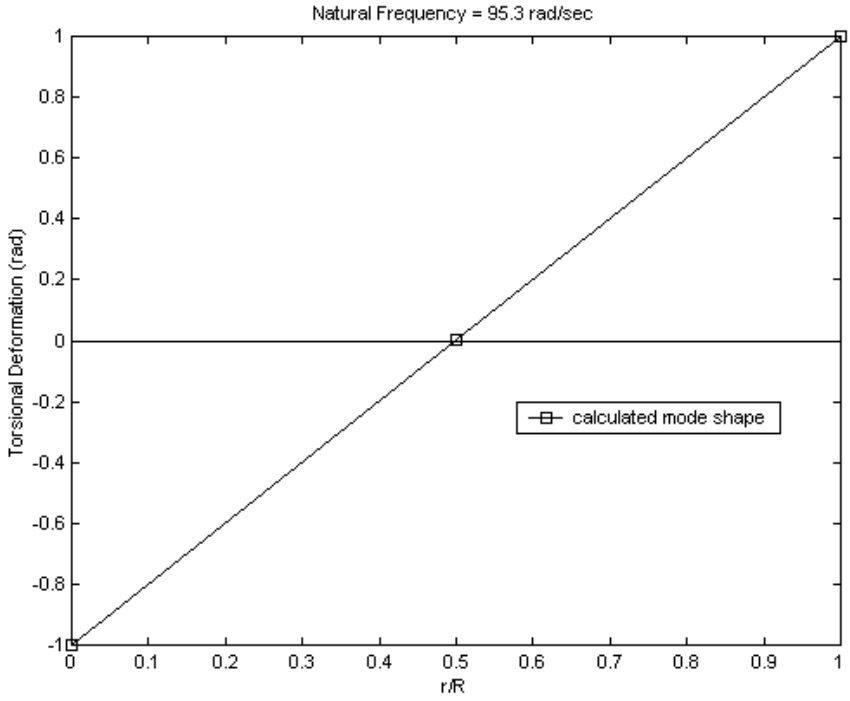

Figure 14. Free-Free, Uniform First Mode Shape.

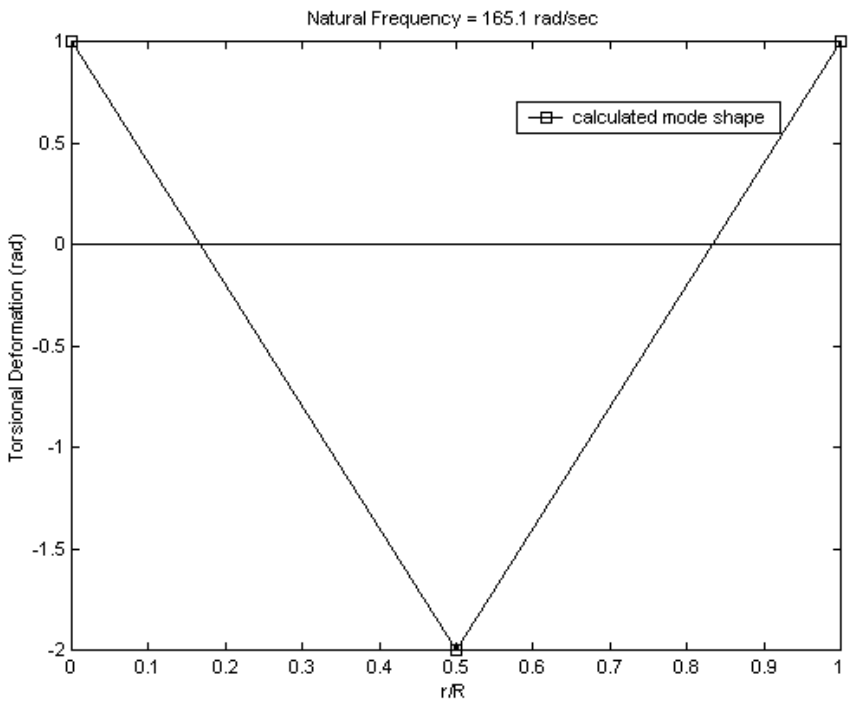

Figure 15. Free-Free, Uniform Second Mode Shape.

The results of this uniform reduced case from Thomson are consistent with the non-uniform case presented next. The Holzer program is valid for the uniform, Free-Free case.

b. Non-Uniform

This test case is Thomson's example 12.4.1 for a slightly non-uniform, Free-Free beam. Table 5 shows the structural properties for the individual segments. [Ref. 11]

3-Segment Lumped-Mass Model			
Segment Number	**I** kg-m^2	**Δr** m	**GJ** N-m^2
1	22	0	8.0E+06
2	11	40	8.0E+06
3	5	40	4.0E+06

Table 5. Structural Properties for Non-Uniform, Non-Rotating, Free-Free Beam.

The natural frequency solutions are shown in Figure 16 where the root boundary condition for the Free-Free case is a torsion moment equal to zero. The natural frequencies are marked with a square. The line simply connects each test frequency's

root torsion moment result at test frequency increments of five (rad/sec) from zero to 300 (rad/sec).

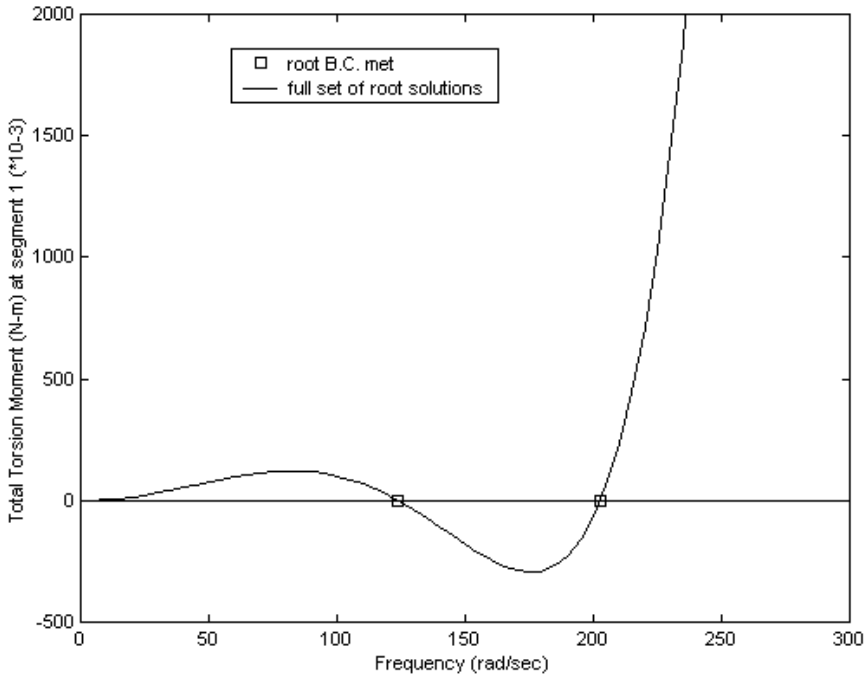

Figure 16. Natural Frequency Graphical Solution to the Free-Free, Non-Uniform Beam.

The Holzer program gives the exact answers found in the Thomson textbook for frequencies and mode shapes. The first natural frequency is at 123.6 (rad/sec) and the second natural frequency is at 202.5 (rad/sec). Figures 17 and 18 show the first and second mode shapes. The squares mark each segment's deflection and the line connects the data points.

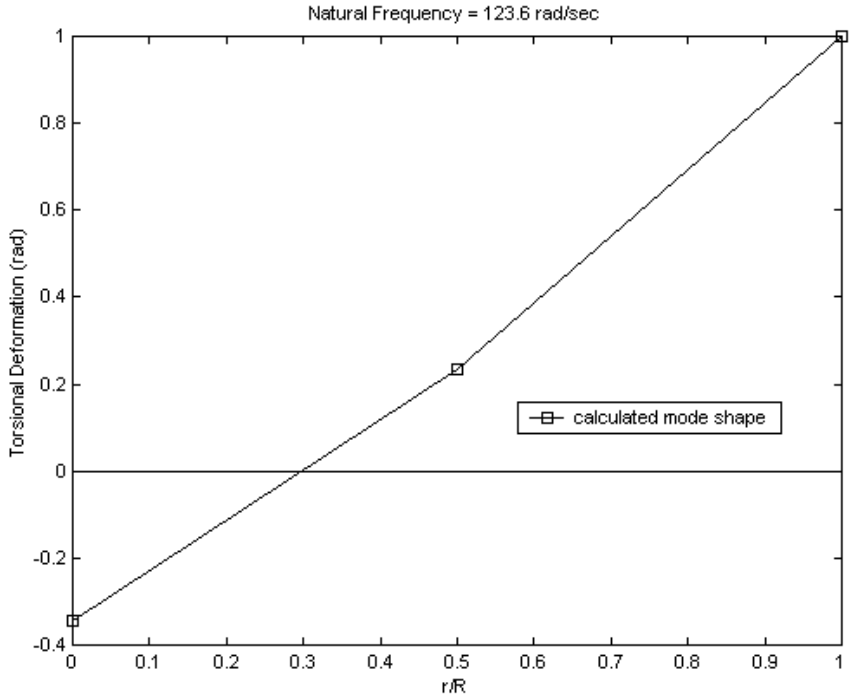

Figure 17. Non-Uniform, Free-Free First Mode Shape.

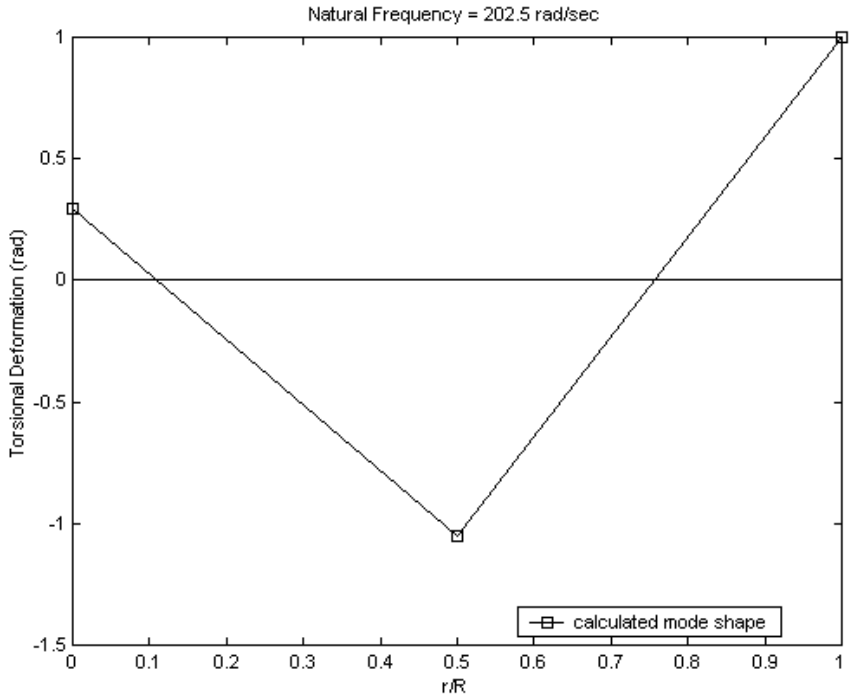

Figure 18. Non-Uniform, Free-Free Second Mode Shape.

This test case is only slightly non-uniform and therefore the mode shapes shown in the previous test case can be compared to Figures 17 and 18 for a general

comparison. When Figures 14 and 15 are compared to Figures 17 and 18 the mode shapes follow the same general trend. Based on the presented results the Holzer program is valid for the non-uniform, Free-Free case.

3. Non-Uniform, Fixed-Free Test Cases

a. Non-Rotating Wing

This test case is Scanlan's example 7.4. The structural properties are listed in Table 6 are for each segment. This example is a model of a fixed-wing aircraft. [Ref. 12]

7-Segment Lumped-Mass Model			
Segment Number	**I** lb-ft-sec^2	**Δr** ft	**GJ** lb-ft^2
1	0	0	4.0E+09
2	350	16	4.0E+09
3	250	34	1.6E+09
4	200	50	4.0E+08
5	150	40	1.4E+09
6	135	40	1.1E+09
7	110	40	1.2E+09

Table 6. Structural Properties for Non-Uniform, Non-Rotating, Fixed-Free Wing.

The Holzer program gives the exact answers found in the Scanlan textbook for natural frequencies and mode shapes. The natural frequency solutions are listed in Table 7.

	ω_1 rad/sec	ω_2 rad/sec	ω_3 rad/sec
Non-Rotating	98.8	351.9	439.1

Table 7. Natural Frequency Results for the Non-Uniform, Non-Rotating, Fixed-Free Wing.

Figures 19, 20 and 21 plot the first three mode shapes. The individual segment deformation value is marked with a square. The line simply connects the data points.

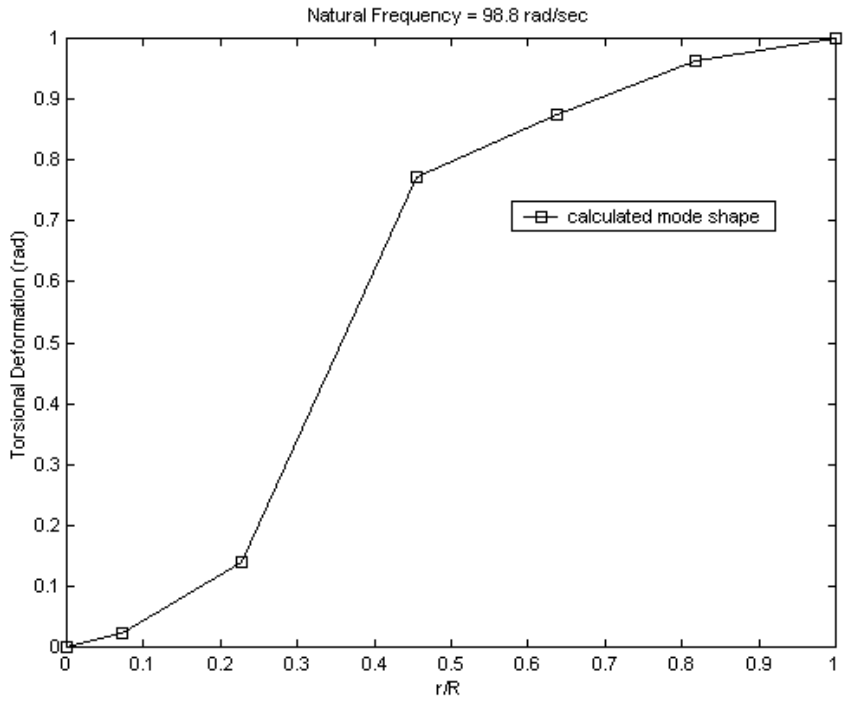

Figure 19. Non-Rotating Wing First Mode Shape.

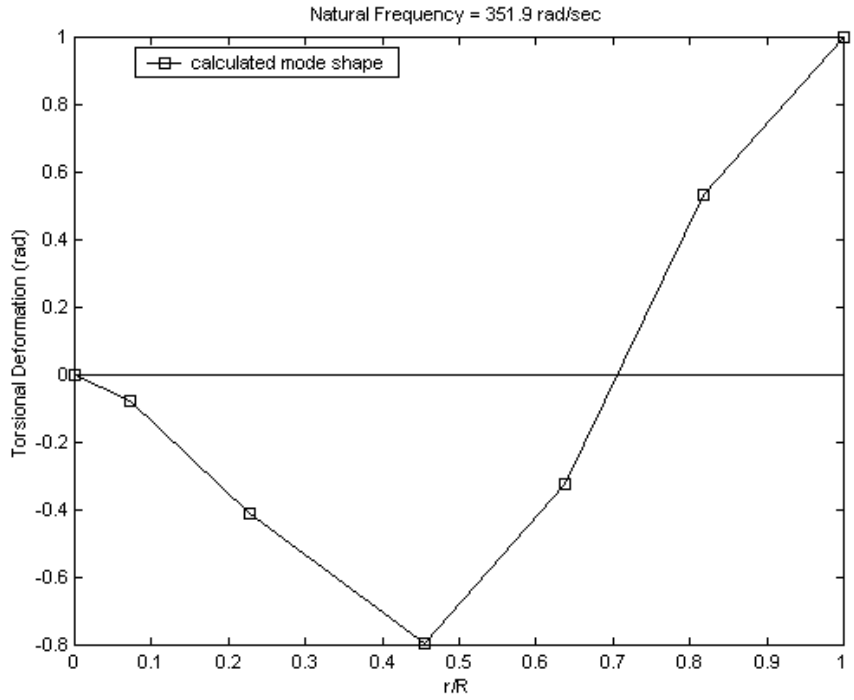

Figure 20. Non-Rotating Wing Second Mode Shape.

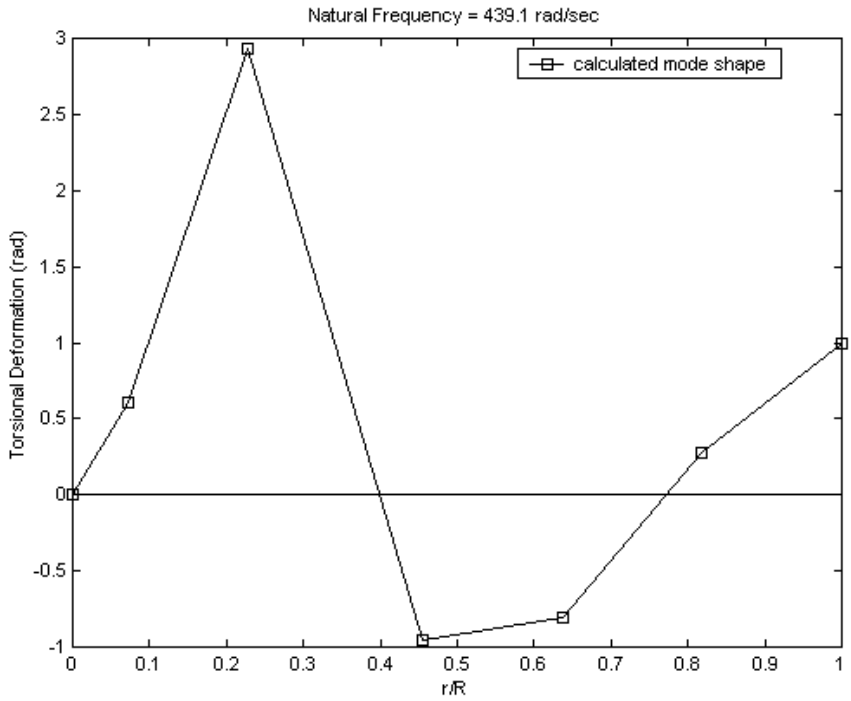

Figure 21. Non-Rotating Wing Third Mode Shape.

The Holzer results for the non-rotating, non-uniform, Fixed-Free case of the Scanlan wing are exact with the published solution. The Holzer program is valid for this test case.

b. Rotating Wing

This test case takes the structural properties listed in Table 4 and applies a rotational speed of 150 (rad/sec). The rotating natural frequencies from the Holzer program are identical to the exact solution. The exact rotating natural frequency solution is obtained using Equation 3.3 and the non-rotating natural frequencies from Table 7. Table 8 lists the rotating natural frequency results.

	ω_1 rad/sec	ω_2 rad/sec	ω_3 rad/sec
Rotating	179.6	382.6	464.0

Table 8. Natural Frequency Results for the Non-Uniform, Rotating, Fixed-Free Wing.

Theoretically the mode shapes in rotation are identical to those for the non-rotating condition. In reality there is some deviation between rotating and non-rotating mode shapes. Figure 22 presents the mode shape deviation between the rotating

and non-rotating mode shapes for the first three modes. Each symbol marks the deviation at an individual segment and mode. The lines connect the data points for each mode.

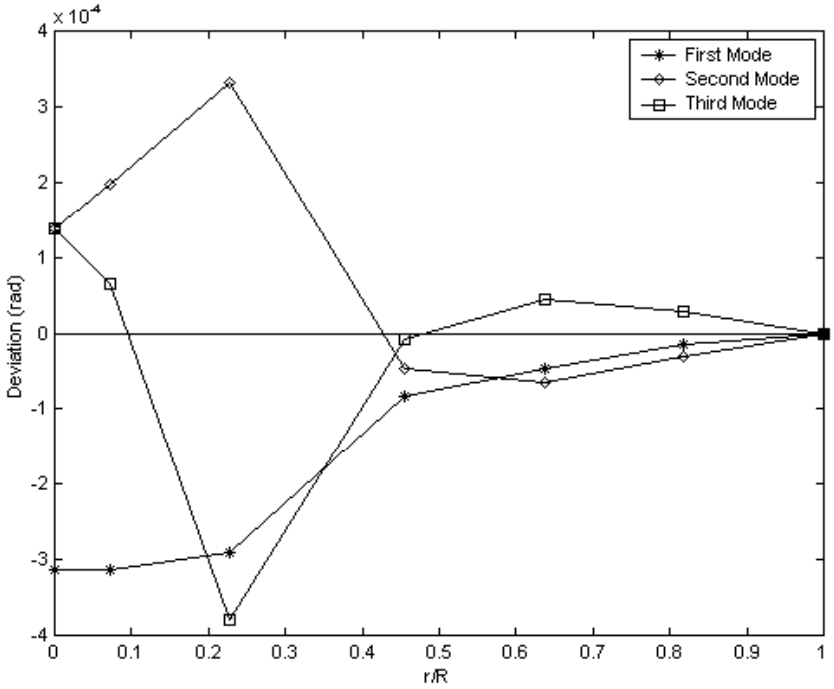

Figure 22. Deviation of Rotating versus Non-Rotating Wing Mode Shapes.

The deviations in Figure 22 are extremely small with the largest value being less than 0.0004 radians. Based on the presented results the Holzer program is valid for the non-uniform, Fixed-Free, rotating test case.

C. NON-UNIFORM ROTOR BLADE TEST CASES

1. Full Scale UH-60 Rotor Blade

a. Overview of Experiment

In November 1990, Engineers at the NASA-Ames Research Center measured dynamic properties of a full-scale production and instrumented UH-60A Black Hawk rotor blades. NASA measurements from the shake tests of a production blade will be compared against the Holzer program results. [Ref. 15]

The UH-60A rotor blade is 24.15 feet in radius and is composed of a titanium spar, a honeycomb core, fiberglass skin, and an aluminum tip cap. The root offset is 2.65 feet. [Ref. 15]

b. Non-Rotating, Free-Free Natural Frequencies and Mode Shapes

Table 9 shows the structural properties for the full-scale UH-60A rotor blade from a NASA database [Ref. 16]. The list of structural properties does not include terms required to generate the tension-torsion or the "tennis racket" terms because these terms are only a factor for rotating test cases.

GJ lb-ft^2	I lb-ft-sec^2	r ft	GJ lb-ft^2	I lb-ft-sec^2	r ft
4.88E+05	3.84E-03	2.7	1.72E+05	2.53E-02	17.6
4.88E+05	0.00E+00	2.7	1.72E+05	0.00E+00	17.6
4.88E+05	6.45E-03	3.1	1.72E+05	2.71E-02	18.4
3.46E+05	0.00E+00	3.1	1.72E+05	2.89E-02	19.1
3.46E+05	6.99E-03	3.4	1.72E+05	0.00E+00	19.1
3.46E+05	1.75E-02	4.2	1.72E+05	3.08E-02	19.7
3.46E+05	0.00E+00	4.2	1.72E+05	0.00E+00	19.7
3.46E+05	1.68E-02	4.9	1.72E+05	2.88E-02	20.4
1.80E+05	0.00E+00	4.9	1.72E+05	0.00E+00	20.4
1.80E+05	8.20E-03	5.2	1.72E+05	3.20E-02	21.1
1.80E+05	2.50E-02	6.3	1.71E+05	0.00E+00	21.1
1.80E+05	0.00E+00	6.3	1.71E+05	2.57E-02	21.7
1.80E+05	1.35E-02	6.7	1.71E+05	0.00E+00	21.7
1.69E+05	0.00E+00	6.7	1.71E+05	1.54E-02	22.1
1.69E+05	8.76E-03	7.0	1.71E+05	1.35E-02	22.4
1.69E+05	2.23E-02	7.6	1.71E+05	2.28E-02	22.9
1.69E+05	0.00E+00	7.6	1.71E+05	1.38E-03	22.9
1.69E+05	4.45E-02	9.1	1.69E+05	0.00E+00	22.9
1.69E+05	0.00E+00	9.1	1.69E+05	4.64E-03	23.1
1.69E+05	4.45E-02	10.4	1.69E+05	0.00E+00	23.1
1.69E+05	2.23E-02	11.2	1.69E+05	3.37E-03	23.2
1.69E+05	2.23E-02	11.8	1.69E+05	1.80E-05	23.2
1.69E+05	0.00E+00	11.8	1.69E+05	0.00E+00	23.2
1.69E+05	7.93E-03	12.1	1.69E+05	1.49E-02	23.6
1.71E+05	0.00E+00	12.1	1.69E+05	1.83E-02	24.1
1.71E+05	1.43E-02	12.5	1.69E+05	0.00E+00	24.1
1.71E+05	2.23E-02	13.3	1.69E+05	6.70E-03	24.3
1.71E+05	0.00E+00	13.3	1.69E+05	2.50E-02	24.7
1.71E+05	2.89E-03	13.3	1.69E+05	1.41E-02	24.9
1.71E+05	1.99E-02	13.9	1.69E+05	1.72E-02	25.2
1.72E+05	0.00E+00	13.9	1.69E+05	0.00E+00	25.2
1.72E+05	2.48E-03	14.0	1.69E+05	1.67E-02	25.5
1.72E+05	2.53E-02	14.7	1.69E+05	1.33E-02	25.9
1.72E+05	0.00E+00	14.7	1.69E+05	0.00E+00	25.9
1.72E+05	2.53E-02	15.4	1.69E+05	1.22E-02	26.2
1.72E+05	2.53E-02	16.2	1.69E+05	1.22E-02	26.5
1.72E+05	0.00E+00	16.2	1.69E+05	0.00E+00	26.5
1.72E+05	2.53E-02	16.9	1.69E+05	1.27E-02	26.8

Table 9. 76-Segment Full-Scale UH-60A Blade Structural Properties. [After: Ref. 16]

Table 10 presents the natural frequency results and errors in comparison to the NASA measurements.

	ω_1 Hz	**error** %	ω_2 Hz	**error** %
Holzer	46.1	-1.1	93.0	9.3
NASA Measurement	46.6		85.1	

Table 10. Natural Frequencies for the Full-Scale UH-60A Rotor Blade. [After: Ref. 15]

The result for the first natural frequency barely exceeds one-percent compared to the experimental result. The error for the uncoupled Holzer calculated second natural frequency is significant at greater than nine-percent. The results are acceptable since coupling effects are expected to have a greater influence over the second mode frequencies than they do for the first mode frequencies.

Figures 23 and 24 give the first and second mode shapes plotted versus the NASA measured mode shapes. The data points represent each segment's deflection for the Holzer results and the solid line connects the data for the NASA results. It is important to note that the span locations for the models used do not match between the Holzer and NASA results.

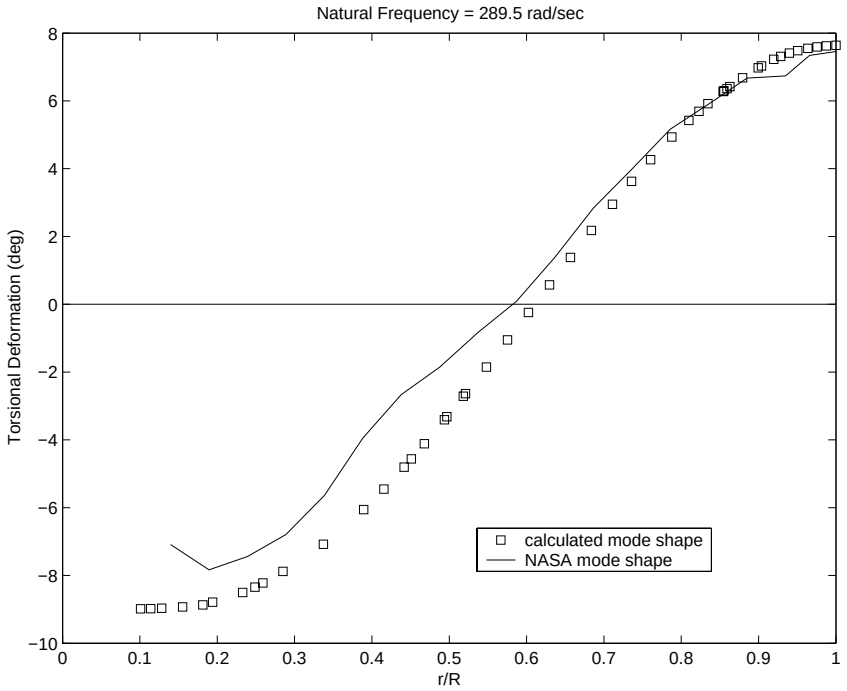

Figure 23. Full-Scale UH-60A Free-Free First Mode Shape. [After: Ref. 15]

From mid-span to tip the Holzer mode shape compares well with the NASA mode shape, but the match is poor from root to mid-span where the mass and stiffness is greater.

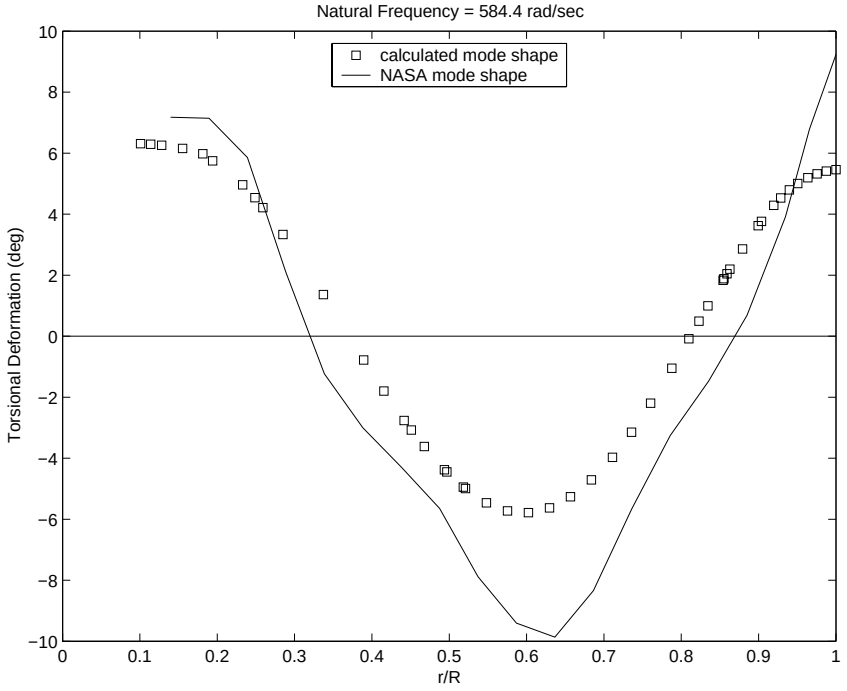

Figure 24. Full-Scale UH-60A Free-Free Second Mode Shape. [After: Ref. 15]

For an uncoupled solution, the Holzer method compares reasonably with the NASA mode shape. These differences are consistent with the errors presented for the second natural frequency.

The Holzer program is valid for the first natural frequency and mode shape calculations for a realistic, Free-Free, full-scale, non-uniform rotor blade. The Holzer program results for the second mode shape and frequency calculations are an acceptable match considering the solution is uncoupled. Use of the Holzer program for higher than the first mode of a free-free, non-uniform rotor blade should be confirmed with other methods to validate the results. A possible source of error is the fact that the Holzer program did not account for shake test boundary conditions. The shake test boundary conditions include the effects of the shaker, bungee cords and gravity [Ref. 15].

2. United Technologies Research Center (UTRC) Model-Scale UH-60 Flex-Free Rotor Blade

a. Description of UTRC model-blade

In 1984 UTRC manufactured a four-bladed (1:5.73) model-scale UH-60A rotor system developed for wind tunnel testing. The blade radius is 56.22 inches, both the radial and feathering axis pitch link offsets are three inches and the chord is 3.643 inches. The blade aspect ratio is 15.3 and the solidity is 0.0825. The blade is dynamically and geometrically scaled. Two different airfoils are used throughout the blade span. Figure 25 shows the actual size of the model-scale airfoils. Pressure transducers; strain gages and temperature sensors were installed in the blades. [Ref. 14]

a) SC 1095 airfoil.

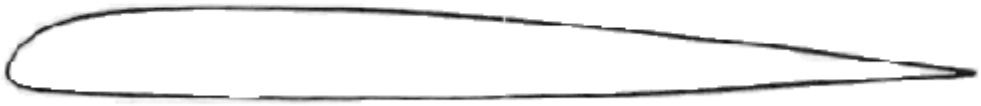

b) SC 1095R8 airfoil.

Figure 25. Airfoil Sections, Actual Size. [From: Ref. 14]

The rotor blades are constructed from graphite-epoxy spars, fiberglass skin, foam trailing edge pockets, and tungsten counterweights [Ref. 14]. Tables 16 through 20 in Appendix C, present the structural properties based on the UTRC data [Ref. 17]. For all the structural property tables the value increase from left to right and coincide with the span locations in Table 16. The tension-torsion term is presented in Table 19 without the square of rotation speed, which is multiplied internally in the Holzer program. The tension-torsion term is already multiplied by the square of the radius of gyration. The torsional stiffness is determined by measuring deflection resulting from point calibration loads. The instrumented rotor blade is thirty-percent heavier than the

scale weight of a full-scale blade without instruments. The added weight caused natural frequencies to change by as much as ten-percent. [Ref. 14]

The root restraint was modeled to be flexible like the actual UH-60A model rotor . The value of k_{Root} is 10,300 (in-lb/rad) and Equation 2.14 results in a root torsional deformation boundary condition of 0.0904 rad. [Ref. 14]

b. Non-Rotating Natural Frequencies and Mode Shapes

This test case is the first examination of the Flex-Free root boundary condition. In addition, this is the first test case to investigate the effects of the tension-torsion and "tennis racket" terms on natural frequencies and mode shapes. Figure 26 shows the graphical solution to the Flex-Free Condition. The root flexibility allows for deflections up to 0.0904 rad. The Holzer program assumes the maximum allowed deflection will be achieved at the natural frequencies. The odd modes have a positive, k_{Root}, and the even modes have a negative, k_{Root}. [Ref. 1]

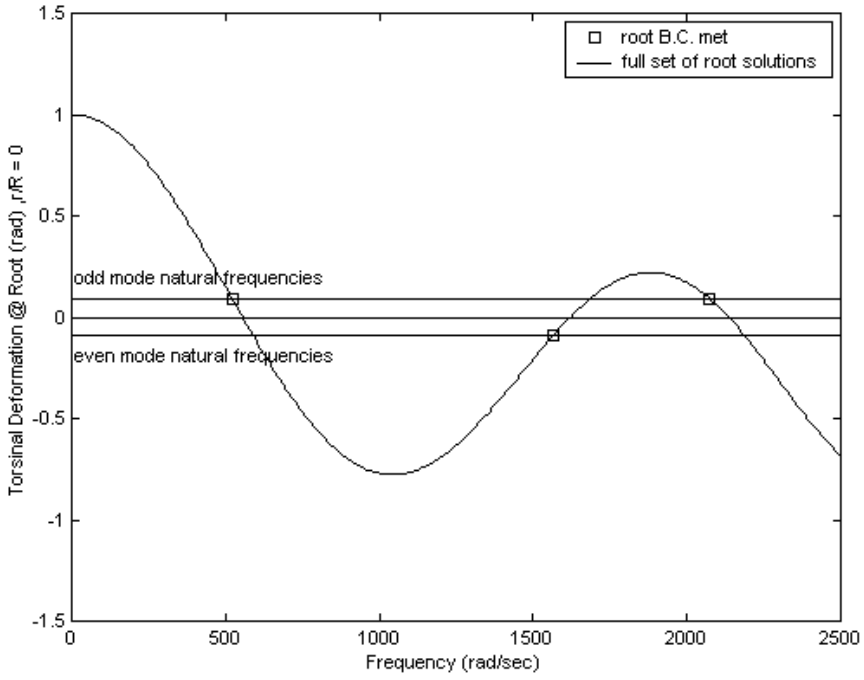

Figure 26. Graphical Solution to the Non-Rotating, Non-Uniform, Flex-Free Natural Frequency.

Table 11 presents the natural frequency solutions for the non-rotating, Flex-Free Holzer calculations, the Myklestad based Sikorsky calculations, and rap test data. Table 11 also shows the calculated natural frequencies for Free-Free solutions.

Non-Rotating	Flex-Free ω_1 (Hz)	error %	Free-Free ω_1 (Hz)	error %
Holzer	83.2	2.7	124.8	2.1
Sikorsky	86.6	6.9	129.8	1.8
Rap Test	81.0		127.5	

Table 11. Natural Frequencies for the Non-Uniform, Non-Rotating, Flex-Free Rotor. [After: Ref. 14]

Results of the Holzer program's Flex-Free first natural frequency agrees better with rap test data than do Sikorsky calculations. The Free-Free first frequency result for the Holzer method is in slightly closer agreement with rap test values than the Flex-Free value.

Figures 27, 28 and 29 show first, second and third mode shapes respectively. Data points represent individual segment deflections with the line connecting the data points.

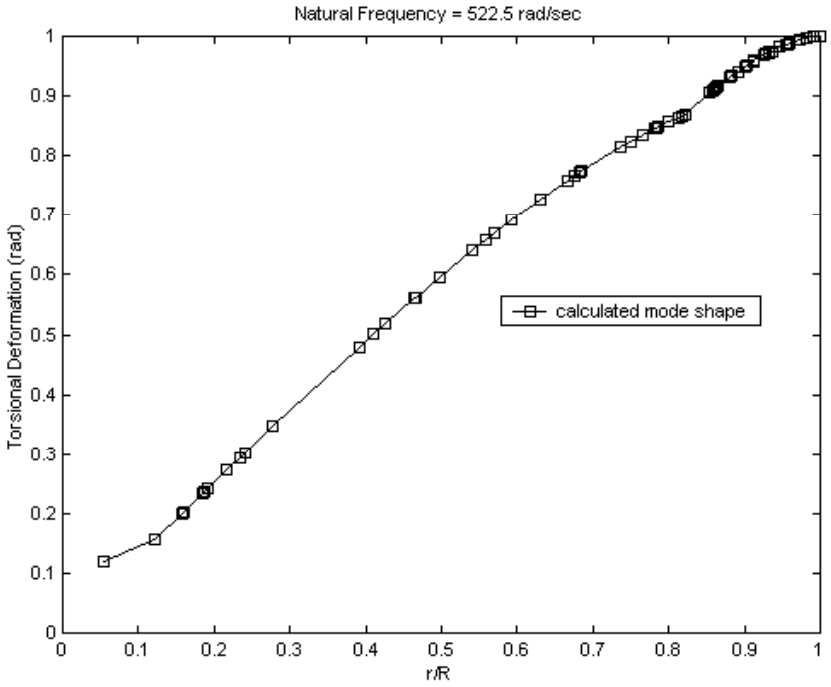

Figure 27. First Mode Non-Rotating Model Rotor Natural Frequency.

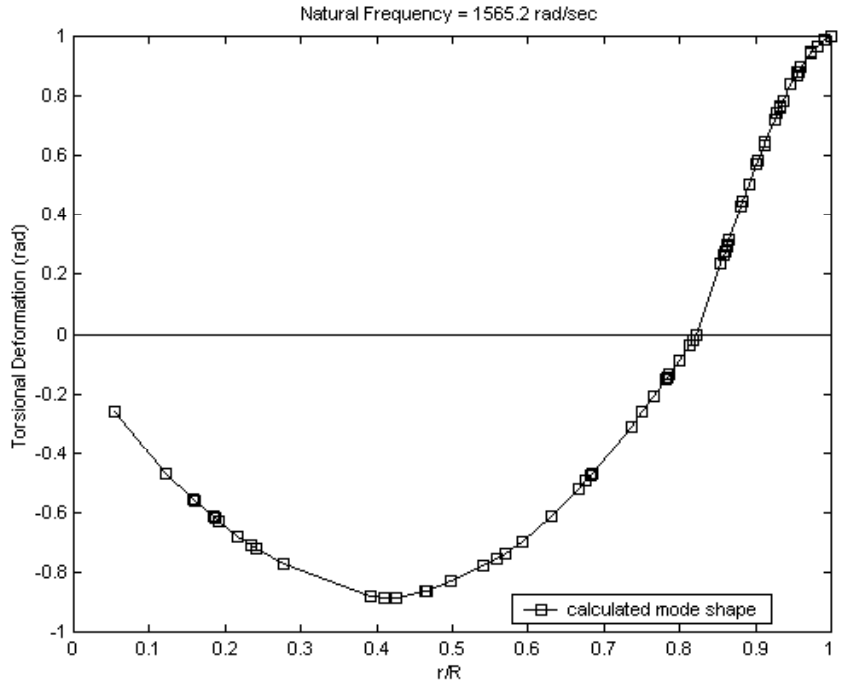

Figure 28. Second Mode Non-Rotating Model Rotor Natural Frequency.

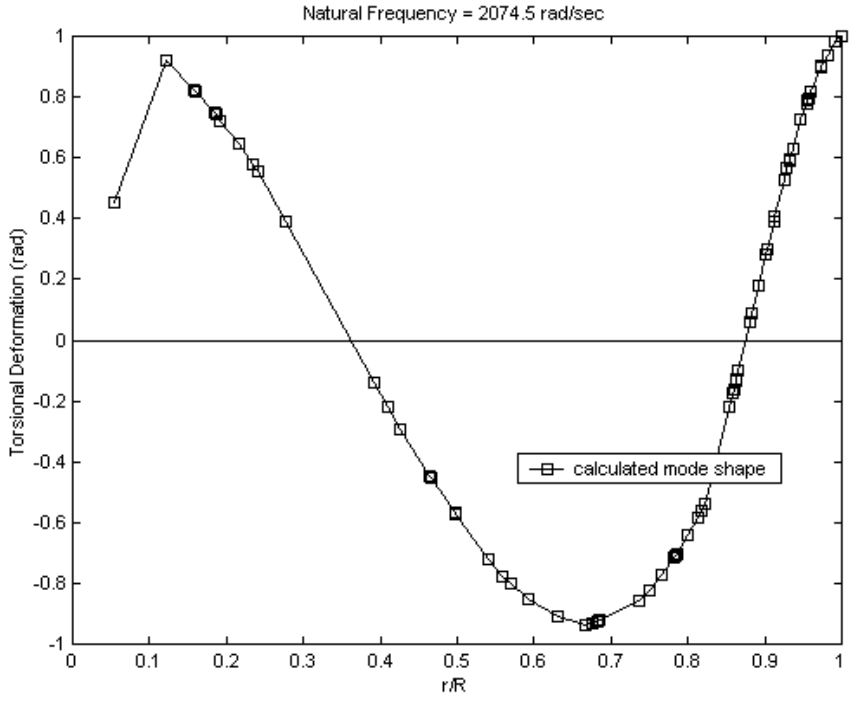

Figure 29. Third Mode Non-Rotating Model Rotor Natural Frequency.

There are no exact mode shapes to compare the Holzer generated mode shapes against. It is noted that the mode shapes do follow expected trends for the first

three modes for a Fixed-Free case. The Holzer program results for the non-rotating, model-scale UH-60A rotor are valid.

c. Rotating Natural Frequencies and Mode Shapes

The ultimate purpose for the Holzer method described here is to calculate mode shapes for a rotating, non-uniform, Flex-Free rotor blade. This section explores results of the Holzer method with and without inclusion of the tension-torsion and "tennis racket" terms. The case considered has a rotational speed of 1,442 RPM (151 rad/sec or 24 Hz). Sikorsky has calculated the natural frequencies for the UTRC blade. Sikorsky calculations are based on a coupled Myklestad method. Table 12 shows Holzer method and Sikorsky calculated rotating natural frequencies and deviation. There are no measured or calculated mode shapes available for comparison with the Holzer generated mode shapes.

Rotating, Ω=1442 RPM	**ω_1** (Hz)	**dev** %	**ω_2** (Hz)	**ω_3** (Hz)
Holzer	86.4	-3.0	250.1	330.9
Sikorsky (coupled Myklestad)	89.1			

Table 12. Natural Frequencies for Non-Uniform, Rotating, Flex-Free Rotor. [After: Ref. 14]

Observe that the first uncoupled Holzer natural frequency is three percent less than the Sikorsky coupled value. No comparison solutions are available for the second and third modes. Figure 30 shows the differences between the rotating and non-rotating mode. The lines connect the deviation data points for each mode shape.

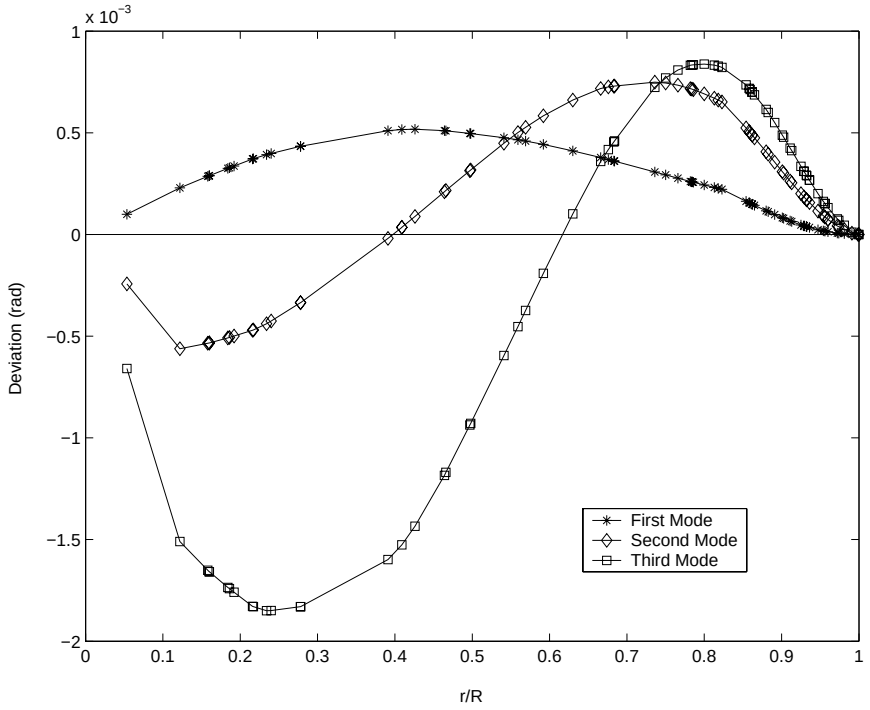

Figure 30. Deviation $\left(x10^{-3}\right)$ Between Rotating and Non-Rotating Mode Shapes.

The variation between rotating and non-rotating mode shapes is insignificant with the largest deviation being less than –0.002 for the third mode (tip deflection equals 1.0) as shown in Figure 30. Another way to analyze the effect of rotational effects on natural frequency calculations is with a Southwell plot. Figure 31 is a Southwell plot displaying the first four elastic mode natural frequencies as they vary with rotor speed with Sikorsky coupled data shown in solid lines [Ref. 14]. Circles at zero RPM mark the rap test results [Ref. 14]. Multiples of rotor speeds are represented by dotted lines that are labeled along the right side of the plot as 1P (one-per revolution) through 6P. The Holzer calculated, uncoupled torsion natural frequencies are marked by an "x" every five RPM and are connected by a dotted line.

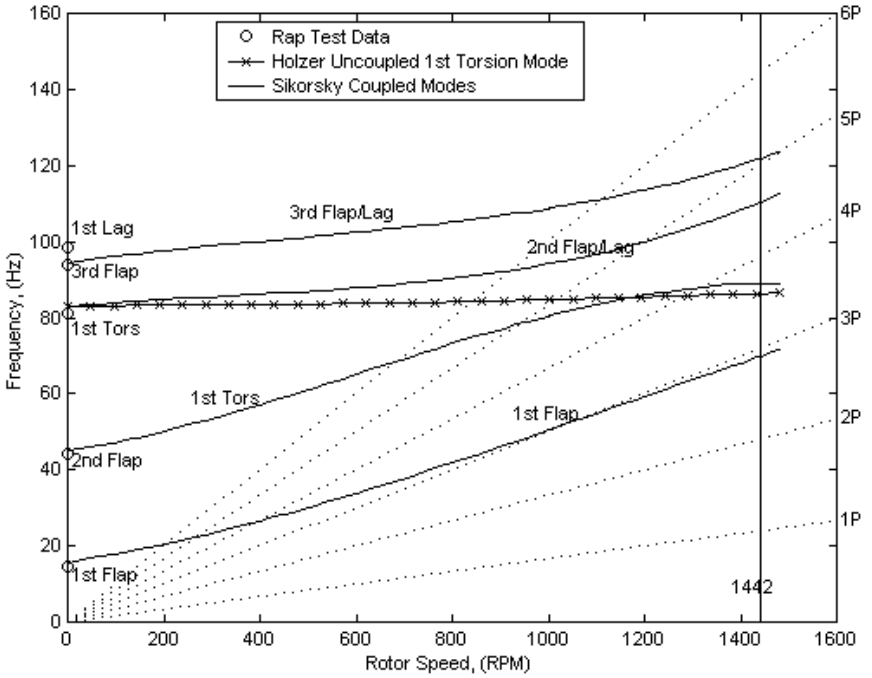

Figure 31. Southwell Plot of Model UH-60 Blade Modes. [After: Ref. 14]

The Sikorsky calculations show strong coupling between the first torsion and second flap modes. Where this coupling is strongest, between 600 and 1,000 RPM, the frequencies of these coupled modes are widely separated from the uncoupled torsion mode calculated with the Holzer method. Above 1,000 RPM, however there is good agreement between the Sikorsky calculations and the Holzer method.

Based on the results presented the Holzer method is valid for the Flex-Free, rotating, non-uniform rotor blade case. The Holzer method has been demonstrated to be of sufficient accuracy to apply to the calculation of mode shapes required for Strain Pattern Analysis (SPA)

IV. DNW RUN 13.20 OF THE MODEL UH-60 ROTOR BLADE

A. INTRODUCTION

To test the Strain Pattern Analysis (SPA) program listed in Appendix B, an available database of strain measurements and the rotor blade structural properties must be available. The structural properties are used in the Holzer program (Appendix A) to generate mode shapes needed for the SPA method. The SPA method can be tested by applying the calculated mode shapes and measured torsion moment data to Equations 1.7 through 1.9. The model UH-60A blade used in the final Holzer test case in Chapter III has an extensive database of wind tunnel test results available. The database includes torsional strain measurements at six span locations that are sufficient to use as the test case for the developed SPA program. [Ref. 14]

The 1989 test of the UTRC manufactured (1:5.73) scaled UH-60A rotor blade at DNW represented the most extensive model rotor test ever conducted at that time. The test program is documented in a seven-volume set of reports plus digital data tapes. The UTRC model blade is described in Chapter III.C.2. The rotor system is a four-bladed (1:5.73) model-scale UH-60A rotor system developed for wind tunnel testing. The blade radius is 56.22 inches, both the radial and feathering axis pitch link offsets are three inches and the chord is 3.643 inches. The blade aspect ratio is 15.3 and the solidity is 0.0825. The test measured blade pressures, acoustics, dynamics, and performance during numerous test runs including 42 separate level flight conditions, 43 descent conditions and 19 hover conditions. Test run number 13.20 was chosen from the level flight condition runs based on availability of the data from previous correlation studies. Instrumentation installed throughout the four rotor blades included 176 pressure transducers, 16 strain gages, eight temperature detectors, and 12 hot film anemometers. Each strain gage measured 1,024 samples per rotor revolution. For the purpose of this thesis only the torsional strain gage measurements are used. The rotor system was mounted on a fully articulated hub and the hub was mounted onto the Army Aeroflightdynamics Directorate (AFDD) rotary wing test stand. The test program was a joint effort between the AFDD, NASA, UTRC and Sikorsky Aircraft. [Ref. 14]

B. DNW FACILITY AND TEST AND RUN 13.20 CONDITIONS

The German-Dutch wind tunnel, (DNW), is a joint aerospace research laboratory run by Germany's DLR and the Netherlands' NLR research organizations. The wind tunnel complex opened in 1980 and is Europe's largest and most extensive wind tunnel. Test data for the model UH-60A blade was taken in the open-jet configured tunnel with maximum flow velocities of up to 262.5 ft/sec (155 knots). The test area dimensions are (170 x 98 x 65 ft). Table 13 provides the details for DNW run 13.20. [Ref. 14]

UH-60A MODEL ROTOR, RUN 13, POINT 20 date: 3/22/89				
Velocity	213.26 ft/sec			
Rotor Speed, Ω	24 Hz 1442 RPM 151 rad/sec			
Density	0.002321 slugs/cu. ft.			
Temperature	64.5 deg Fahreinheit			
Rotor Tip Path Plane Angle	-3.5 deg			
θ_o	10.06 deg			
θ_{1c}	2.25 deg			
θ_{1s}	-7.66 deg			
Advance Ratio, μ	0.301			
Azimuth (deg)	0	90	180	270
Tip Reynolds Number	1,278,729	1,662,969	1,278,730	894,489
Tip Mach Number	0.6324	0.8224	0.6324	0.4424

Table 13. DNW Run 13.20 Data. [After: Ref. 14]

The advance ratio is 0.301, the advancing blade Mach number is 0.8224 and the average Reynolds number is 1,278,729.

C. DNW MEASURED TORSIONAL MOMENTS

Three (four-active arm) strain gage bridges are located at five span locations (0.2, 0.35, 0.5, 0.675 and 0.745). At each of the five locations the first gage measures flapwise bending, the second gage measures chordwise bending and the third gage measures torsion moments. The sixteenth strain gage is located at 0.875 r/R and measures torsion. The torsional moments were determined by applying a calibration matrix from static load tests to the strain gage output voltages. Figure 32 presents the torsion moment time histories at all six span locations. [Ref. 15]

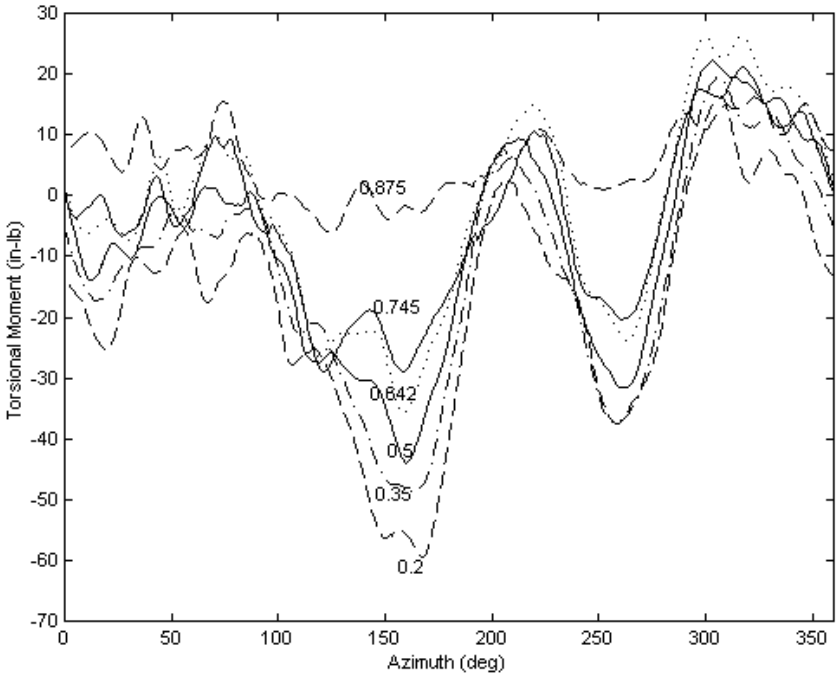

Figure 32. Torsion Moment Time History for DNW Run 13.20.

The torsion moments in Figure 32 have their r/R span locations labeled on their curves from 0.2 to 0.875. Each span location's torsion moment is transformed into harmonic terms using a Fourier transform and the first ten terms are used in the SPA program.

D. DNW STATIC DEFLECTION CALCULATION

Dr. Lorber of UTRC [Ref. 14] calculated the torsional deflection as described in the description of the static method in Chapter I. The DNW results were replicated by applying the static method to the DNW measured torsion moments and given stiffness property of the model-scale blade. Figures 33 to 42 present DNW's calculated torsional deflection compared with the replicated static method calculations. The torsional stiffness from Table 17, Appendix C and the measured torsion moments for run 13.20 were interpolated to a step size of 0.5 r/R. The tip torsion moment was assumed to be zero and the torsion moments between the last strain gage at 0.875 r/R and 1.0 were

assumed to linearly decrease to zero at the tip. The root torsion moment was extrapolated to the 0.534 radial axis pitch offset location. [Ref. 14]

UH-60A Model Rotor, DNW Run 13.20, $\mu = 0.301$

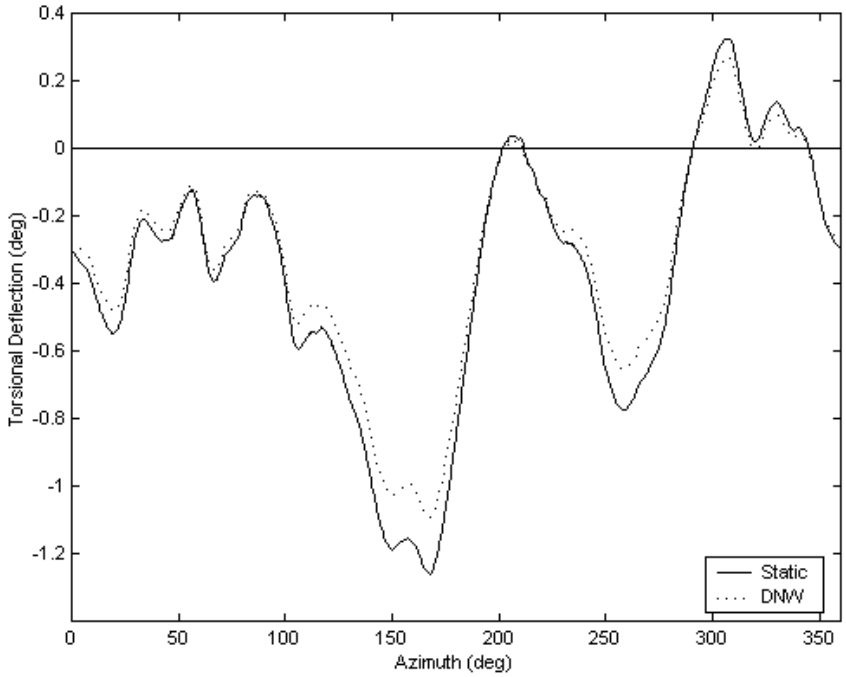

Figure 33. Static Method versus DNW Calculated Torsional Deflection at 0.225 r/R.

UH-60A Model Rotor, DNW Run 13.20, $\mu = 0.301$

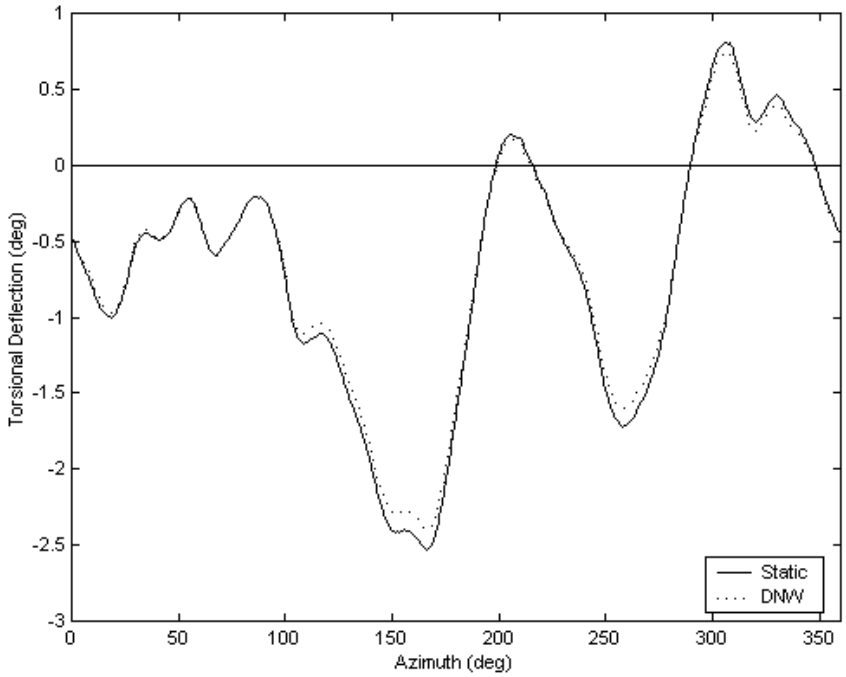

Figure 34. Static Method versus DNW Calculated Torsional Deflection at 0.4 r/R.

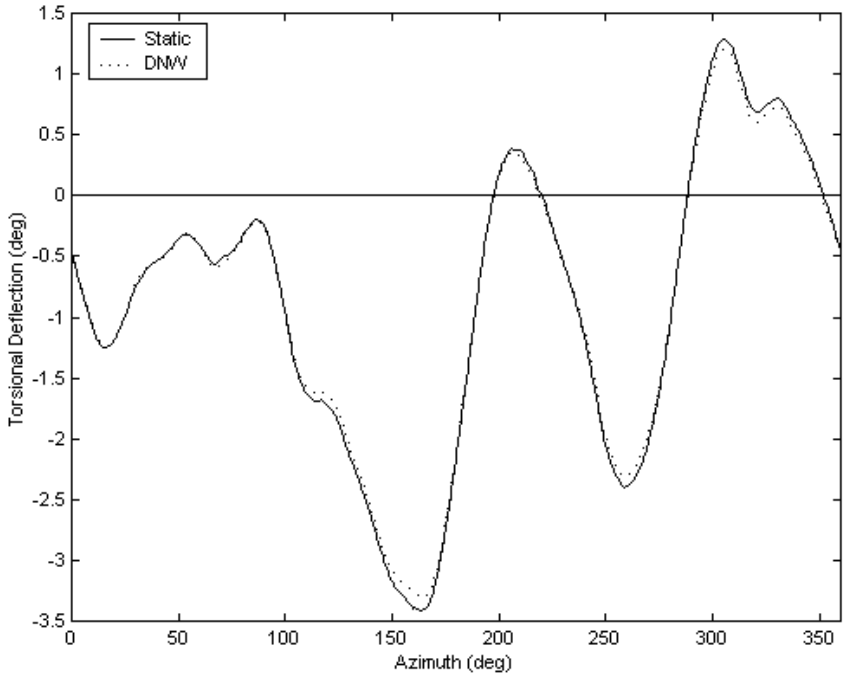

Figure 35. Static Method versus DNW Calculated Torsional Deflection at 0.55 r/R.

UH-60A Model Rotor, DNW Run 13.20, $\mu = 0.301$

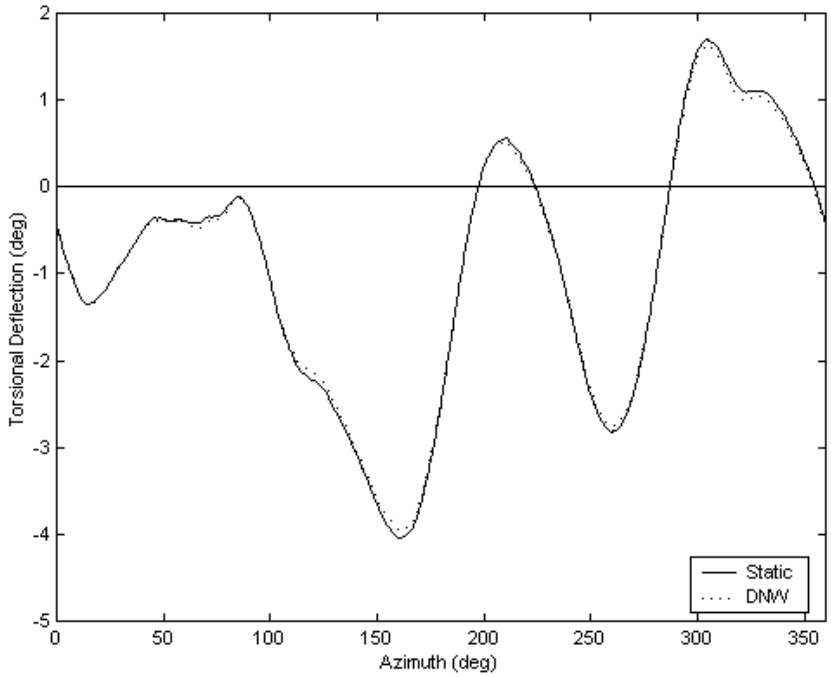

Figure 36. Static Method versus DNW Calculated Torsional Deflection at 0.675 r/R.

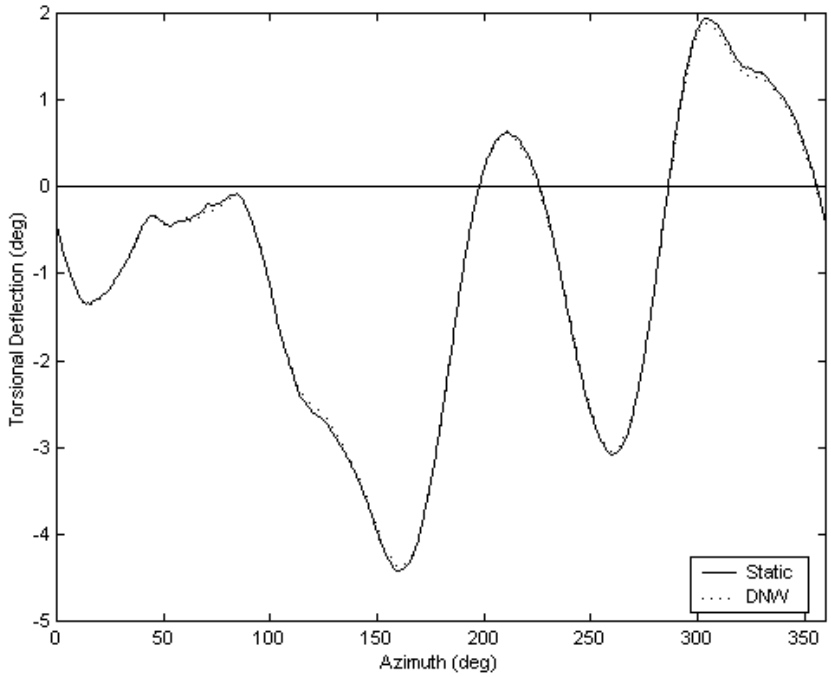

Figure 37. Static Method versus DNW Calculated Torsional Deflection at 0.775 r/R.

UH-60A Model Rotor, DNW Run 13.20, $\mu = 0.301$

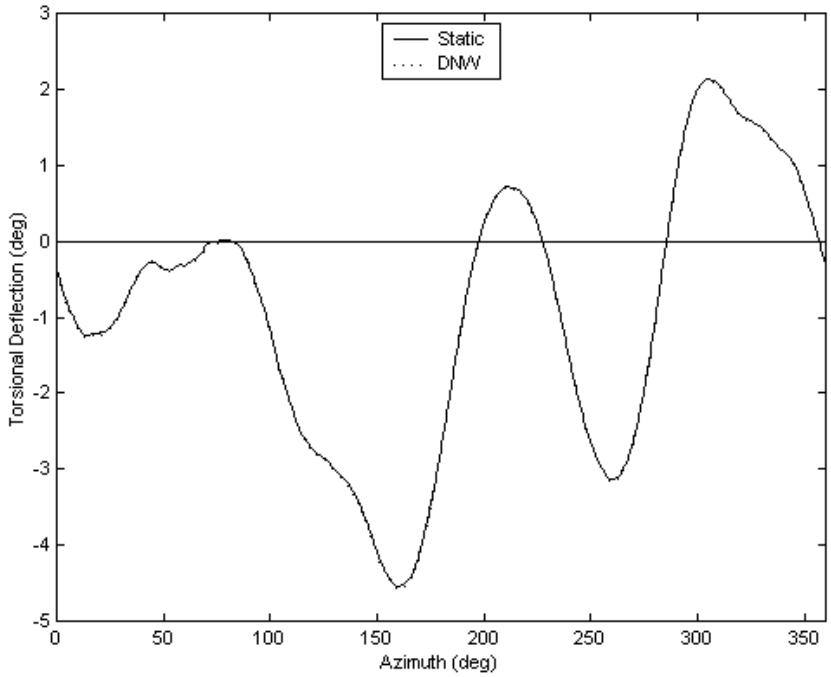

Figure 38. Static Method versus DNW Calculated Torsional Deflection at 0.865 r/R.

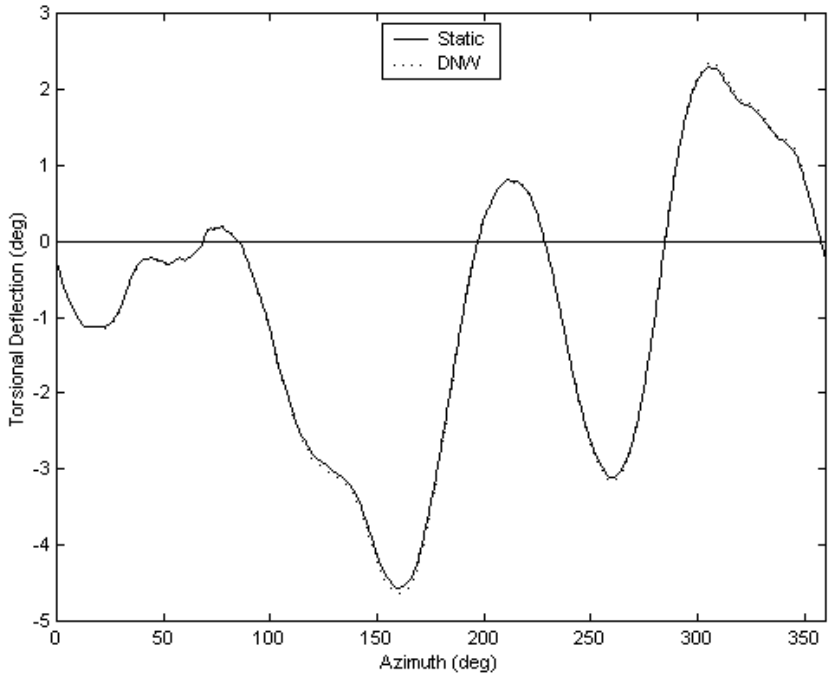

Figure 39. Static Method versus DNW Calculated Torsional Deflection at 0.92 r/R.

UH-60A Model Rotor, DNW Run 13.20, $\mu = 0.301$

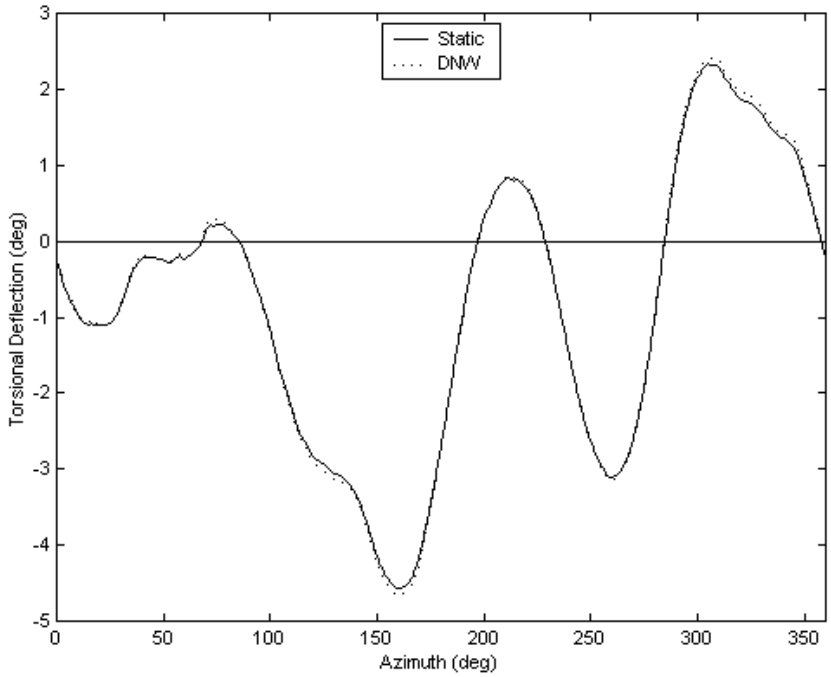

Figure 40. Static Method versus DNW Calculated Torsional Deflection at 0.945 r/R.

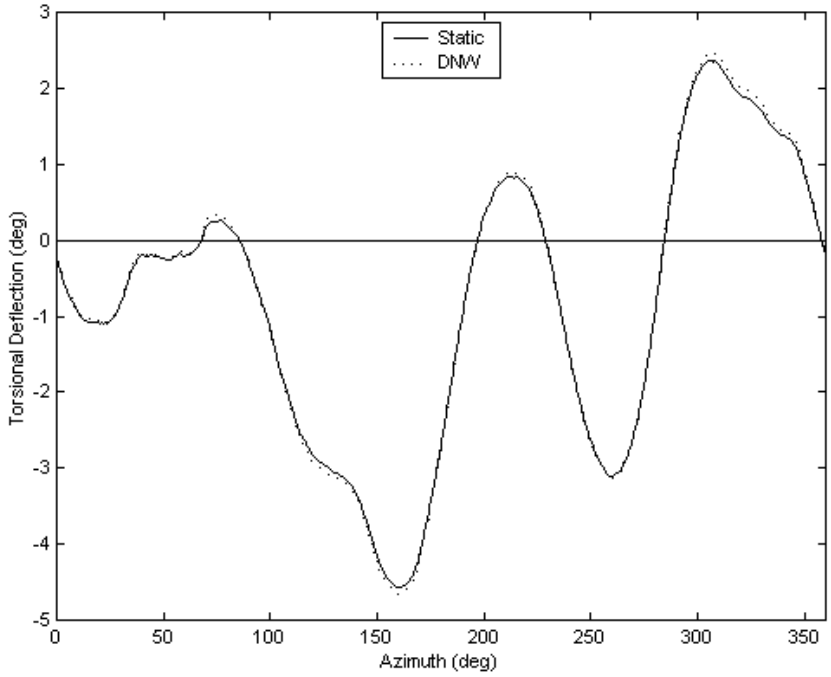

Figure 41. Static Method versus DNW Calculated Torsional Deflection at 0.965 r/R.

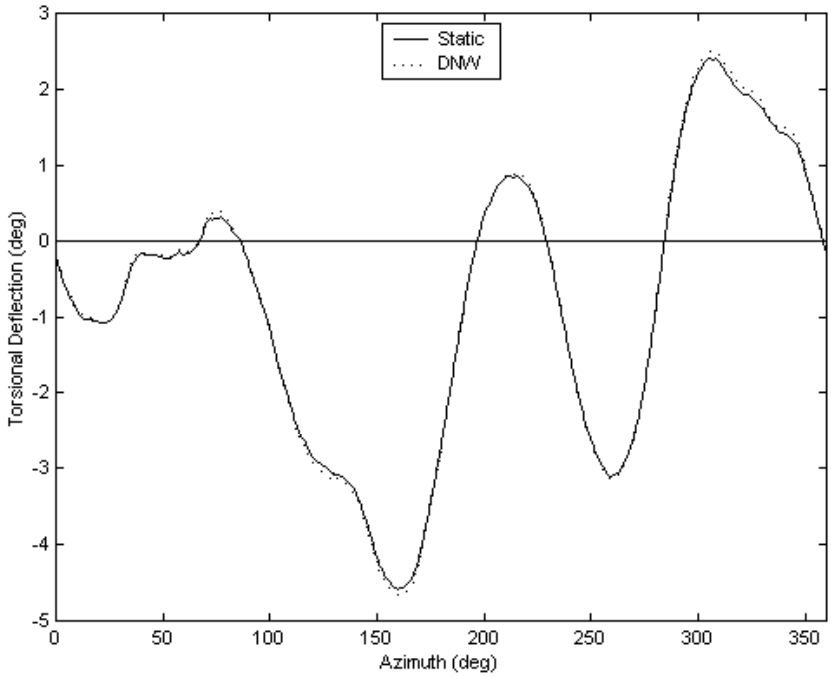

Figure 42. Static Method versus DNW Calculated Torsional Deflection at 0.99 r/R.

The replicated torsional deflections from the 0.55 span location to 0.99 r/R are excellent. Minor differences in Figures 35 through 42 could be the result of differences in interpolation and rounding. The differences are more apparent for the span locations from 0.225 to 0.4. The differences near the root are due to different integration step sizes between the replicated static method and the DNW calculations. The DNW static deflection results will be used to evaluate SPA method deflections.

THIS PAGE INTENTIONALLY LEFT BLANK

V. APPLICATION OF STRAIN PATTERN ANALYSIS

A. INTRODUCTION

A comparison between the developed SPA method and the DNW static method will be conducted for the torsional deformation results of the UTRC model UH-60A rotor blade during run 13.20 of the DNW test presented in Chapter IV. The SPA method is applied to the Holzer program generated mode shapes as presented in Chapter III for the UTRC blade. The application of the SPA method is done with the SPA program listed in Appendix B. The SPA method follows steps one through three as presented in Chapter I with calculations based on Equations 1.7 through 1.9.

B. SPA STEP ONE

The SPA vector, {q}, is derived for the first 21 harmonics using Equation 1.7 restated below.

$$\{q\} = ([T]^T[T])^{-1}[T]^T\{M\} \tag{1.7}$$

Each of the first 21 measured harmonic terms of the measured torsion moment is represented as a vector {M}. The calculated torsion moment mode shape matrix, [T], is an output of the Holzer program. There were six strain gage locations that were used to measure torsion moments for the UTRC blade. From the SPA theory in Chapter I, the maximum number of modes for use in the SPA method (columns of the [T] matrix) is five, one less than strain gage locations. The SPA program will be run five separate times to study the effect the number of modes used in the SPA method has on the results. The five separate SPA solutions are for each number of mode shapes used from one mode shape to the maximum of five mode shapes.

In Appendix D, Figures 44 through 53 show the solution for the SPA vector, {q}, for all 21 harmonic terms for the five-mode SPA solution. The lines connect the data points for each harmonic. The value of the SPA vector term for each mode determines that mode's contribution to the least squares fit of the measured torsion moment and ultimately the deflection solution. The contribution of each mode decreases for higher modes. The SPA vectors converge to zero as they approach the fifth mode.

C. SPA STEP TWO

To confirm the accuracy of the SPA vector {q} Equation 1.8, given below, is used.

$$\{M\} \cong [T]\{q\} \tag{1.8}$$

The SPA vector is multiplied with the calculated torsion moment matrices, [T], from the five runs of the Holzer program. The result of Equation 1.8 is the SPA method's least square fit of the measured torsion moment data for the first through fifth mode SPA vector. The estimated torsion moment is plotted against the measured torsion moment on Figures 54 through 68 in Appendix D for each of the first 21 harmonics for the first through fifth mode solution. A "+" marks the measured torsion moment values and the dotted line connects the measured moment data points. A diamond marks the SPA calculated torsion moment values resulting from Equation 1.8, and the solid line connects the SPA data points. We observe that the results are poor for the one-mode SPA torsion moment estimation on Figures 54 through 56. The two-mode SPA torsion moments in Figures 57 through 59 are a great improvement over the one-mode solutions, but are still a poor fit to the measured data. In Figures 60 through 62 the three-mode SPA torsion moments are shown to be the first SPA solutions to accurately fit the measured data. The three-mode SPA results significantly miss the peaks and valleys of the measured data. The four-mode SPA results shown in Figures 63 through 65 are an improvement upon the three-mode solution, but still significantly miss some peaks and valleys of the measured data. Figures 66 through 68 show the five-mode SPA results are clearly the best fit of the measured data. The SPA method will continue to be applied using only the five-mode SPA vectors.

Figures 69 through 74 show the time histories of the five-mode SPA torsion moment compared to the measured torsion moment for each strain gage location. The measured moment dotted line clearly shows where the discrepancies between the SPA results and measured values are located. The five-mode SPA fits the measured torsion moment time histories well, but the fit is not perfect. Higher harmonic influences may be the cause of the mismatch between the SPA moments and the measured moment values.

D. SPA STEP THREE

The final step of the SPA method applies Equation 1.9, shown below, to estimate the deformation, $\{\phi\}$, using the torsional deformation matrix, [D], multiplied by the five-mode SPA vector, {q} derived in step one and validated in step two.

$$\{\phi\} = [D]\{q\} \tag{1.9}$$

The multiplication is done twenty-one times, once per harmonic. Figures 75 to 84 plot the time histories of the SPA torsional deflection against the DNW static method results from Chapter IV for each reported span location. It is important to note that there is no exact solution available for this test case. The deviations between the DNW results and the SPA results are not an indication of either method's inaccuracy. The overall similarities between the two methods establish confidence in both methods' validity. Optical method results are unavailable for comparison. Both methods calculate a similar deflection pattern at each span location. The maximum deviation between the two methods is approximately 1.1 degrees and occurs at approximately 172 degrees azimuth. There are also relatively large deviations in the region between 60 and 90 degrees azimuth. The differences between the two methods in the noted locations are large as a percentage of total deflection. Tables 14 presents the maximum, minimum and mean deflection values for each span location.

UH-60A Model Rotor, DNW Run 13.20, $\mu = 0.301$

	SPA (deg)			DNW (deg)		
r/R	**max**	**min**	**mean**	**max**	**min**	**mean**
0.225	0.43	-2.25	-0.65	0.27	-1.09	-0.33
0.400	0.83	-3.47	-0.99	0.74	-2.40	-0.69
0.550	1.31	-4.36	-1.15	1.20	-3.31	-0.87
0.675	1.74	-5.04	-1.25	1.61	-3.95	-0.95
0.775	2.04	-5.46	-1.29	1.88	-4.37	-0.99
0.865	2.33	-5.67	-1.23	2.13	-4.59	-0.96
0.920	2.50	-5.66	-1.12	2.33	-4.64	-0.88
0.945	2.55	-5.62	-1.07	2.42	-4.65	-0.85
0.965	2.58	-5.58	-1.03	2.46	-4.65	-0.83
0.990	2.61	-5.54	-0.99	2.49	-4.66	-0.82

Table 14. Maximum and Minimum Torsional Deflection by Span Location.

The mismatch between the static method and SPA method may be a result of higher harmonics influencing the static method result versus the SPA method that only includes harmonics up to the 10th sine term. An attempt was made to include harmonics through the 20th sine and no significant change in the SPA result was identified. Figure 43 shows the mean values of SPA and DNW deflection from Table 14 plotted versus span location. The lines connect the data points for the SPA deflections and the DNW deflections. It is important to only use this figure in the context of the actual deflection time histories or the significance of torsional deformations around the entire rotor azimuth will be overlooked. Comparing the maximum and minimum values in Table 14 with Figure 43 is a good indication that the average deflection values do not give a complete picture of torsional deformation.

UH-60A Model Rotor, DNW Run 13.20, $\mu = 0.301$

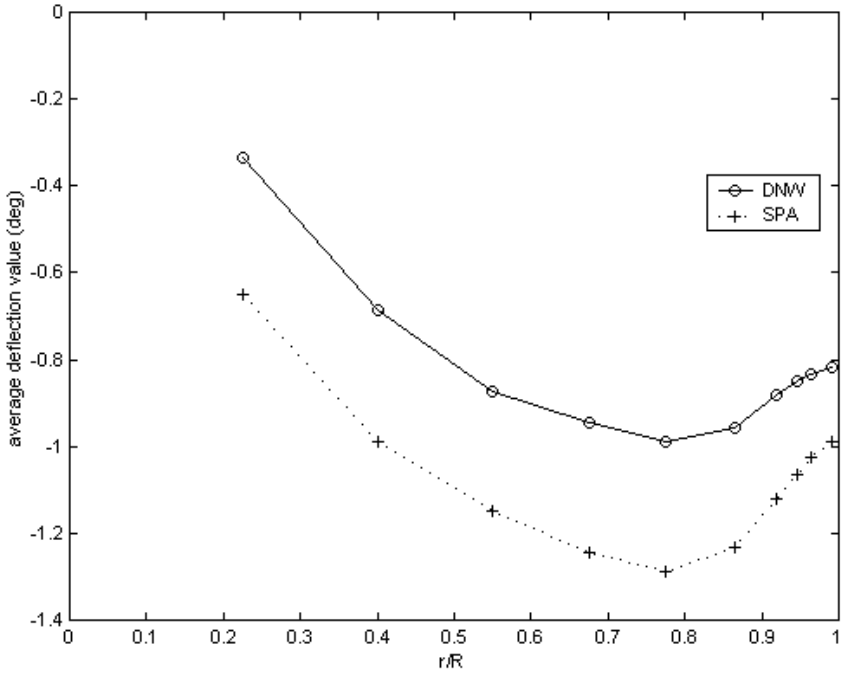

Figure 43. Five-Mode SPA versus DNW Average Deflection by span location.

Figure 43 shows how the overall pattern of the SPA deflection is similar to the DNW deflections, but the SPA deflections are offset by approximately three-tenths of a degree from the root to 0.865 r/R. The average (steady) values for torsional deflection are sensitive to the number of modes used in the solution. To analyze the differences

using the first ten harmonics of the SPA estimated deflections and the DNW static method deflection calculations Figures 85 to 94 present linear regression plots for each reported span location. Figures 85 to 94 plot the SPA deflection on the y-axis against the DNW deflection on the x-axis. Any deviation from the diagonal axis signifies a deviation between the two techniques. Figures 85 to 94 show that many of the harmonic terms are huddled near the zero axes and are therefore insignificant contributors to the deflection solution. The significant terms are marked with the harmonic term they represent. Close to the root only the steady, first cosine, first sine and third sine terms stand out as strong influences to the deflection solution. Throughout the entire span these four harmonic terms continue to dominate the behavior of torsional deformation. As the tip is approached six additional harmonic terms significantly influence the torsional deflection including the fourth cosine, third cosine, seventh sine, second sine, fifth cosine and fourth sine terms.

Along the bottom of the regression plots the y-intercept (b), correlation coefficient, and slope are displayed for the line that best fits the data (the line is not plotted). The correlation coefficient is the statistical measure of the degree of association between the x-axis (DNW) and y-axis (SPA) data [Ref. 8]. The correlation coefficient equals the covariance between the DNW and SPA data divided by the product of their standard deviations [Ref. 8]. For a perfect match between SPA and DNW deflection the y-intercept would be equal to zero, the correlation coefficient would be equal to one, and the slope would be equal to one. Figures 95 through 97 plot the values of the y-intercept, correlation coefficient and slope versus span. In Figure 95, the y-intercept remains relatively constant just below the ideal zero. The correlation coefficient converges towards one as the span locations approach the tip. This indicates a better match between the two methods from 0.865 to 0.99 span. The good correlation near the tip can also be seen in the time history plots discussed previously. The slope near the root is well off the ideal value of one. Near the root the deflections are small due to high stiffness values and the harmonic terms cluster near zero and lose statistical significance. The harmonic terms increase in significance as the stiffness decreases towards the tip and the regression plots and the slope values become a significant indication of the better agreement

between the SPA and DNW results toward the tip. As the span locations increase towards the tip the slope values converge towards the ideal value of one.

The similar torsional deformation results for the five-mode SPA method and the static method verify the applicability of each method in estimating torsional deflection from measured strain data. No further analysis can be accomplished without optical measurements to compare with the SPA results.

E. EVALUATE THE ROBUSTNESS OF THE SPA METHOD

1. Effect of Changes in Mass and Stiffness Properties

The SPA method is dependent upon the measured structural properties of stiffness and mass. Errors in the measurement of the structural properties manifest themselves in inaccurate mode shapes and ultimately incorrect deflection estimates. The Holzer program includes an option to randomly vary the mass and stiffness properties plus or minus a chosen percentage at each span location to test the SPA method's robustness to structural property inaccuracies. The five-mode SPA test case for the UTRC model UH-60A blade was recalculated using a random five percent variance in structural properties. Figures 98 and 99 present the deflection results using varied structural properties on time history plots for the 0.4 and 0.775 radial stations compared to the original five-mode deflection result. The result of varying mass and stiffness properties appears to be insignificant to the validity of the SPA deflection result.

2. Effect of Number of Measurement Stations

A strain gage failure during a test program can also affect the ability to estimate deflections using the SPA method. The SPA program allows for the elimination of all data from a failed strain gage. To test the robustness of the SPA method to eliminating one strain gage's measurements from the torsion moment data another run of the Holzer and SPA programs was conducted where the data from the strain gage at 0.642 was eliminated.

Figures 100 and 101 show the time histories for the 0.4 and 0.775 radial stations compared with the original five-mode SPA result. The maximum number of modes allowed to fit measured data from five strain gages is four modes. With only six strain gages in the DNW test of the UH-60A model blade the loss of any one strain gage has a

significant impact on the final SPA result. The loss of one strain gage has a two-fold impact on the SPA technique. First, there is less available data to fit the sets of calculated modes to. Second, the SPA solution process must reduce the maximum number of modes used to estimate the deflection.

3. Effect of Measurement Error

Short of a strain gage failure it is normal to have errors in experimental measurements of rotor blades [Ref. 3]. Measurement errors include calibration error, static error, and random error [Ref. 3]. The SPA program was run for five modes using a random error from minus five to plus five percent at each of the six strain gage locations on the DNW blade. Figures 102 and 103 show the time history plots for the deflection results at 0.4 and 0.775 radial stations compared with the original five-mode SPA result. The solution for each harmonic term changed negligibly from the original five-mode SPA test case. The method is insensitive to the randomly occurring measurement error of five percent.

THIS PAGE INTENTIONALLY LEFT BLANK

VI. SUMMARY

A. CONCLUSIONS

The Strain Pattern Analysis (SPA) method has been developed and tested for torsional deformation using data from the model-scale UH-60A rotor blade wind tunnel test conducted at DNW. The Holzer method was used to provide the SPA method with the calculated torsion moment mode shapes and torsional deflection mode shapes for the rotor blade. The measured torsion moments are from wind tunnel tests conducted by the Army, NASA, UTRC, and Sikorsky at DNW with a (1:5.73) model-scale UH-60A rotor blade with an advance ratio of 0.301, an advancing tip Mach number of 0.8224 and an average Reynolds number of 1,278,729. The SPA method estimates torsional deflections in two steps. First, the mode shapes of a rotating blade in a vacuum are calculated. Second, the modal amplitudes are identified using a least squares fit to the measured data. The mode shape calculation only has to be done once unless more than one rotor speed is evaluated.

The SPA method torsional deflections compare well with the overall trend and range of static method integrated deflections from the DNW database. The SPA method predicts slightly larger deflections than the static method. Differences between the two methods of estimating torsional deflection are expected. No additional validation of the SPA results can be done without results from optical methods of measuring torsional deformation.

Possible sources of error in the application of the SPA method include the Holzer method's approximate solution to the equation of motion, inaccurate strain gage measurements and inaccurate rotor blade structural properties. The Holzer calculated mode shapes are based on the developed uncoupled rotor blade equation of motion for torsion. Coupling effects could change the mode shapes and the final SPA deflection estimate. The possibility of a faulty strain gage was tested and the SPA program proved to be sensitive to the decrease in available strain gages for the six strain-gage UH-60A blade. The SPA method was demonstrated to be tolerant to variations in blade properties and measurement errors.

B. RECOMMENDATIONS FOR FURTHER RESEARCH

Further areas of study should include the evaluation of the SPA method for other test runs from the DNW database for the model UH-60A rotor blade. A complete evaluation of the SPA program developed in this thesis would require data from test programs with available optical measurement results to compare to. Improvements can also be made in the calculation of rotor blade mode shapes. The Holzer program developed in this thesis can be improved by using the coupled equations of motion and developing the Myklestad method for determining natural frequencies and mode shapes as presented in [Ref. 9] and [Ref. 18], in which the fully coupled Myklestad method is developed for specific application to rotary wing aircraft. The sensitivity towards a decrease in modes caused by a simulated strain gage failure should be investigated further by using test cases with more measurement stations. The higher mode's contribution to the SPA deflection estimate is expected to become increasingly insignificant and therefore the method should prove tolerant to the loss of a strain gage for tests involving a greater number of measurement stations. Further research could determine the minimum number of measurement stations required for the SPA method to be insensitive to the loss of a strain gage and a decrease in the number of contributing modes.

APPENDIX A. HOLZER PROGRAM

A. INSTRUCTIONS FOR RUNNING THE HOLZER PROGRAM

1. Holzer Program Set Up

To start the Holzer program type "SPAholzer" in the MATLAB™ command window. The program queries the user for the information necessary to calculate the torsional mode shapes. After you select to enter your own test case or to use one of the built-in test cases (line 8) you will be asked for the number of modes to solve for (line 20). The number you select will determine how many mode shape plots are displayed and how many modes are used in the SPA solution. Choose zero modes if you choose to solve for natural frequencies over a range of rotational speeds or to individually choose modes for plotting after the natural frequencies are found. For brevity the program listing presented does not list the structural properties for the built-in test cases. The next option selects the Fixed or Flex-Free versus Free-Free boundary condition (line 30).

If you opt to enter your own data you will first be asked for the number of stations you have structural properties for (line 32). If you choose to enter your own data it is important to be consistent with units. The program asks for (lb-ft-sec^2) for the torsional mass moment of inertia (line 41), (ft^2-lb) for torsional stiffness (line 43) and (ft) for the distance between segments (line 46). In all cases the first segment is the one closest to the root. Table 15 gives the input units you may use and the corresponding output variable units. The input and output units for rotational speed and frequency will always be rad/sec.

I	GJ	Δr	Torsion Moment	Deflection
slug-ft^2 or lb-ft-sec^2	lb-ft^2	ft	ft-lb	rad
lb-in-sec^2	lb-in^2	in	in-lb	rad
kg-m^2	N-m^2	m	N-m	rad

Table 15. Input and Output Units of Measure.

The built-in plot labeling will always give the English units in feet and is easily changed using the option to change axes properties from the edit option on the figure toolbar. If you will be using your own test case you must have matrices of structural data ready to paste into the command window. When the program queries for a specific

variable copy the corresponding matrix from its location, then on the command window type a matrix symbol "[ ]" and paste your matrix in the middle of the brackets. Each structural property matrix must have the same number of terms, but the matrices can have different numbers of rows and columns. If you will be using centrifugal terms you must prepare the blade angle prior to deformation, β, in degrees for each station (line 105) and the tension-torsion term (lines 33-38) in the form, $((1/2)(mass/\Delta r)(R^2 - r^2) * k_A^2)$. In this form the Holzer program will multiply by the appropriate rotational speed to include the stiffening effect of the tension-torsion term.

Whether you enter your own data or use a built-in test case you will be presented with a number of options prior to solving for natural frequencies and mode shapes. You may opt to not include the "tennis racket" term in your calculations (line 103). If your structural properties do not extend all the way to the tip (1.0) location you can apply the properties from the closest station to the tip to create a final station where deflection will equal one (line 40 and lines 195-207). This option forces the boundary condition of one radian tip deflection to be applied at the tip instead of the last location available. These options are designed to allow the effects of individual terms to be evaluated on the final result.

The program will ask for the measurement stations for test data you have for use with the SPA program (lines 49 & 51). This information is used to interpolate the calculated torsion moment mode shape to the same span locations as the measured data to allow for the SPA vector to be calculated (lines 370-378) for Fixed & Flex-Free, (lines 430-439) for Free-Free. Enter the locations between "[ ]" symbols in non-dimensional r/R form. After choosing your rotational speed or range of rotational speeds (lines 126-137) you will be asked for test frequency parameters (lines 139-150). The most useful method of solving natural frequencies is to enter a range of "test" frequencies from zero (lower limit) to the an applicable upper limit that will allow for your desired number of modes to be found. I suggest using the highest mode you wish to solve for times 1,000 as an upper limit (i.e.: if you want five modes, enter 5,000 as your upper limit). The Holzer program will locate all the natural frequencies between your lower limit and upper limit by testing each frequency from zero to the upper limit at the entered step size. Your last

options are to include a random variation to the mass and stiffness properties to allow for a test of program robustness (lines 156-181).

The first step of the Holzer method is Equation 2.10 on line 211. Step two is on line 212 using Equation 2.21. Step Three is on line 218 using Equation 2.23. Step Four is on line 267 with Equation 2.21. The program loops as many times as required to repeat steps three and four until the root solution for each tested frequency is calculated. When each test frequency root solution is completed the program will execute step six to find the natural frequencies. Step six uses the bisection method to find where the root deflection equals zero for the Fixed-Free condition or the allowed deflection for the Flex-Free condition on lines 221 to 263. For the Free-Free condition the bisection method searches for where the root torsion moment equals zero on lines 270 to 292.

2. Holzer Program Operation

As the Holzer program finds natural frequencies it will display the frequency in rad/sec, the mode number, and the rotational frequency in rad/sec on the screen. The program will display a graphical solution plot (lines 306-320/322-329) to the natural frequency when it completes the full range you entered. The graphical solution can be used to confirm no natural frequencies were missed. It is possible to miss a higher mode when the step size is larger than one. If a mode is missed you must start over and use a smaller step size. You are given the option to delete a measurement station location to test the effects of a bad strain gage (lines 350-361/410-429). The program will now display the deflection mode shapes for only the number you selected (lines 384-401/447-459). If you chose zero for number of modes you will have the option to individually enter frequencies and rotational speed to plot mode shapes for (line 464). The outputs from the Holzer program are listed in the next section.

B. HOLZER PROGRAM VARIABLES

DD (n x m) Torsional Deformation Mode Shapes (rad) where each row corresponds to the stations structural properties were provided for and each column is a separate mode (line 346 for Fixed/Flex-Free) and (line 406 for Free-Free).

GG (n x m) Torsion Moment Mode Shapes ( ) where each row corresponds to the stations where structural properties were provided and each column is a separate mode (line 347 for Fixed/Flex-Free) and (line 407 for Free-Free).

G (g x m) Torsion Moment Mode Shapes ( ) interpolated to measurement station locations for rows and each column is a separate mode (line 377 Fixed/Flex) and (line 438 Free-Free).

WNF# WNF1 is the first natural frequency (rad/sec) in order of increasing rotational speed (rad/sec) and WNF2 is for the second natural frequency (line 240 & 245).

OMEGA# The rotational speeds (rad/sec) that correspond to WNF1,WNF2 (line 241 &246).

rootfreq The natural frequencies (rad/sec) in mode order if a single rotational speed was selected (line 234 Fixed/Flex) and (line 282 Free-Free).

x(n) The non-dimensional calculation stations where structural properties were provide, increases by one station if you forced the tip boundary condition (line 98).

span(g) The non-dimensional measurement stations (line 51).

C. HOLZER PROGRAM LISTING

```
1    %Holzer's method for ROTATING Torsion Mode approximation
2    clc
3    clear
4    eliminate=2;
5    %create the 1x1024 matrix of azimuth locations for DNW cases
primarily
6    NEWAZIMUTH=[0:(360/57.3)/1024:((360/57.3)-(360/57.3)/1024)];
7    CNEWAZIMUTH=NEWAZIMUTH(:);
8    choice=input('enter 1 to input your own blade properties \n or 2
for 126 segment DNW\n or 3 for Full-Scale UH-60A data\n or 4 for the
Scanlan Wing example\n or 5 for the 49 segment uniform, fixed test
case\n');
10   if choice==3
11   col=1;
12   end
13   y1=1;%These variables are needed for WNF1, OMEGA1 for southwell
plots
14   y2=1;
15   disp('for all inputs you must use a full matrix')
16   disp('add zeros if required even if it exceeds your number of
nodes')
17   disp('the total number of elements in each matrix must be the same
size')
18   disp('but rows & columns do not have to be the same length')
19   disp('  ');
```

```
20   modenumber=input('enter 0 to individually select (also for range of
omegas)\n or enter desired # to preset how many natural frequencies to
do mode shape plot and/or SPA analysis for\n');
22   modec=modenumber;
23   CTLSTIFF=input('For Flex-Free enter the root torsion displacement\n
(zero for Fixed-Free and Free-Free, .0904 rad for DNW)\n');
24   if CTLSTIFF~=0
25   mult=2;
26   end
27   if CTLSTIFF==0
28   mult=1;
29   end
30   choice4=input('enter 1 if this is a Flex-Free or Fixed-Free
boundary condition or zero for Free-Free\n');
31   if choice==1
32   nodes=input('enter the number of segments\n to evaluate');
33   tension=input('enter 1 to enter your own tension-torsion term\n
(without rotation speed) or zero to not include\n');
34   if tension~=1
35   TENS=zeros(nodes,1);
36   end
37   if tension==1
38   TENS=input('enter the vector of tension-torsion terms\n')
39   end
40   force=input('enter 1 to force the tip boundary condition or zero to
apply deflection of one radian at your last station');
41   CITHETA=input('enter your Torsional Mass Moment of Inertia (lb-ft-
s^2) matrix,\n');
42   [CITHETArow CITHETAcol]=size(CITHETA);
43   CGJ=input('enter your NON-ZERO GJ (ft^2-lb) matrix,\n ensure same
number of elements as segments chosen (theoretical fixed segment gets
arbitrary non-zero value)\n');
45   [CGJrow CGJcol]=size(CGJ);
46   Cdeltax=input('enter your delta r (feet) matrix,\n ensure same
number of elements as segments chosen,(theoretical fixed segment=0)\n');
48   [Cdeltaxrow Cdeltaxcol]=size(Cdeltax);
49   experiment=input('Enter 1 if you have experimental measured data to
use with SPA\n or zero if you only want modes calculated\n');
50   if experiment==1
51   span=input('enter the r/R Strain Gage locations=\n');
52   end
53   if experiment~=1
54   span=[0:0.1:1];
55   end
56   %The following loops are to make column vectors out of all matrices
entered%%%%%%%%%%%%
57   i=1;
58   j=1;
59   k=1;
60   for i=1:nodes
61   if j==CITHETAcol+1
62   j=1;
63   k=k+1;
64   end
65   ITHETA(i,1)=CITHETA(k,j);
66   i=i+1;
67   j=j+1;
68   end
69   i=1;
70   j=1;
71   k=1;
72   for i=1:nodes
73   if j==CGJcol+1
74   j=1;
```

```
75   k=k+1;
76   end
77   GJ(i,1)=CGJ(k,j);
78   i=i+1;
79   j=j+1;
80   end
81   i=1;
82   j=1;
83   k=1;
84   for i=1:nodes
85   if j==Cdeltaxcol+1
86   j=1;
87   k=k+1;
88   end
89   deltax(i,1)=Cdeltax(k,j);
90   i=i+1;
91   j=j+1;
92   end
93   sumdeltax(1)=0;
94   for count=2:1:nodes
95   sumdeltax(count)=deltax(count)+sumdeltax(count-1);
96   count=count+1;
97   end
98   x=sumdeltax/sumdeltax(nodes);
99   end
100  %NOW COS2Beta For all cases except DNW which has it built-in
101  if choice~=0
102  if choice~=2
103  choice5=input('enter 0 to enter a Beta (collective+cyclic+built-in)
matrix or 1 to not include the tennis-racket term\n');
104  if choice5==0
105  THETA=input('enter the Beta sectional blade angle matrix in
degrees\n')
106  [THETArow THETAcol]=size(THETA);
107  i=1;
108  j=1;
109  k=1;
110  for i=1:nodes
111  if j==THETAcol+1
112  j=1;
113  k=k+1;
114  end
115  CTHETA(i,1)=THETA(k,j);
116  i=i+1;
117  j=j+1;
118  end
119  COS2THETA=cos(2*CTHETA/57.3);
120  end
121  if choice5==1
122  COS2THETA=[ones(nodes,1)];
123  end
124  end
125  end
126  choice3=input('enter 0 to set range or enter 1 to input specific
omega (rad/sec)\n');
127  if choice3==1
128  omega=input('enter the blade rotational speed you want evaluated
(rad/sec)\n');
129  loweromega=0;
130  upperomega=0;
131  end
132  if choice3==0
133  loweromega=input('enter lower limit of omega (rad/sec)\n');
134  upperomega=input('enter upper limit of omega (rad/sec)\n');
```

```
135  %omega is rad/sec NOT RPM!!!
136  omega=[loweromega:5:upperomega];
137  end
138  %w is rad/sec
139  choice2=input('enter 0 to set range of frequencies or 1 to input a
specific frequency (rad/sec)\n');
140  if choice2==1
141  w=input('enter frequency to check in rad/sec\n');
142  stepsize=1;
143  upper=0;
144  lower=0;
145  end
146  if choice2==0
147  lower=input('enter lower limit of frequency search(ensure enough
range to support # of modes you want solved for)\n');
148  upper=input('enter upper limit of frequency search\n');
149  stepsize=input('enter the stepsize between frequency values\n start
with five, but if a root is missed decrease the stepsize\n');
150  w=[lower:stepsize:upper];
151  end
152  zz=1; %need this for next line
153  alternate=(-1)^(zz+1); %Need this for the first mode pass thru
bisector
154  %%%%%%%%%%%%%%%%%%%%%%%%%%%%%%%%%%%%%%%%%%%%%%%%%%%%%%%%%%%%%%%%
155  %%Designed to loop as long as desired for specific natl freq
testing
156  %This is to test robustness
157  mass=input('enter the max percentage you wish to randomly (+/- from
zero to max) change TENSION & ITHETA by\n to test robustness of
solution to mass changes\n');
159  stiffness=input('enter the max percentage you wish to randomly (+/-
from zero to max)change GJ by\n to test robustness of solution to
stiffness changes\n');
161  if mass~=0
162  for n=1:nodes
163  randomass=randperm(mass);
164  randomsign=randperm(2);
165  sign=(-1)^randomsign(1);
166  permass=1+sign*randomass(1)/100;
167  TENS(n)=TENS(n)*permass;
168  ITHETA(n)=ITHETA(n)*permass;
169  n=n+1;
170  end
171  end
172  if stiffness~=0
173  for n=1:nodes
174  randomstiff=randperm(stiffness);
175  randomsign=randperm(2);
176  sign=(-1)^randomsign(1);
177  perstiff=1+sign*randomstiff(1)/100;
178  GJ(n)=GJ(n)*perstiff;
179  n=n+1;
180  end
181  end
182  ccontinue=1;
183  mode=0;
184  while ccontinue==1
185  for j=1:((upperomega-loweromega)/5+1)
186  if mode==0
187  disp('Natural Frequency(rad/sec)  Mode       Rotational Frequency
(rad/sec)')
188  end
189  mc=1;
190  zz=1;
```

```
191  alternate=1;
192  for i=1:((upper-lower)/stepsize+1)
193  %THE HOLZER METHOD
194  n=nodes;%This will be overwritten if force tip option used
195  if force==1
196  if x(nodes)~=1
197  n=nodes+1;
198  x(n)=1.0;
199  deltax(n)=x(n)-x(n-1);
200  %Assume strux properties for point nodes+1 is same
201  %as properties at point nodes
202  GJ(n)=GJ(n-1);
203  ITHETA(n)=ITHETA(n-1);
204  TENS(n)=TENS(n-1);
205  COS2THETA(n)=COS2THETA(n-1);
206  end
207  end
208  %For the Torsion to the right of the last segment
209  T(n+1,i,j)=0;%A Holzer Method Boundary Condition
210  %For the deflection at the last segment
211  theta(n,i,j)=1;%STEP ONE EQN 2.10
212  %For the Torsion at the last segment-STEP TWO EQN 2.21
213  T(n,i,j)=T(n+1,i,j)+((w(i))^2-
(omega(j))^2*(COS2THETA(nodes,1)))*ITHETA(nodes)*theta(n,i,j);
214  Nodes=n;
215  p=n-1;
216  for m=1:p;
217  e=n-1;
218  %this subtracts previous delta theta from previous theta-STEP THREE
EQN 2.23
219  theta(e,i,j)=theta(n,i,j)-
T(n,i,j)*(deltax(n))/(TENS(n)*(omega(j))^2+GJ(n));
220  %STEP 6: Find the Natl Freq's is done only at root for each tested
frequency
221  %BISECTION METHOD WITH OFFSET FOR CONTROL STIFFNESS%%%
222  sign=(-1)^(mc+1);
223  if choice4==1 %fixed free
224  if e==1 %Root location
225  if choice2==0 %range of w
226  if i>=2 %i=1 is at lower limit freq
227  %This simply finds where sign changes
228  if alternate>0
229  signchange=(theta(e,i,j)-sign*CTLSTIFF)*(theta(e,(i-1),j)-
sign*CTLSTIFF);
230  if signchange<0
231  twotheta=[theta(e,i,j) theta(e,(i-1),j)];
232  twofreq=[w(i) w(i-1)];
233  coeff=polyfit(twofreq,twotheta,1);
234  rootfreq(mc)=(sign*CTLSTIFF-coeff(2))/coeff(1);
235  yaxis(mc)=sign*CTLSTIFF;
236  [rootfreq(mc)         mc     omega(j)]
237  SOL(zz,:)=[rootfreq(mc),omega(j)];
238  %for southwell plots
239  if mc==1
240  WNF1(y1)=rootfreq(mc);
241  OMEGA1(y1)=omega(j);
242  y1=y1+1;
243  end
244  if mc==2
245  WNF2(y2)=rootfreq(mc);
246  OMEGA2(y2)=omega(j);
247  y2=y2+1;
248  end
249  mc=mc+1;
```

```
250  end%for if signchange<0
251  end%for if alternate>0
252  if (theta(e,i,j)-sign*CTLSTIFF)*(theta(e,(i-1),j)-sign*CTLSTIFF)<0
253  zz=zz+1;
254  alternate=(-1)^(zz+1);%for an even zz we get an odd alternate
255  end
256  if CTLSTIFF==0 %don't want to alternate solutions
257  alternate=1;
258  end
259  end%for if i>=2
260  end%for if choice2==0 %range of w
261  end%for if e==1
262  end%for if choice4==1 %fixed free
263  %%%%%BISECTION ROOT FINDER ENDS HERE FOR FIXED-FREE%%%%%
264  %This is the total Torque,
265  %STEP 4: EQN 2.21 on line 267
266  %(STEP 5: Repeats Steps 3 & 4 until at root for each tested
frequency)
267  T(e,i,j)=T(n,i,j)+((w(i))^2-
(omega(j))^2*(COS2THETA(e,1)))*ITHETA(e)*theta(e,i,j);
268  n=n-1;
269  m=m+1;
270  %%%BISECTION METHOD WITHOUT OFFSET%%%%%%
271  %FOR FREE FREE, STEP 6 for when at root for each tested frequency
272  if choice4==0 %free free
273  if e==1
274  if choice2==0 %range of w
275  if i>=2
276  %This simply finds where sign changes
277  signchange=(T(e,i,j))*(T(e,(i-1),j));
278  if signchange<0
279  twotheta=[T(e,i,j) T(e,(i-1),j)];
280  twofreq=[w(i) w(i-1)];
281  coeff=polyfit(twofreq,twotheta,1);
282  rootfreq(mc)=(-coeff(2))/coeff(1);
283  yaxis(mc)=0;
284  [rootfreq(mc)                          mc          omega(j)]
285  SOL(zz,:)=[rootfreq(mc),omega(j)];
286  mc=mc+1;
287  end
288  end
289  end
290  end
291  end
292  %%%BISECTION ROOT FINDER ENDS HERE FOR FREE-FREE%%%%%%%%%%
293  %This end is for the m=1:p loop
294  end
295  i=i+1;%NEXT FREQ
296  %This end is for the range of frequencies loop
297  end
298  %This loop works with numerous frequencies and one omega
299  if choice2==0
300  if choice3==1
301  xl=w;
302  yl=zeros(size(xl));
303  yll(1,1:size(xl))=-CTLSTIFF;
304  yul(1,1:size(xl))=+CTLSTIFF;
305  if choice4==1
306  figure
307  plot(rootfreq,yaxis,'s',w,theta(1,:,1),'k-')
308  line(xl,yl)
309  line(xl,yll)
310  line(xl,yul)
311  if CTLSTIFF~=0
```

```
312  text(10,(+CTLSTIFF+0.1),'odd mode natural frequencies')
313  text(10,(-CTLSTIFF-0.1),'even mode natural frequencies')
314  end
315  axis([0 upper -1.5 1.5])
316  xlabel('Frequency (rad/sec)')
317  ylabel(['Torsinal Deformation @ Root (rad)',' ,r/R =
',num2str(x(1))])
318  title('Graphical Solution to Natural Frequency (Fixed-Free)')
319  legend('root B.C. met','full set of root solutions');
320  end
321  if choice4==0
322  figure
323  plot(rootfreq,yaxis,'s',w,T(1,:,1)/1000,'k-')
324  line(xl,yl)
325  xlabel('Frequency (rad/sec)')
326  ylabel('Total Torsion Moment (Ft-Lbs) at segment 1 (*10-3)')
327  title('Graphical Solution to Natural Frequency (Free-Free)')
328  legend('root B.C. met','full set of root solutions');
329  end
330  end
331  end
332  %if checking a range of omegas this will work
333  if choice3==0
334  j=j+1;%NEXT OMEGA
335  end
336  %This end is for the loop for a range of omega(j)
337  end
338  %%%%%%%%%%%%%%%%%%%%%%%%
339  %This works with one frequency & one omega
340  if choice2==1
341  if choice3==1
342  if choice4==1 %Fixed Free
343  if modenumber==0
344  mode=input('input mode number you are checking\n');
345  end
346  DD(:,mode)=theta(:,1,1);
347  GG(:,mode)=T(:,1,1);
348  sign=(-1)^(mode+1);
349  [rowgage,gages]=size(span);
350  %Eliminate a Bad Strain Gage???
351  if eliminate==2
352  eliminate=input('enter 1 if you want to zero out a strain gage or
zero not to eliminate any\n');
353  if eliminate==1
354  maxmodes=gages-2;
355  disp(['If the number of modes calculated exceed ',
num2str(maxmodes) ,' your result will be incorrect']);
356  killit=input('enter the strain gage location number\n (closest to
the root = 1) you want to eliminate\n');
357  for g=1:gages
358     if g<killit
359  span(rowgage,g)=span(rowgage,g);
360  end
361  if g>killit
362  span(rowgage,g-1)=span(rowgage,g);
363  end
364  end
365  gages=gages-1;
366  span=span(rowgage,1:gages)
367  end
368  end
369  %%%%%%%END OF ELIMINATION ROUTINE%%%%%%%%%
370  %Interpolate calculated harmonic torques to span locations for
direct comparison
```

```
371  for kkk=nodes:-1:2
372  for ccc=1:gages
373  if x(kkk)>=span(ccc)
374  twotorque=[GG(kkk,mode) GG(kkk-1,mode)];
375  twox=[x(kkk) x(kkk-1)];
376  coeff=polyfit(twox,twotorque,1);
377  G(ccc,mode)=coeff(1).*span(ccc)+coeff(2);
378  end
379  ccc=ccc+1;
380  end
381  end
382  xl=0:1;
383  yl=zeros(size(xl));
384  figure
385  if choice==5
386  plot(x,theta(:,1,1),'ks',x,(sign*sin((mode-0.5)*pi*x)),'k-')
387  end
388  if choice~=2
389  if choice~=5
390  plot(x,theta(:,1,1),'k-s')
391  end
392  end
393  if choice==2
394  plot(x(3:nodes),theta(3:nodes,1,1),'k-s')
395  end
396  line(xl,yl)
397  xlabel('r/R')
398  ylabel('Torsional Deformation (rad)')
399  title(['Mode Shape # ',num2str(mode),'-- ',num2str(nodes),'
Segments -- ','Wn = ',num2str(w),' rad/sec'])
400  legend('calculated mode shape',0)
401  end %for choice4==1
402  if choice4==0 %FREE FREE
403  if modenumber==0
404  mode=input('input mode number you are checking\n');
405  end
406  DD(:,mode)=theta(:,1,1);
407  GG(:,mode)=T(:,1,1);
408  sign=(-1)^(mode+1);
409  [rowgage,gages]=size(span);
410  %Eliminate a Bad Strain Gage???
411  if eliminate==2
412  eliminate=input('enter 1 if you want to zero out a strain gage or
zero not to eliminate any\n');
413  if eliminate==1
414  maxmodes=gages-2;
415  disp(['If the number of modes calculated exceed
',num2str(maxmodes),' your result will be incorrect']);
416  killit=input('enter the strain gage location number\n (closest to
the root = 1) you want to eliminate\n');
417  for g=1:gages
418  if g<killit
419  span(rowgage,g)=span(rowgage,g);
420  end
421  if g>killit
422  span(rowgage,g-1)=span(rowgage,g);
423  end
424  end
425  gages=gages-1;
426  span=span(rowgage,1:gages)
427  end
428  end
429  %%%%%%%END OF ELIMINATION ROUTINE%%%%%%%%%
```

```
%Interpolate calculated harmonic torques to span locations for
direct comparison
if choice~=3
for kkk=nodes:-1:1
for ccc=1:gages
if x(kkk)>=span(ccc)
twotorque=[GG(kkk,mode) GG(kkk-1,mode)];
twox=[x(kkk) x(kkk-1)];
coeff=polyfit(twox,twotorque,1);
G(ccc,mode)=coeff(1).*span(ccc)+coeff(2);
end
ccc=ccc+1;
end
if kkk>1
kkk=kkk-1;
end
end
end
if choice~=2
plot(x,theta(:,1,1),'k-s')
end
if choice==2 %plots DNW from offset to tip
plot(x(3:nodes),theta(3:nodes,1,1),'k-s')
end
line(xl,yl)
xlabel('r/R')
title(['Mode Shape #',num2str(mode),'--',num2str(nodes),' Segments
-- ','Wn = ',num2str(w),' rad/sec'])
if choice~=3
ylabel('Torsional Deformation (rad)')
legend('calculated mode shape',0)
end
end %for choice4==0 loop
end %for choice3==1 line
end %for choice2==1 line
if modenumber==0
ccontinue=input('enter one to try an exact frequency to check or
zero to quit\n');
end
if ccontinue==1
if modenumber==0
w=input('enter frequency to check in rad/sec\n');
omega=input('enter rotational speed to check in rad/sec\n');
end
choice3=1;
choice2=1;
upper=0;
lower=0;
upperomega=0;
loweromega=0;
end
if modenumber==0
if ccontinue~=1
ccontinue=input('press zero if you are sure you want to quit, else
press 1?');
end
end
if modenumber~=0
if mode==modenumber
ccontinue=0;
end
if mode<modenumber
mode=mode+1;
w=rootfreq(mode);
```

```
490  choice3=1;
491  choice2=1;
492  upper=0;
493  lower=0;
494  upperomega=0;
495  loweromega=0;
496  ccontinue=1;
497  end
498  end
499  end
   500  modenumber=mode;
```

THIS PAGE INTENTIONALLY LEFT BLANK

APPENDIX B. STRAIN PATTERN ANALYSIS PROGRAM

A. INSTRUCTIONS FOR RUNNING THE SPA PROGRAM

The option to run the SPA program is given after the Holzer program generates the number of mode shapes desired. Your initial choice of how many mode shapes to generate cannot be changed unless you start over and run the Holzer program again. If you choose to run the SPA program line 4 gives the option to see plots of SPA estimated torsion moments versus measured torsion moments for each harmonic (lines 68 to 78). Similarly, line 5 of the program gives the option to plot the SPA vector by mode number (lines 81 to 154). These options are not recommended if you are only concerned with the final estimated deflection result of the SPA program. You will also have the option to choose to estimate the first 10 harmonics (21 terms through the 10th sine) or 20 harmonics (41 terms through the 20th sine). The matrix of measured torsion moments you enter must be equal to or greater than your choice of harmonics to estimate. Enter the measured torsion moments in the same units that correspond to those you chose in Table 15. The columns of your measured torsion moment matrix are the harmonics and the rows are the measurement stations. After entering the measured moments you can opt to randomly vary the measured data to replicate measurement error. Line 20 asks for a vector of span locations of comparison deflection data to compare against the SPA estimated deflection. Lines 24 to 37 eliminate an entire set of strain gage data from the measured moment matrix if you selected this option during the Holzer program. Lines 39 to 48 interpolate the calculated mode shapes to the same span locations of the comparison deflection values entered in line 20. Line 62 is Step One of the SPA method using Equation 1.7 to calculate the SPA vector. Line 63 is Step Two of the SPA method using Equation 1.8 to calculate the estimated torsion moment matrix to compare against the measured torsion moment matrix. Line 64 is Step Three of the SPA method using Equation 1.9 to calculate the estimated deflection. All three Equations are inside a loop that runs once for each harmonic term. Each SPA vector is stored as a column in a matrix of {q}. Similarly, each harmonic of the estimated deflection solution {deflsol} and estimated moments {Checkq} are stored as columns of their respective matrix. The remainder of the program produces plots based on the earlier choices and converts the

harmonics of measured torsion moments and estimated deflections (radians) into the time domain.

B. SPA PROGRAM VARIABLES

steadytendefl The (nx1024) matrix of estimated SPA deflection (radians) where each row corresponds to the span locations entered for the comparison data and the 1,024 columns range from zero to 2π radians (line 193).

deflsol The (nxh) matrix of harmonics of SPA estimated deflection where the rows correspond to the interpolation stations chosen for comparison and the columns correspond to harmonic terms (line 64).

newxaxis The final SPA estimated deflection in deflsol or steadytendefl may not be available at all comparison stations if the last calculated mode shape location did not exceed the last comparison deflection location. This variable contains all of the span locations that the SPA deflection values can be compared to the chosen set of deflections (line 67).

steadyten The (gx1024) matrix of measured torsion moment values (ft-lb) where each row corresponds to the measurement span locations and the 1,024 columns range from zero to 2π radians (line 173).

M The (gxh) matrix of harmonic terms for the measured torsion moment entered by the user (ft-lb or N-m) (line 16).

xaxis The user input span locations to interpolate values of the torsional deflection mode shape [DD] from the Holzer program (non-dimensional, r/R) (line 20).

D The (xaxis,m) matrix of Hozler calculated deflection mode shapes interpolated to the desired span locations by row and each column corresponds to a separate mode (line 47).

q The (mxh) matrix of SPA vectors where each column is the SPA vector for each harmonic, and the rows correspond to mode numbers (line 62).

checkq The (gxh) matrix of SPA estimated torsion moments where rows correspond to measurement span locations and columns correspond to harmonic terms

C. SPA PROGRAM LISTING

```
1    %START OF SPA PROGRAM, PART 2%
2    GOSPA=input('enter 1 if you want to conduct Strain Pattern
Analysis\n');
3    if GOSPA==1
4    figyes=input('press 1 if you want to see a plot of Test Data vs SPA
Torsion Moment vs. r/R by Harmonic\n');
5    figyes2=input('press 1 if you want to see the proportions (q) SPA
vector plotted vs. mode number by harmonic\n');
6    harmonic=input('enter the 10 (through 10th Sine) or 20 (through
20th Sine) for the number of harmonics you want to solve\n');
7    harmonicterm=2*harmonic+1;
8    if harmonic==10
9    fortyone=0;
10   end
11   if harmonic==20
12   fortyone=1;
13   end
14   if choice~=0
15   if choice~=2
16   M=input('enter the harmonic torsion moment (FT-LBS)\n');
18   %THE NEXT inputs ARE REQUIRED if you want to plot you're results
against other results??
19  %Locations entered below are used to interpolate deflection mode
shape data for final SPA result to be easily compared to other methods
20   xaxis=input('enter the vector of r/R locations for the comparison
set of deflection information\n');
21   end
22   end
23   [rowM colM]=size(M);
24   %If you chose to eliminate a Bad Strain Gage???
25   if eliminate==1
26   for g=1:rowM
27   if g<killit
28   M(g,:)=M(g,:);
29   end
30   if g>killit
31   M(g-1,:)=M(g,:);
32   end
33   end
34   rowM=rowM-1;
35   M=M(1:rowM,:);
36   end
37   %%%%%%%END OF ELIMINATION ROUTINE%%%%%%%%%
38   [rowxaxis colxaxis]=size(xaxis);
39   %Interpolate mode shape to xaxis locations to be able to compare
test to SPA
40   for mmode=1:mode
41   for kkk=Nodes:-1:1
42   for ccc=1:colxaxis
43   if x(kkk)>=xaxis(ccc)
44   twodefl=[DD(kkk,mmode) DD(kkk-1,mmode)];
45   twox=[x(kkk) x(kkk-1)];
46   coeff=polyfit(twox,twodefl,1);
47   D(ccc,mmode)=coeff(1).*xaxis(ccc)+coeff(2);
48   end
49   ccc=ccc+1;
50   end
51   if kkk>1
52   kkk=kkk-1;
53   end
54   end
55   mmode=mmode+1;
```

```
56   end
57   %Size of G (Referred to as [T] in thesis) is (#r/R stations of
Strain Gages  x # modes in solution (#))
58   %Size of M is (#r/R Stations in Test Data  x # Harmonic Terms (21
or 41))
59   %Size of q is #modes x # Harmonic terms
60   for amplitudes=1:harmonicterm;
61   %THIS IS THE SPA Vector {q} with number of modes used for number of
terms
62   q(amplitudes)=inv(G.'*G)*G.'*M(:,amplitudes);%Equation 1.7 Step One
63   checkq(:,amplitudes)=G*q(:,amplitudes);%Equation 1.8 Step Two
64   deflsol(:,amplitudes)=D*proportions(:,amplitudes);%Equation 1.9
Step Three
65   [rowD colD]=size(D);
66   nodes=rowD;
67   newxaxis=xaxis(1:nodes);
68   if figyes==1
69   xl=0:1;
70   yl=zeros(size(xl));
71   figure
72   plot(span,checkq(:,amplitudes),'k-d',span,M(:,amplitudes),'b:+')
73   line(xl,yl)
74   %title([num2str(modenumber) ,' mode solution: Test Data vs SPA
Torsion Moment for Harmonic Term ',num2str(amplitudes)])
75   xlabel('r/R')
76   ylabel('Torsion Moment (ft-lbs)')
77   %legend('SPA Torsion Moment','Measured Torsion Moment',0)
78   end
79   amplitudes=amplitudes+1;
80   end
81   if figyes2==1
82   xl=1:mode;
83   yl=zeros(size(xl));
84   figure
85   plot(1:1:mode,q(:,1),'k-d',1:1:mode,q(:,2),'b-
o',1:1:mode,q(:,3),'g-*')
86   line(xl,yl)
87   xlabel('mode number')
88   ylabel('SPA Vector')
89   title([num2str(modenumber) ,' mode solution: Steady, 1st Cos, and
1st Sin Least Squares Proportions'])
90   legend('Steady','1st Cos','1st Sin',0)
91   figure
92   plot(1:1:mode,q(:,4),'k-d',1:1:mode,q(:,5),'b-o')
93   line(xl,yl);
94   xlabel('mode number')
95   ylabel('SPA Vector')
96   title([num2str(modenumber) ,' mode solution: 2nd Cos and 2nd Sin
Least Squares Proportions'])
97   legend('2nd Cos','2nd Sin',0)
98   figure
99   plot(1:1:mode,q(:,6),'k-d',1:1:mode,q(:,7),'b-o')
100  line(xl,yl)
101  xlabel('mode number')
102  ylabel('SPA Vector')
103  title([num2str(modenumber) ,' mode solution: 3rd Cos and 3rd Sin
Least Squares Proportions'])
104  legend('3rd Cos','3rd Sin',0)
105  figure
106  plot(1:1:mode,q(:,8),'k-d',1:1:mode,q(:,9),'b-o')
107  line(xl,yl)
108  xlabel('mode number')
109  ylabel('SPA Vector')
```

```
110  title([num2str(modenumber) ,' mode solution: 4th Cos and 4th Sin
Least Squares Proportions'])
111  legend('4th Cos','4th Sin',0)
112  figure
113  plot(1:1:mode,q(:,10),'k-d',1:1:mode,q(:,11),'b-o')
114  line(xl,yl)
115  xlabel('mode number')
116  ylabel('SPA Vector')
117  title([num2str(modenumber) ,' mode solution: 5th Cos and 5th Sin
Least Squares Proportions'])
118  legend('5th Cos','5th Sin',0)
119  figure
120  plot(1:1:mode,q(:,12),'k-d',1:1:mode,q(:,13),'b-o')
121  line(xl,yl)
122  xlabel('mode number')
123  ylabel('SPA Vector')
124  title([num2str(modenumber) ,' mode solution: 6th Cos and 6th Sin
Least Squares Proportions'])
125  legend('6th Cos','6th Sin',0)
126  figure
127  plot(1:1:mode,q(:,14),'k-d',1:1:mode,q(:,15),'b-o')
128  line(xl,yl)
129  xlabel('mode number')
130  ylabel('SPA Vector')
131  title([num2str(modenumber) ,' mode solution: 7th Cos and 7th Sin
Least Squares Proportions'])
132  legend('7th Cos','7th Sin',0)
133  figure
134  plot(1:1:mode,q(:,16),'k-d',1:1:mode,q(:,17),'b-o')
135  line(xl,yl)
136  xlabel('mode number')
137  ylabel('SPA Vector')
138  title([num2str(modenumber) ,' mode solution: 8th Cos and 8th Sin
Least Squares Proportions'])
139  legend('8th Cos','8th Sin',0)
140  figure
141  plot(1:1:mode,q(:,18),'k-d',1:1:mode,q(:,19),'b-o')
142  line(xl,yl)
143  xlabel('mode number')
144  ylabel('SPA Vector')
145  title([num2str(modenumber) ,' mode solution: 9th Cos and 9th Sin
Least Squares Proportions'])
146  legend('9th Cos','9th Sin',0)
147  figure
148  plot(1:1:mode,q(:,20),'k-d',1:1:mode,q(:,21),'b-o')
149  line(xl,yl)
150  xlabel('mode number')
151  ylabel('SPA Vector')
152  title([num2str(modenumber) ,' mode solution: 10th Cos and 10th Sin
Least Squares Proportions'])
153  legend('10th Cos','10th Sin',0)
154  end
155  %%%Convert from Torsional Moment Harmonics to Time Domain%%%
156  sta=1;
157  for sta=1:rowM
158  MM=M(sta,:);
159  Harmtors=MM(:);
160  harm=1;
161  for harm=1:harmonic;
162  A(harm)=-1*Harmtors(2*harm);
163  B(harm)=-1*Harmtors(2*harm+1);
164  i=1;
165  for i=1:1024
166  Lattors(harm,i)=A(harm)*cos(harm*CNEWAZIMUTH(i));
```

```
167  Longtors(harm,i)=B(harm)*sin(harm*CNEWAZIMUTH(i));
168  end
169  %Now put collective and cyclic together Harmonic
170  Tors(harm,:)=-Lattors(harm,:)-Longtors(harm,:);
171  harm=harm+1;
172  end
173  steadyten(sta,:)=M(sta,1)+sum(Tors,1);
174  sta=sta+1;
175  end
176  %%NOW Convert DEFL Harmonics to TIME HIST%%%
177  for sta=1:rowD
178  ff=deflsol(sta,:);
179  Harmdefl=ff(:);
180  harm=1;
181  for harm=1:harmonic;
182  A(harm)=-1*Harmdefl(2*harm);
183  B(harm)=-1*Harmdefl(2*harm+1);
184  i=1;
185  for i=1:1024
186  Latdefl(harm,i)=A(harm)*cos(harm*CNEWAZIMUTH(i));
187  Longdefl(harm,i)=B(harm)*sin(harm*CNEWAZIMUTH(i));
188  end
189  %Now put collective and cyclic together Harmonic
190  DEFL(harm,:)=-Latdefl(harm,:)-Longdefl(harm,:);
191  harm=harm+1;
192  end
193  steadytendefl(sta,:)=deflsol(sta,1)+sum(DEFL,1);%Radians
194  sta=sta+1;
195  end
196  end %end for GOSPA==1
```

APPENDIX C. UTRC MODEL-SCALE BLADE PROPERTIES

x (non-dimensional r/R)			
0.00000	0.05290	0.05340	0.05341
0.12200	0.12201	0.15800	0.15801
0.16000	0.16001	0.18400	0.18401
0.18600	0.19200	0.19201	0.21600
0.21601	0.21700	0.23400	0.23401
0.24000	0.24001	0.27800	0.27801
0.39100	0.39101	0.40900	0.40901
0.42600	0.42601	0.46400	0.46401
0.46600	0.49700	0.49701	0.49800
0.49801	0.54100	0.54101	0.55900
0.55901	0.56900	0.56901	0.59200
0.59201	0.63000	0.63001	0.66600
0.66601	0.67600	0.67601	0.68300
0.68301	0.68400	0.68401	0.73600
0.73601	0.75000	0.76600	0.76601
0.78200	0.78400	0.78401	0.78600
0.78601	0.80000	0.80001	0.81300
0.81301	0.81800	0.82300	0.85400
0.85800	0.85801	0.85930	0.85931
0.86200	0.86201	0.86220	0.86221
0.86500	0.86501	0.88000	0.88001
0.88260	0.88261	0.89100	0.90100
0.90260	0.90261	0.91110	0.91111
0.91300	0.92500	0.92501	0.92890
0.92891	0.92900	0.93200	0.93201
0.93250	0.93251	0.93600	0.93601
0.93610	0.93611	0.94700	0.95390
0.95391	0.95600	0.95601	0.95610
0.95611	0.96000	0.96001	0.97200
0.97390	0.97391	0.97400	0.97401
0.98110	0.98111	0.99100	0.99890
0.99891	1.00000		

Table 16. UTRC Blade 126-Segment Span Locations. [After: Ref. 17]

GJ (lb-ft^2)			
416.67	416.67	416.67	416.67
416.67	152.78	152.78	152.78
152.78	152.78	152.78	152.78
152.78	152.78	152.78	152.78
152.78	152.78	152.78	152.78
152.78	152.78	152.78	152.78
152.78	152.78	152.78	152.78
152.78	152.78	152.78	152.78
152.78	152.78	152.78	152.78
152.78	152.78	152.78	152.78
152.78	152.78	152.78	152.78
152.78	152.78	152.78	152.78
152.78	152.78	152.78	152.78
152.78	152.78	152.78	152.78
152.78	152.78	152.78	152.78
152.78	152.78	152.78	152.78
152.78	152.78	152.78	152.78
152.78	152.78	152.78	152.78
152.78	152.78	152.78	72.22
72.22	72.22	72.22	72.22
72.22	72.22	72.22	72.22
72.22	72.22	72.22	72.22
72.22	72.22	72.22	72.22
72.22	72.22	72.22	72.22
72.22	72.22	72.22	72.22
72.22	72.22	72.22	72.22
72.22	72.22	72.22	72.22
72.22	72.22	72.22	72.22
72.22	72.22	72.22	72.22
72.22	72.22	72.22	72.22
72.22	72.22	72.22	72.22
72.22	72.22	72.22	72.22
72.22	72.22	72.22	72.22
72.22	72.22		

Table 17. UTRC Blade Torsional Stiffness. [After: Ref. 17]

I (lb-ft-sec^2)			
0.00E+00	0.00E+00	5.41E-04	5.41E-04
5.41E-04	2.10E-05	2.10E-05	1.09E-05
1.09E-05	1.09E-05	1.09E-05	1.09E-05
1.09E-05	1.09E-05	6.63E-05	6.63E-05
6.63E-05	6.63E-05	6.63E-05	6.63E-05
6.63E-05	3.63E-05	3.63E-05	1.79E-05
1.79E-05	8.29E-05	8.29E-05	8.29E-05
8.29E-05	3.63E-05	3.63E-05	1.79E-05
1.79E-05	1.79E-05	1.86E-05	1.86E-05
1.86E-05	1.86E-05	6.22E-05	6.22E-05
6.22E-05	6.22E-05	6.22E-05	6.22E-05
3.63E-05	3.63E-05	6.48E-05	6.48E-05
6.48E-05	6.48E-05	6.48E-05	6.48E-05
6.48E-05	6.48E-05	4.14E-05	4.14E-05
7.25E-05	7.25E-05	7.25E-05	7.25E-05
7.25E-05	7.25E-05	7.25E-05	7.25E-05
5.61E-05	5.61E-05	5.96E-05	5.96E-05
4.14E-05	4.14E-05	4.14E-05	4.14E-05
4.14E-05	4.14E-05	4.14E-05	2.11E-05
2.11E-05	2.11E-05	2.11E-05	7.10E-05
7.10E-05	9.69E-05	9.69E-05	3.11E-05
3.11E-05	5.18E-05	5.18E-05	5.18E-05
5.18E-05	3.11E-05	3.11E-05	1.04E-04
1.04E-04	1.04E-04	1.04E-04	1.04E-04
3.11E-05	3.11E-05	3.06E-05	3.09E-05
3.08E-05	1.89E-05	1.81E-05	1.76E-05
1.76E-05	1.18E-04	1.09E-04	9.98E-05
0.00E+00	0.00E+00	0.00E+00	0.00E+00
1.44E-04	1.37E-04	1.37E-04	1.08E-04
1.02E-04	0.00E+00	0.00E+00	0.00E+00
0.00E+00	2.27E-04	2.09E-04	1.92E-04
0.00E+00	0.00E+00	0.00E+00	0.00E+00
0.00E+00	0.00E+00		

Table 18. UTRC Blade Torsional Mass Moment of Inertia. [After: Ref. 17]

Ck_A^2/Ω^2 (lb-ft^2-sec^2/rad^2)			
7.39E-10	7.37E-10	7.37E-10	6.05E-09
4.56E-09	5.33E-10	1.87E-10	9.21E-11
9.21E-11	9.21E-11	9.13E-11	5.94E-11
5.93E-11	5.92E-11	5.92E-11	5.86E-11
1.14E-10	1.14E-10	1.13E-10	6.68E-11
6.66E-11	6.66E-11	6.52E-11	6.52E-11
5.99E-11	1.01E-10	9.95E-11	6.65E-11
6.54E-11	6.54E-11	6.27E-11	5.25E-11
5.24E-11	5.04E-11	5.04E-11	5.03E-11
5.03E-11	4.73E-11	8.59E-11	8.35E-11
5.15E-11	5.07E-11	5.07E-11	4.87E-11
4.87E-11	4.52E-11	4.52E-11	4.17E-11
6.53E-11	6.51E-11	6.81E-11	6.64E-11
6.64E-11	6.53E-11	5.21E-11	2.98E-11
2.09E-11	2.00E-11	1.88E-11	2.80E-11
2.63E-11	2.61E-11	2.16E-11	2.14E-11
2.14E-11	2.02E-11	2.02E-11	1.90E-11
1.90E-11	1.85E-11	1.05E-11	8.77E-12
8.55E-12	6.24E-12	6.19E-12	6.19E-12
6.08E-12	6.08E-12	6.07E-12	6.07E-12
5.96E-12	1.00E-11	8.97E-12	8.97E-12
8.78E-12	8.78E-12	8.19E-12	7.48E-12
7.36E-12	7.36E-12	6.75E-12	6.75E-12
6.61E-12	5.74E-12	5.74E-12	5.45E-12
5.45E-12	5.44E-12	4.91E-12	2.06E-12
1.67E-12	1.67E-12	1.59E-12	2.30E-12
2.30E-12	2.30E-12	1.92E-12	1.68E-12
1.68E-12	1.60E-12	1.65E-12	1.64E-12
1.64E-12	1.50E-12	1.38E-12	9.73E-13
9.08E-13	9.08E-13	9.05E-13	4.45E-13
3.25E-13	3.25E-13	1.55E-13	1.91E-14
1.89E-14	0.00E+00		

Table 19. UTRC Blade Tension-Torsion Term without Square of Rotational Speed. [After: Ref. 17]

β (degrees)			
10.00	14.19	14.23	14.23
19.67	19.67	19.67	19.67
19.67	19.67	19.67	19.67
19.67	19.61	19.61	19.36
19.36	19.35	19.05	19.05
18.94	18.94	18.28	18.28
16.29	16.29	15.98	15.98
15.68	15.68	15.01	15.01
14.98	13.43	13.43	13.41
13.41	12.66	12.66	12.35
12.35	12.17	12.17	11.77
11.77	11.10	11.10	10.47
10.47	10.30	10.30	10.17
10.17	10.16	10.16	9.25
9.25	9.00	8.81	8.81
8.62	8.59	8.59	8.57
8.57	8.40	8.40	8.25
8.25	8.19	8.13	8.87
8.77	8.77	8.74	8.74
8.67	8.67	8.66	8.66
8.59	8.59	8.22	8.22
8.15	8.15	7.94	7.31
7.22	7.22	6.75	6.75
6.64	6.44	6.44	6.37
6.37	6.37	6.40	6.40
6.40	6.40	6.43	6.43
6.43	6.43	6.52	6.75
6.75	6.83	6.83	6.83
6.83	6.96	6.96	7.37
7.47	7.47	7.47	7.47
7.84	7.84	8.35	8.82
8.82	8.89		

Table 20. UTRC Blade Feathering Angle Before Deformation. [After: Ref. 14]

THIS PAGE INTENTIONALLY LEFT BLANK

APPENDIX D. STRAIN PATTERN ANALYSIS PLOTS

UH-60A Model Rotor, DNW Run 13.20, $\mu = 0.301$

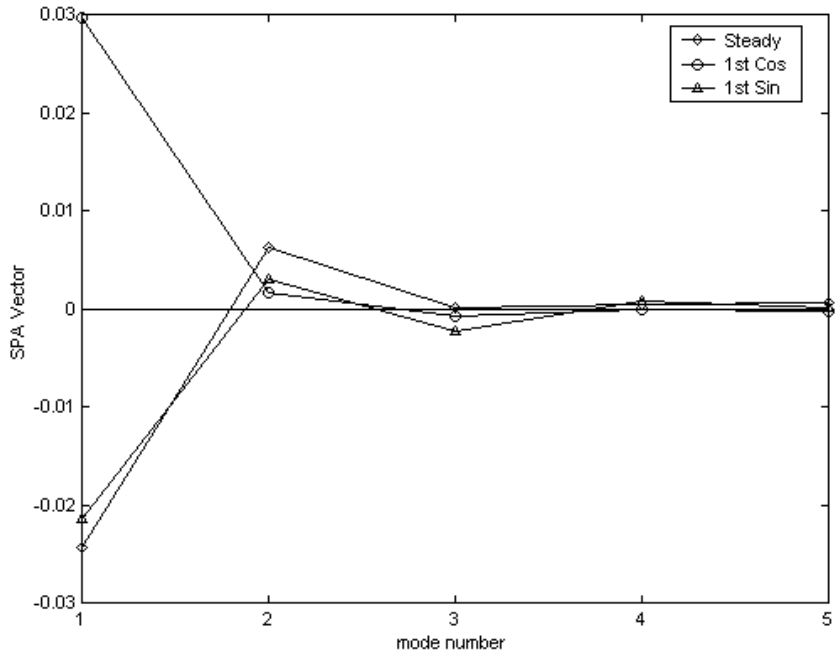

Figure 44. Five-Mode SPA Vector for the Steady, 1st Cosine and 1st Sine Terms.

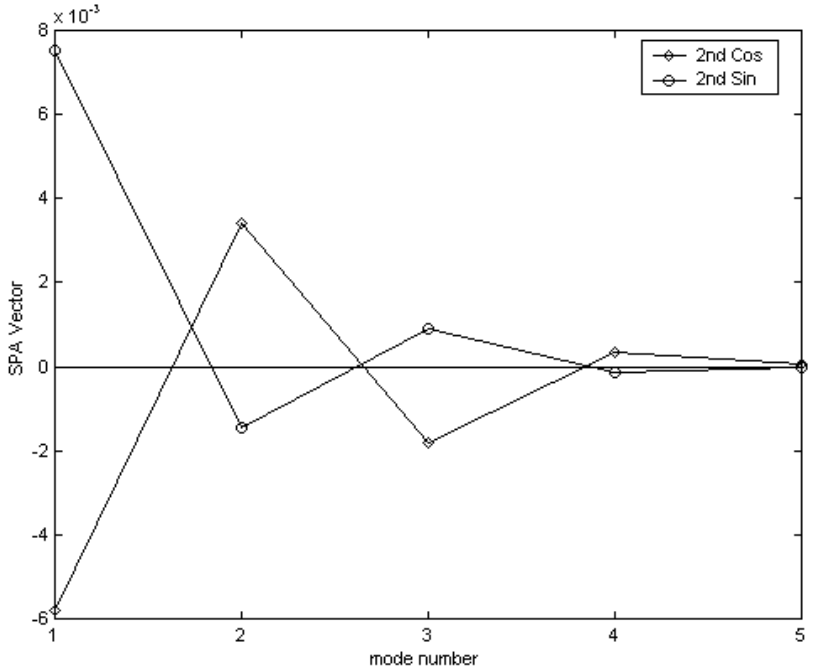

Figure 45. Five-Mode SPA Vector for the 2nd Cosine and 2nd Sine Terms.

UH-60A Model Rotor, DNW Run 13.20, $\mu = 0.301$

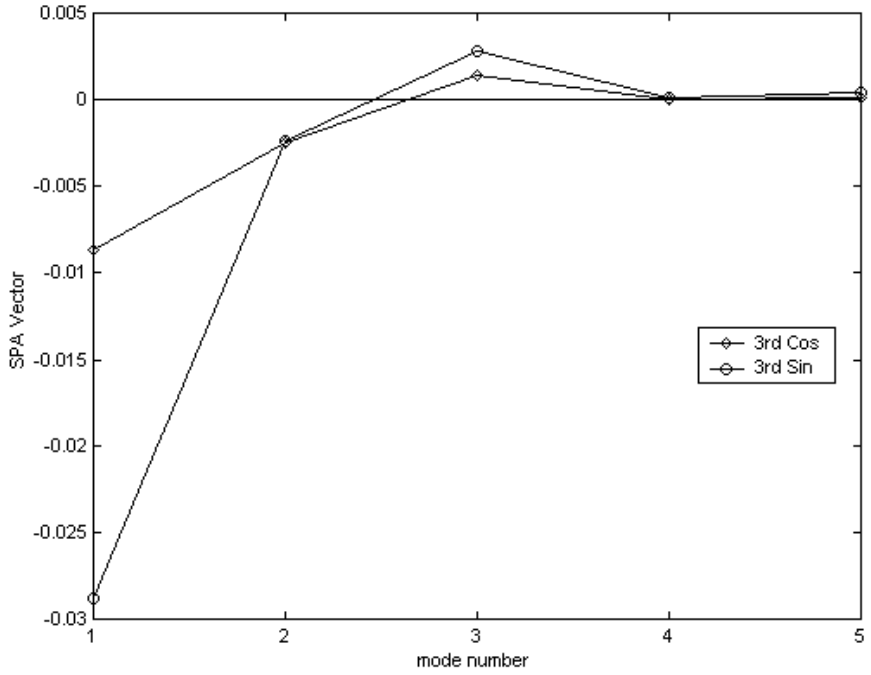

Figure 46. Five-Mode SPA Vector for the 3rd Cosine and 3rd Sine Terms.

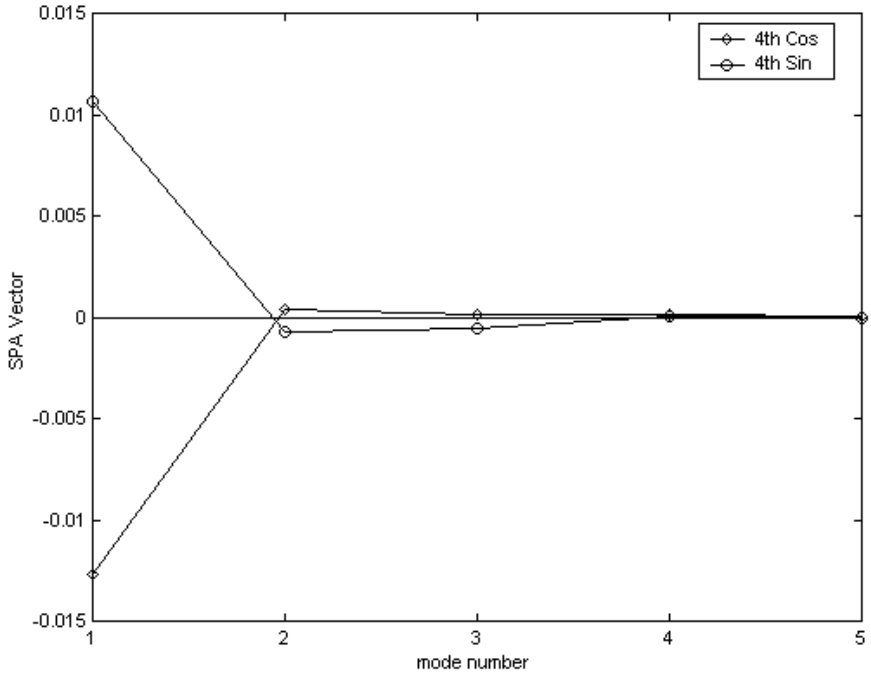

Figure 47. Five-Mode SPA Vector for the 4th Cosine and 4th Sine Terms.

UH-60A Model Rotor, DNW Run 13.20, $\mu = 0.301$

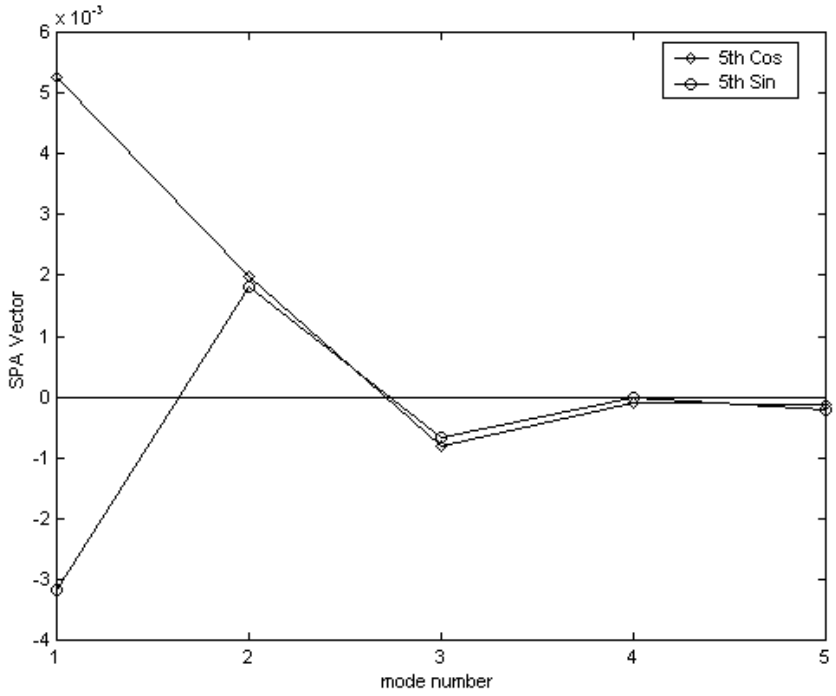

Figure 48. Five-Mode SPA Vector for the 5th Cosine and 5th Sine Terms.

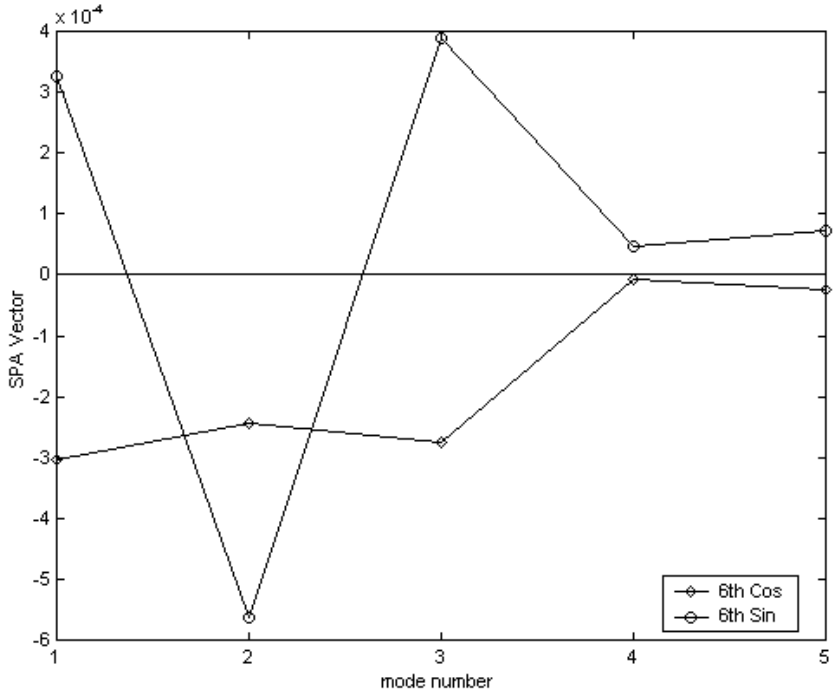

Figure 49. Five-Mode SPA Vector for the 6th Cosine and 6th Sine Terms.

UH-60A Model Rotor, DNW Run 13.20, $\mu = 0.301$

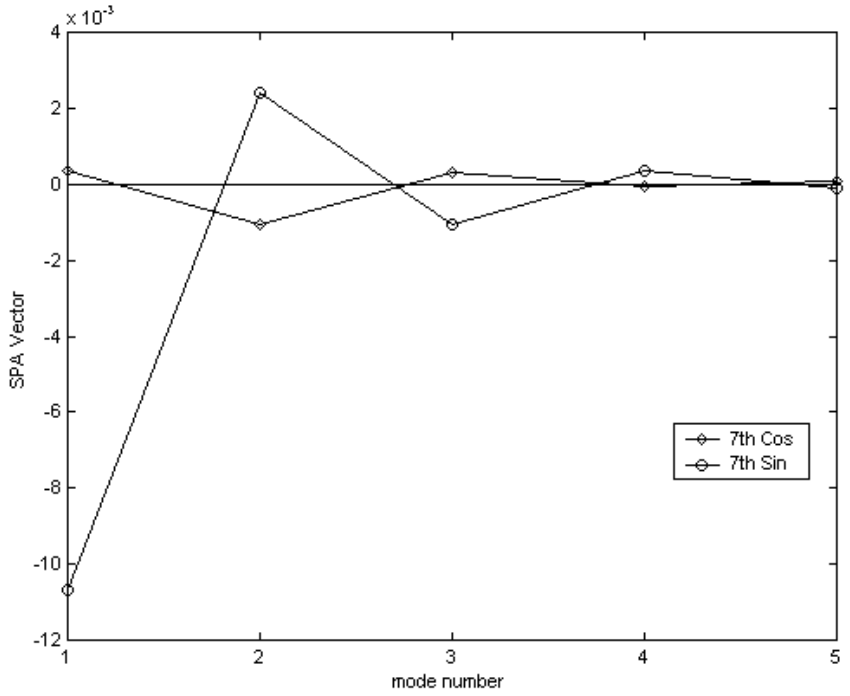

Figure 50. Five-Mode SPA Vector for the 7th Cosine and 7th Sine Terms.

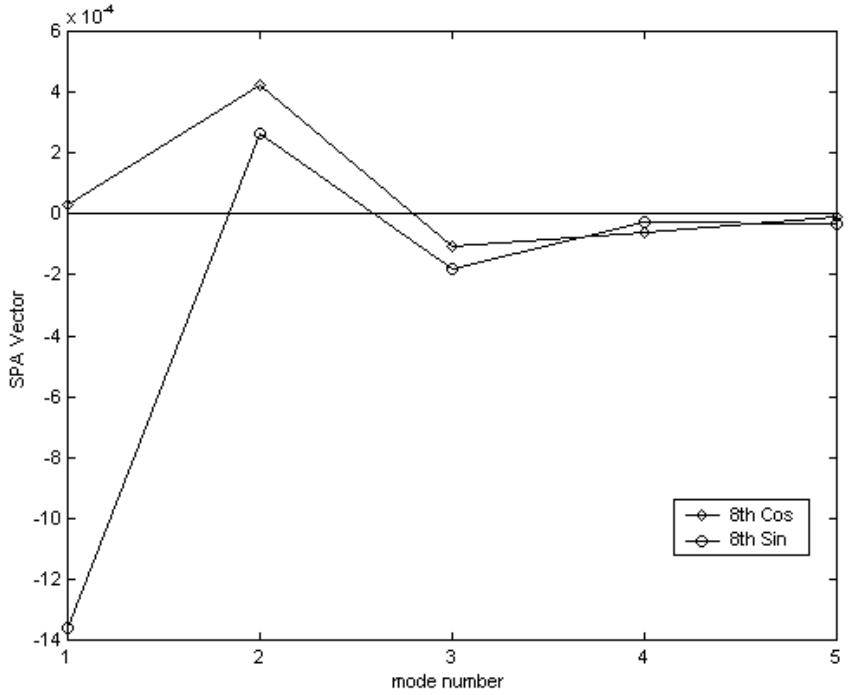

Figure 51. Five-Mode SPA Vector for the 8th Cosine and 8th Sine Terms.

UH-60A Model Rotor, DNW Run 13.20, $\mu = 0.301$

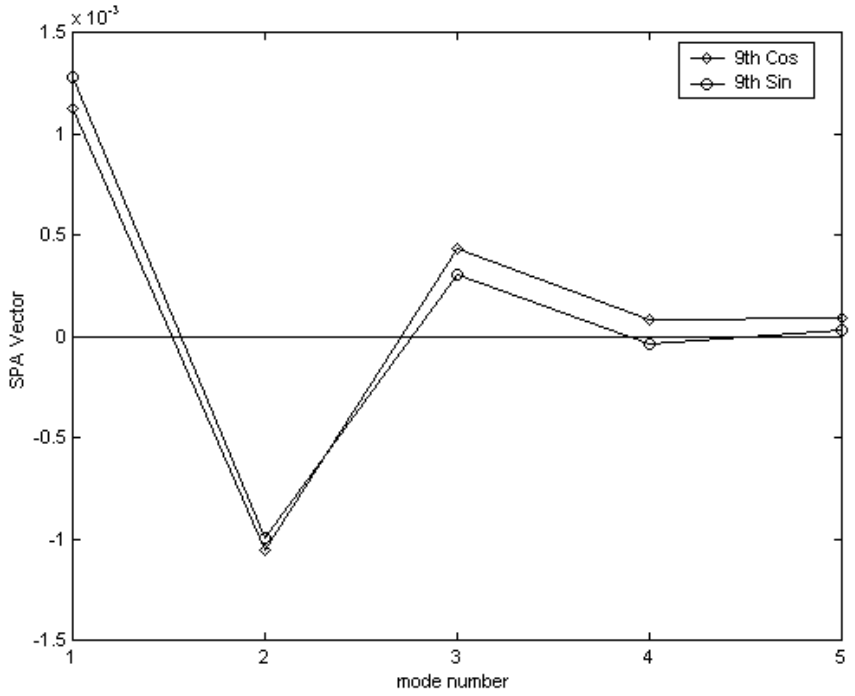

Figure 52. Five-Mode SPA Vector for the 9th Cosine and 9th Sine Terms.

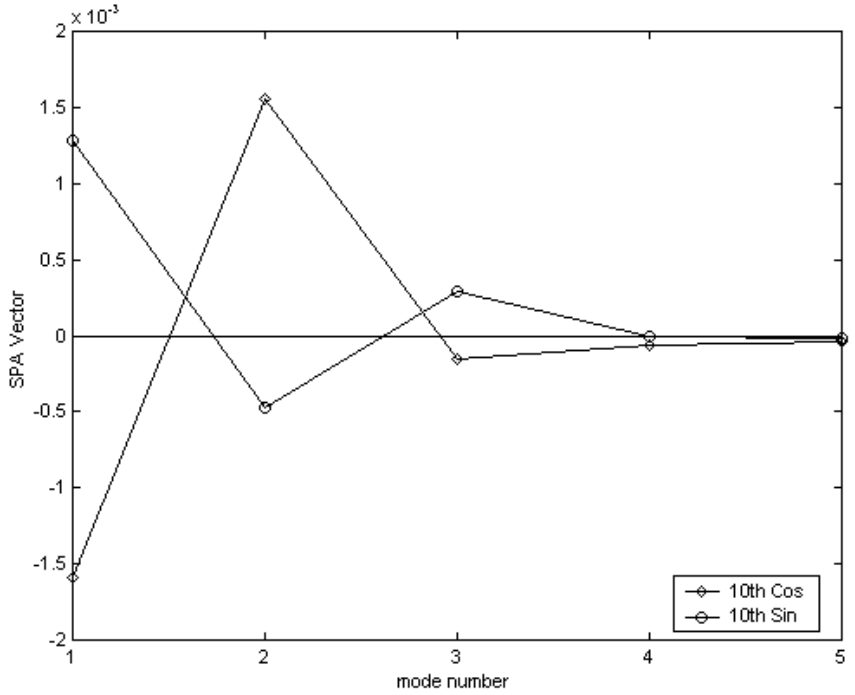

Figure 53. Five-Mode SPA Vector for the 10th Cosine and 10th Sine Terms.

UH-60A Model Rotor, Measured = Dotted Line, SPA = Solid Line

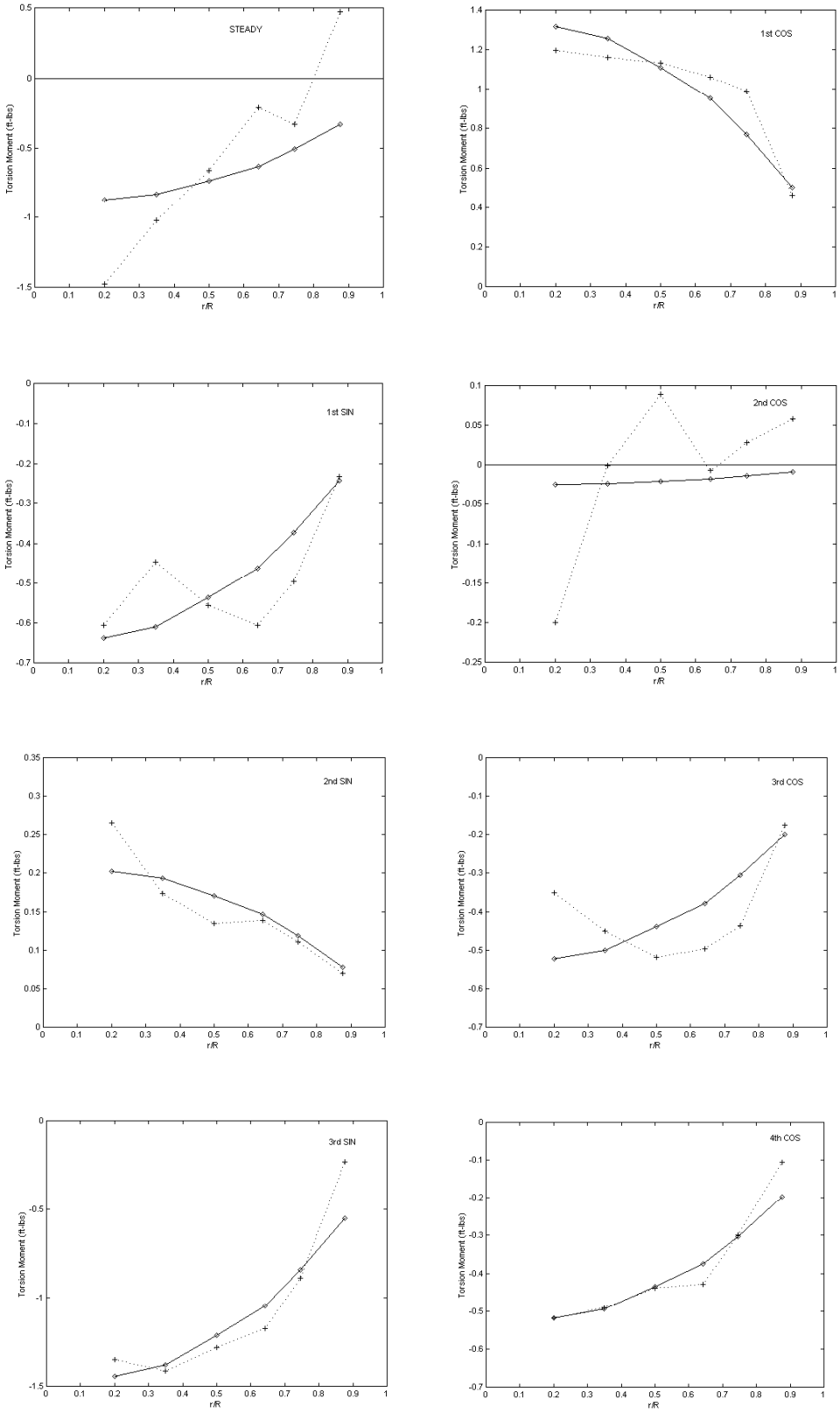

Figure 54. One-Mode SPA versus Measured Torsion Moments for Steady to 4th Cosine.

UH-60A Model Rotor, Measured = Dotted Line, SPA = Solid Line

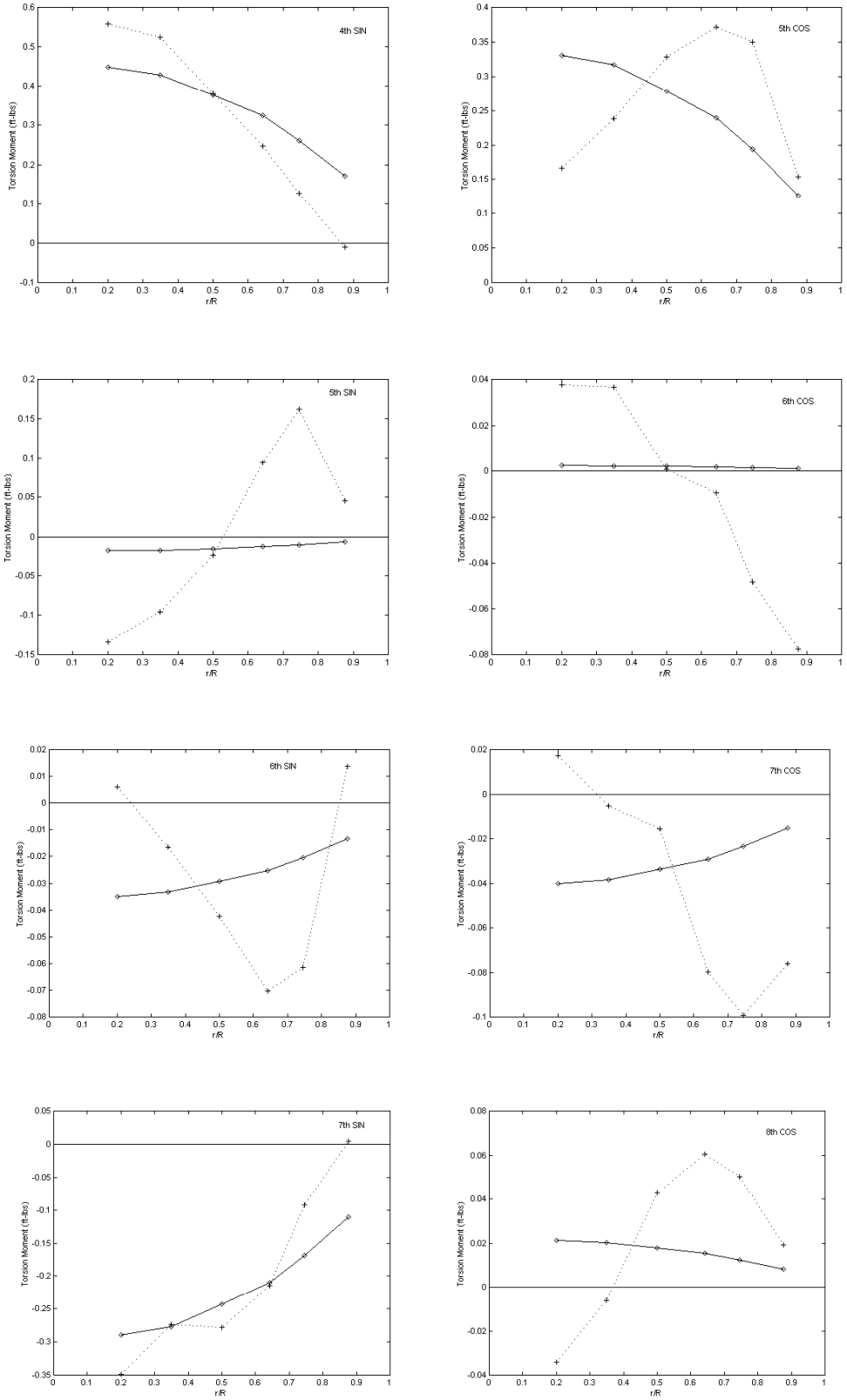

Figure 55. One-Mode SPA versus Measured Torsion Moments for 4th Sine to 8th Cosine.

UH-60A Model Rotor, Measured = Dotted Line, SPA = Solid Line

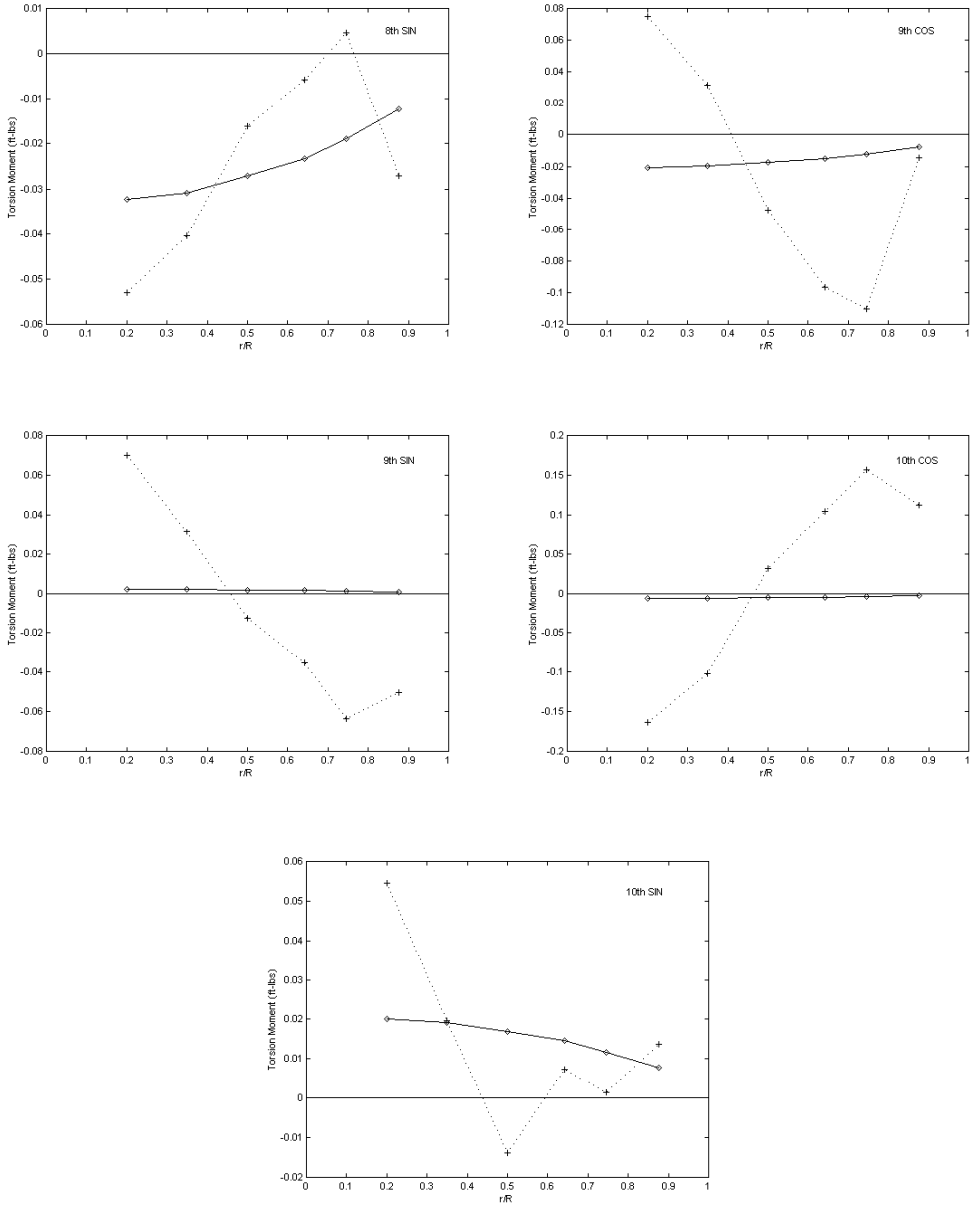

Figure 56. One-Mode SPA versus Measured Torsion Moments for 8th Sine to 10th Sine.

UH-60A Model Rotor, Measured = Dotted Line, SPA = Solid Line

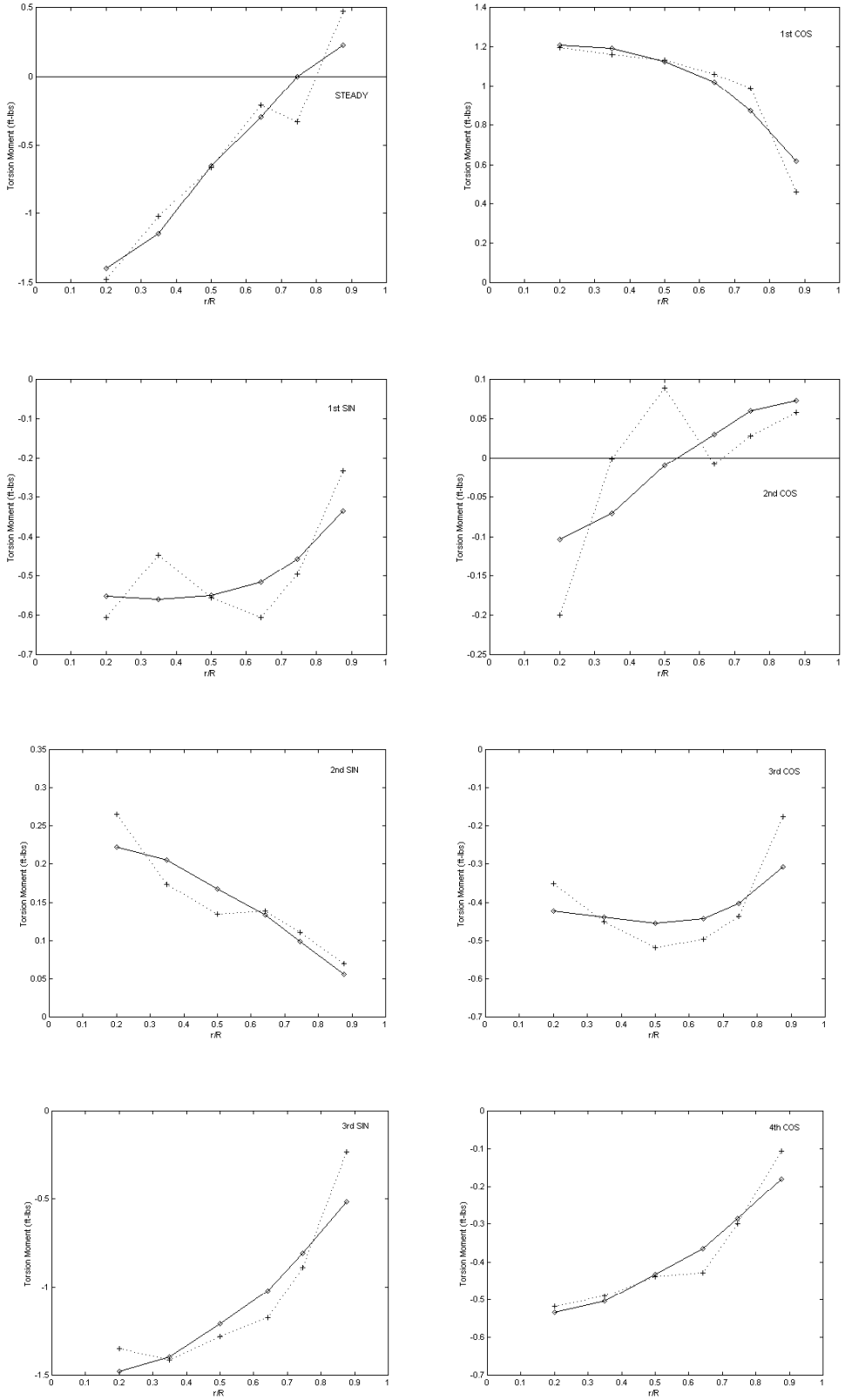

Figure 57. Two-Mode SPA versus Measured Torsion Moments for Steady to 4th Cosine.

UH-60A Model Rotor, Measured = Dotted Line, SPA = Solid Line

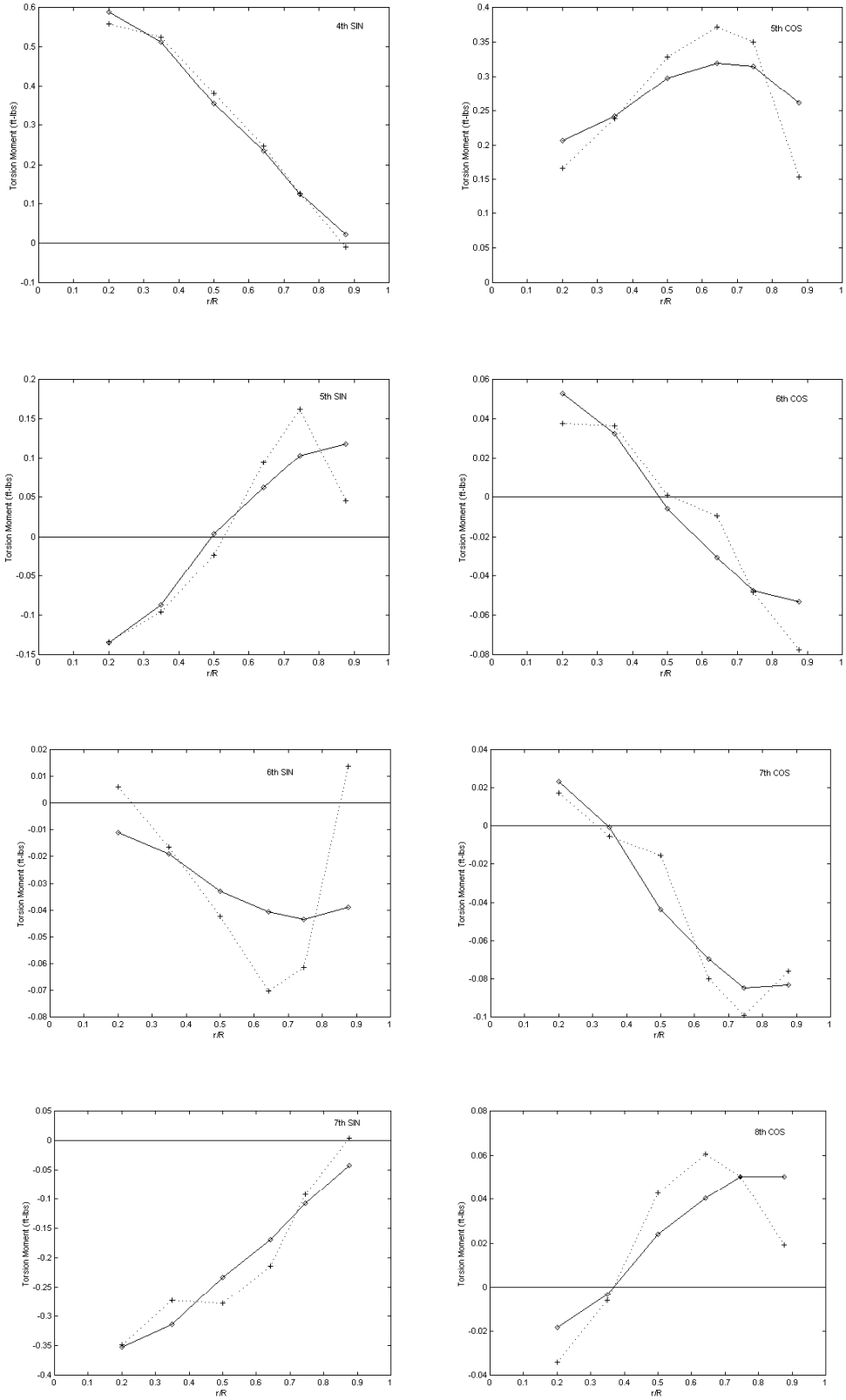

Figure 58. Two-Mode SPA versus Measured Torsion Moments for 4th Sine to 8th Cosine.

UH-60A Model Rotor, Measured = Dotted Line, SPA = Solid Line

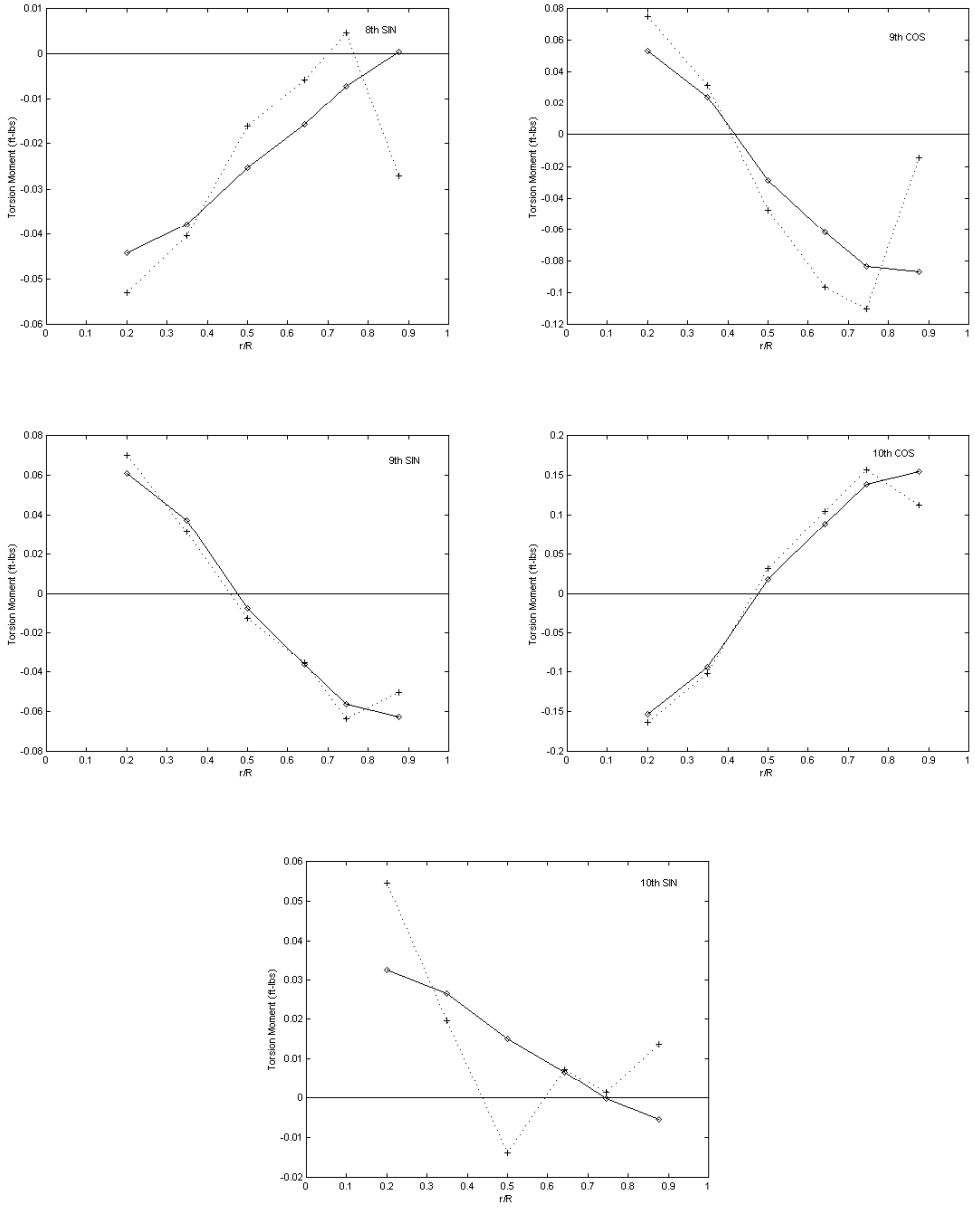

Figure 59. Two-Mode SPA versus Measured Torsion Moments for 8th Sine to 10th Sine.

UH-60A Model Rotor, Measured = Dotted Line, SPA = Solid Line

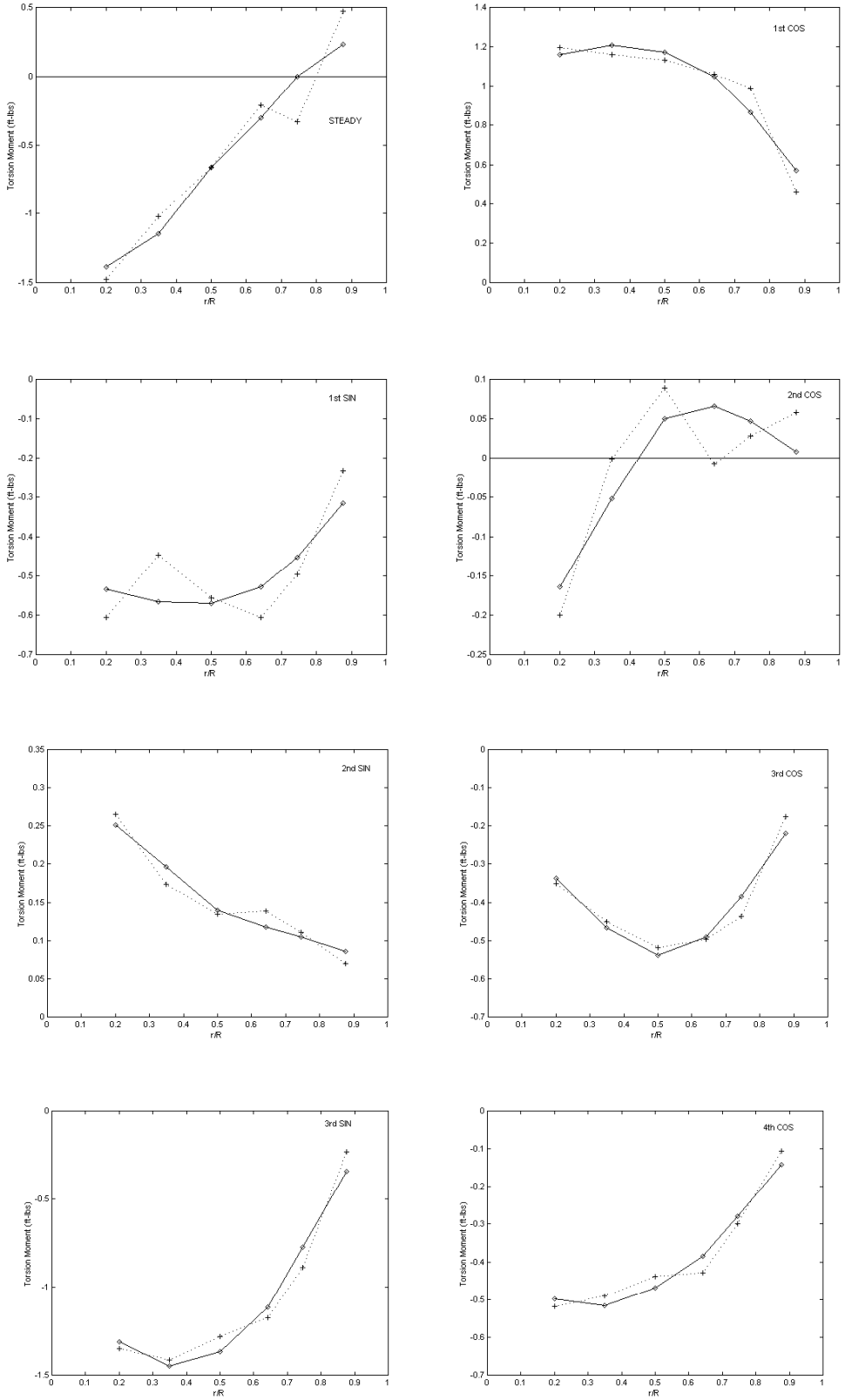

Figure 60. Three-Mode SPA versus Measured Torsion Moments for Steady to 4th Cosine.

UH-60A Model Rotor, Measured = Dotted Line, SPA = Solid Line

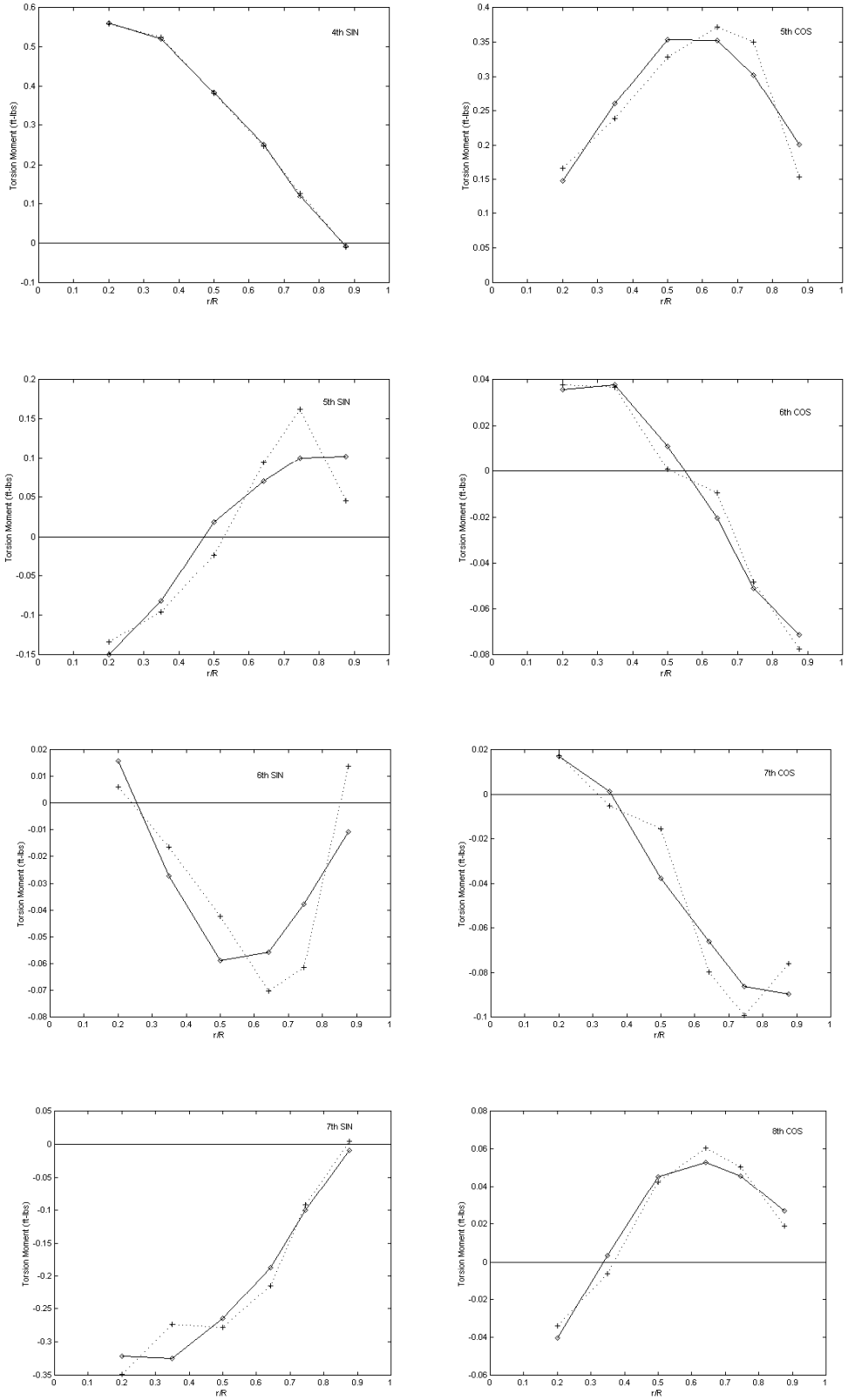

Figure 61. Three-Mode SPA versus Measured Torsion Moments for 4th Sine to 8th Cosine.

UH-60A Model Rotor, Measured = Dotted Line, SPA = Solid Line

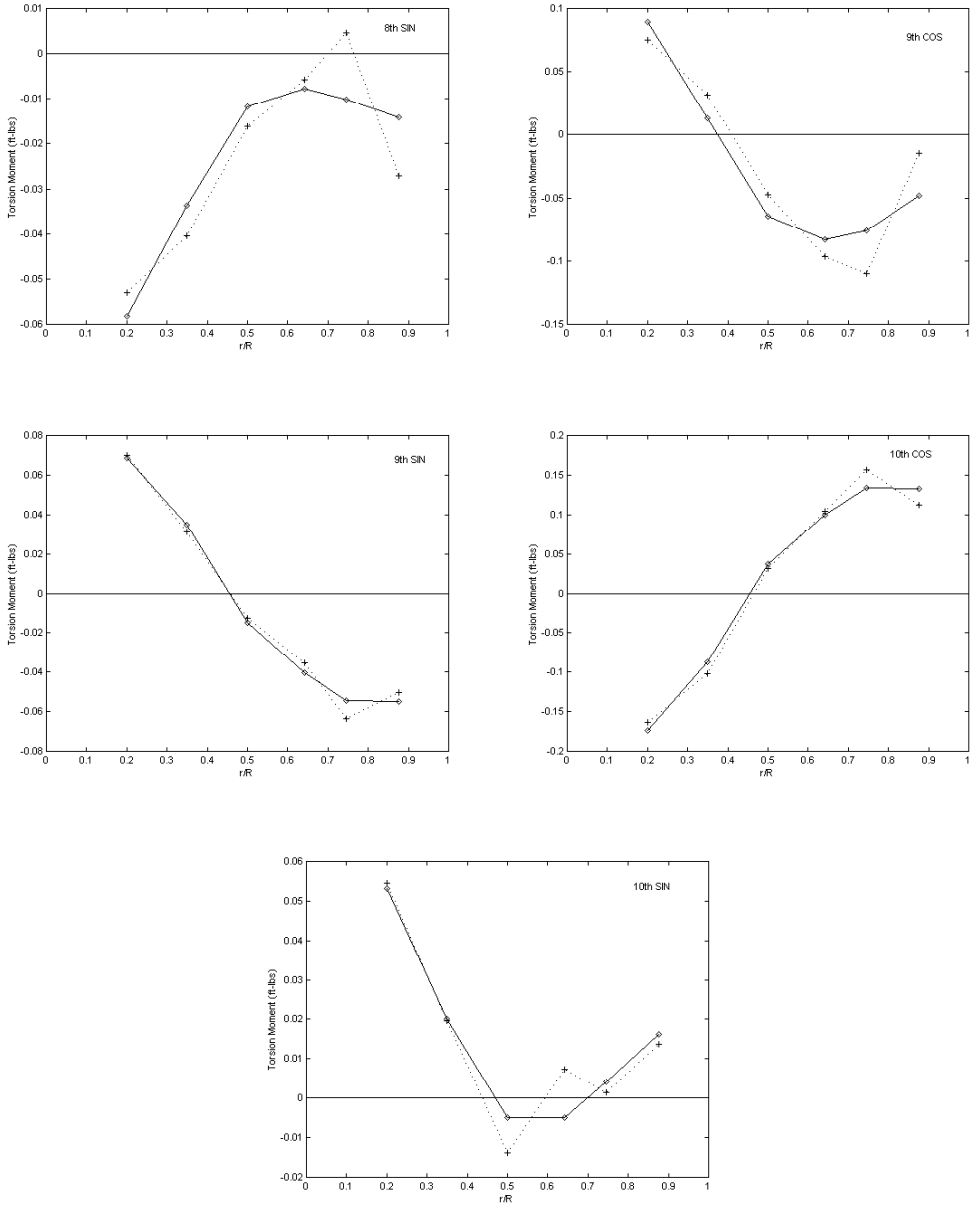

Figure 62. Three-Mode SPA versus Measured Torsion Moments for 8th Sine to 10th Sine.

UH-60A Model Rotor, Measured = Dotted Line, SPA = Solid Line

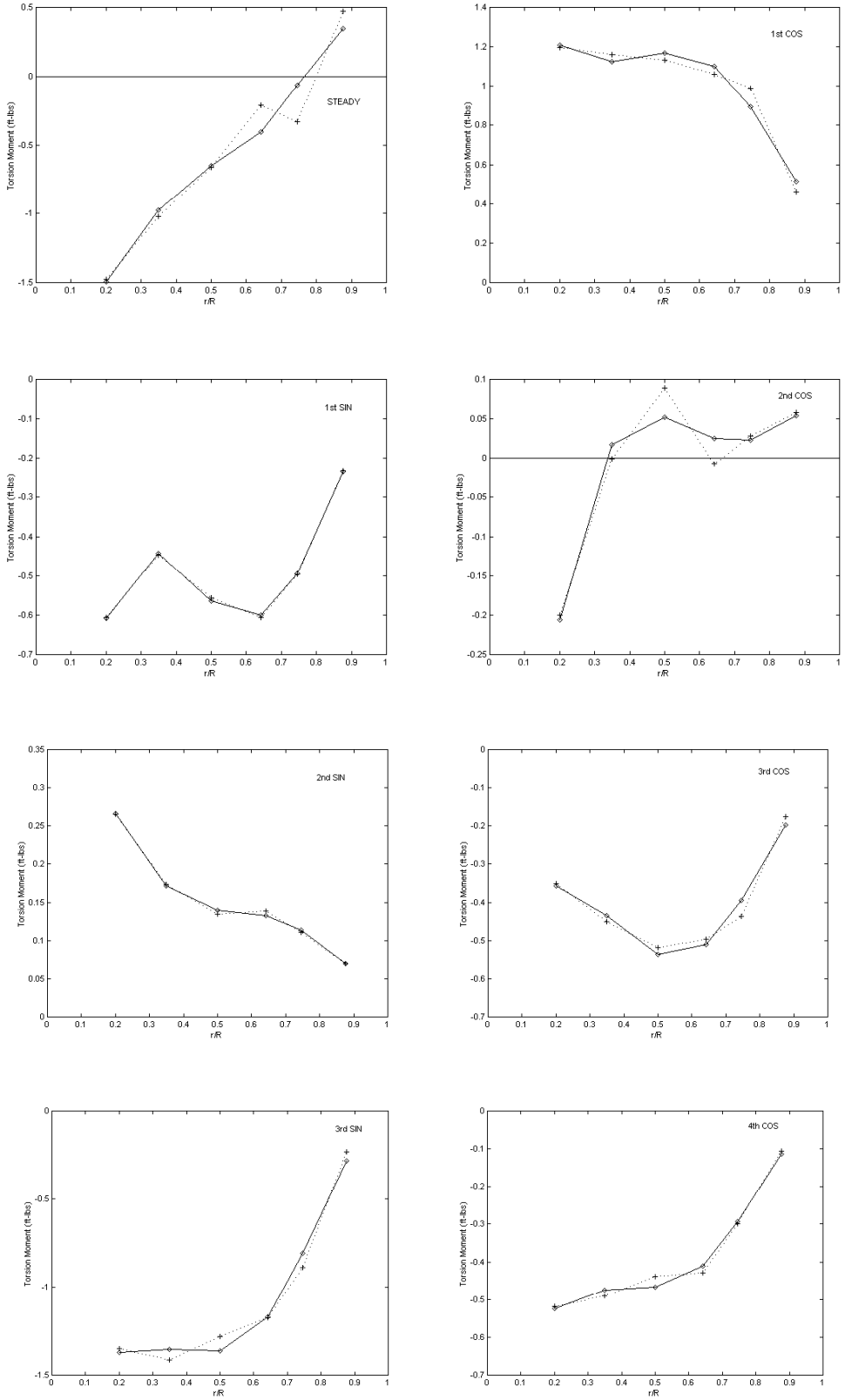

Figure 63. Four-Mode SPA versus Measured Torsion Moments for Steady to 4th Cosine.

UH-60A Model Rotor, Measured = Dotted Line, SPA = Solid Line

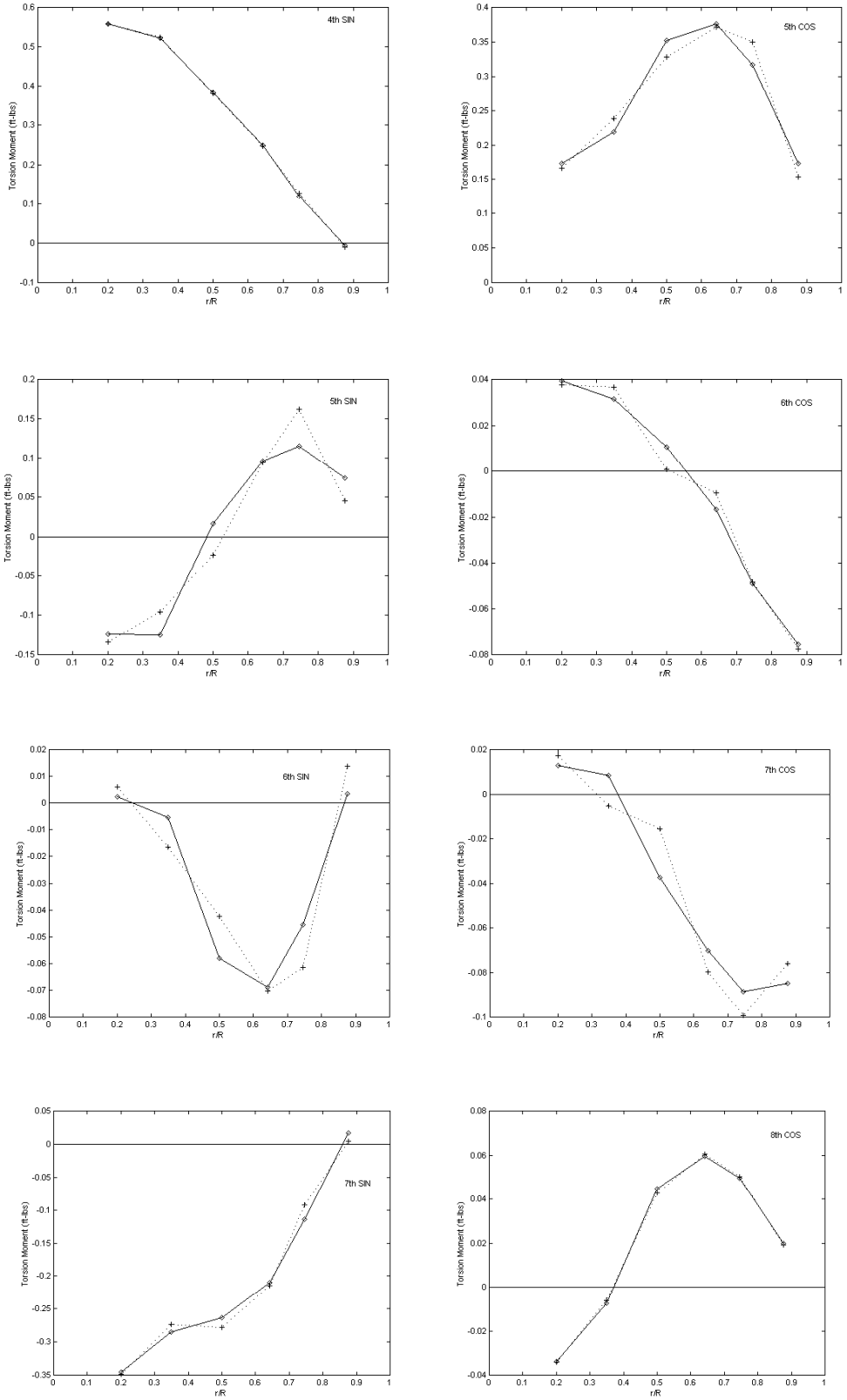

Figure 64. Four-Mode SPA versus Measured Torsion Moment for 4th Sine to 8th Cosine.

UH-60A Model Rotor, Measured = Dotted Line, SPA = Solid Line

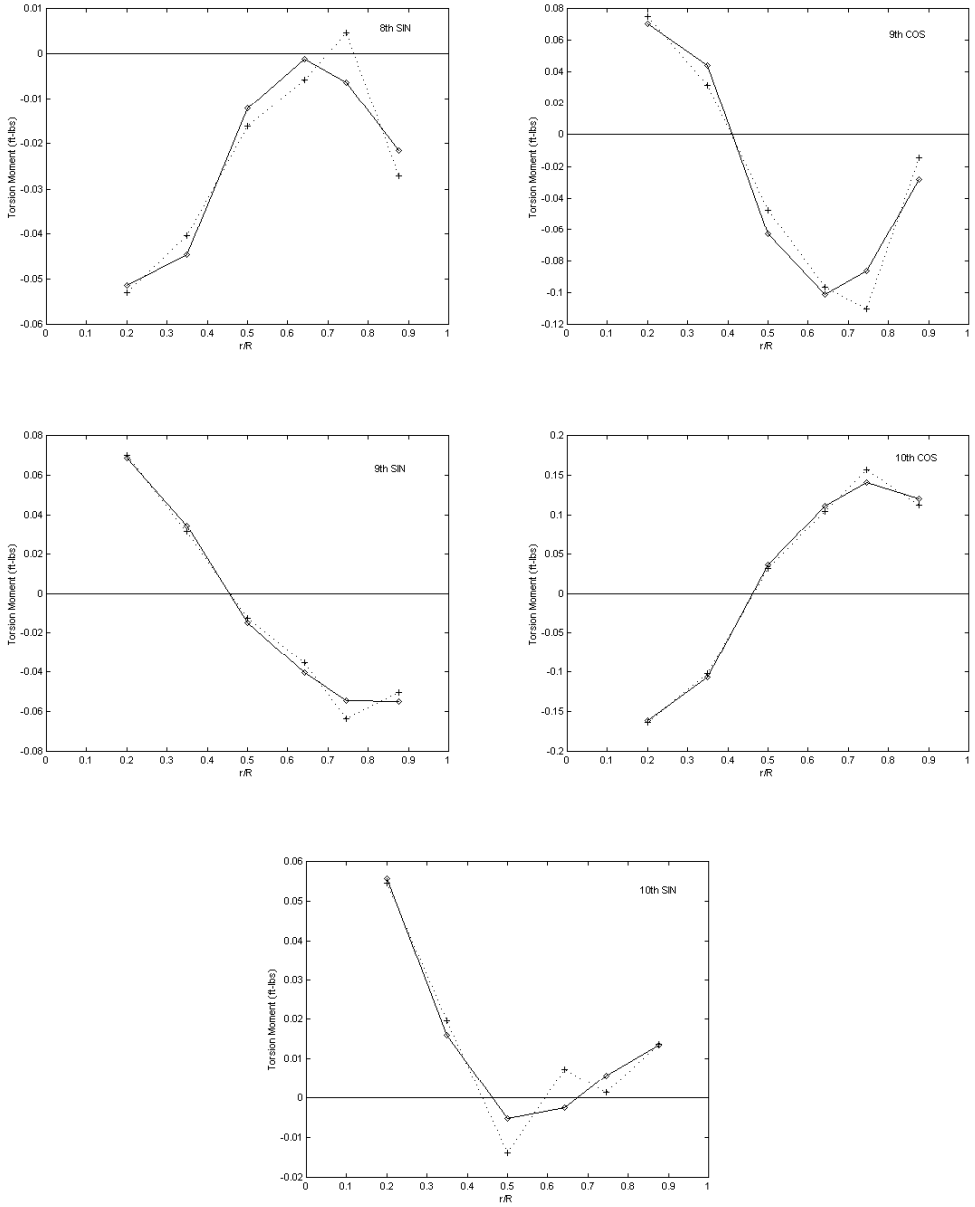

Figure 65. Four-Mode SPA versus Measured Torsion Moment for 8th Sine to 10th Sine.

UH-60A Model Rotor, Measured = Dotted Line, SPA = Solid Line

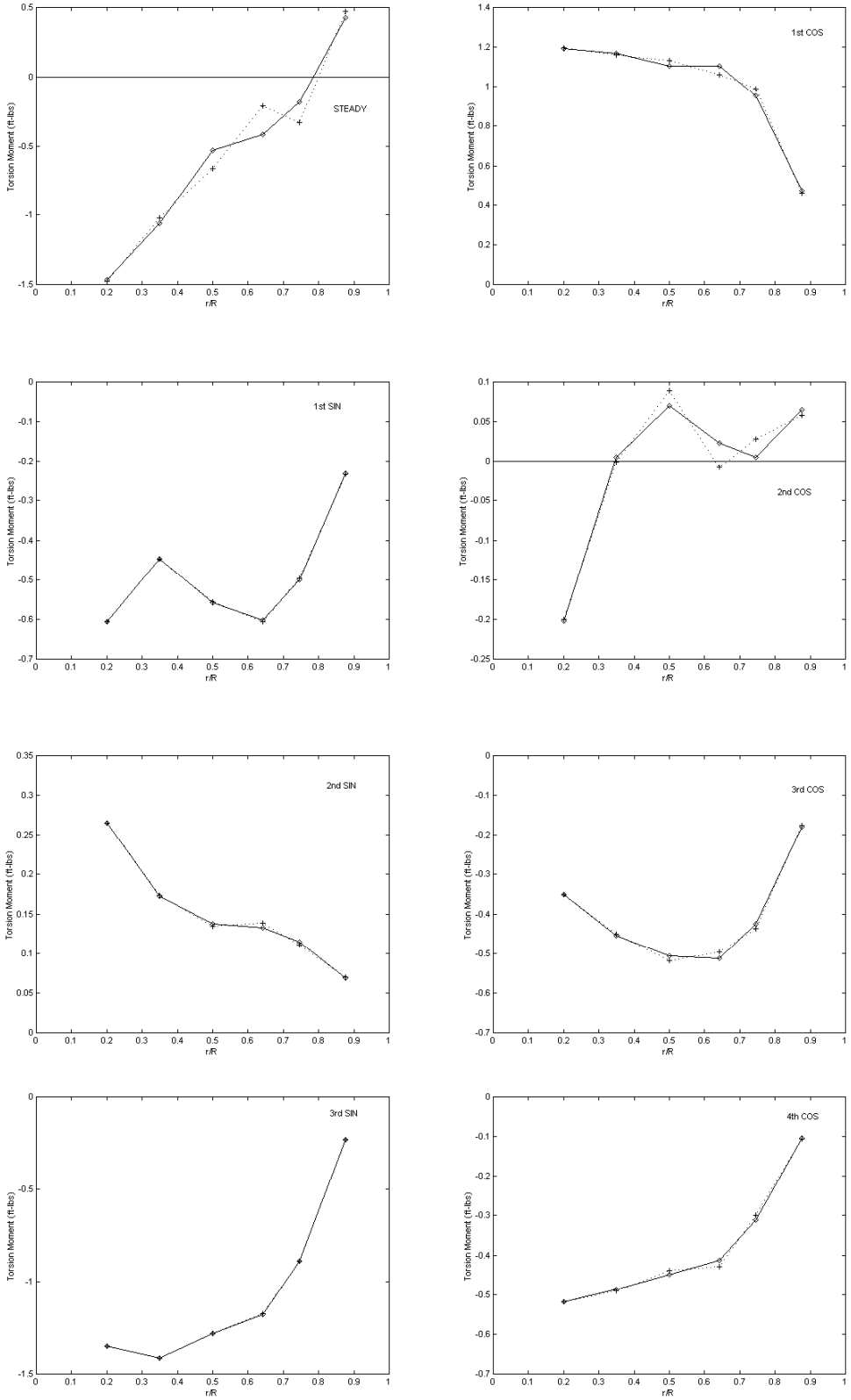

Figure 66. Five-Mode SPA versus Measured Torsion Moments for Steady to 4th Cosine.

UH-60A Model Rotor, Measured = Dotted Line, SPA = Solid Line

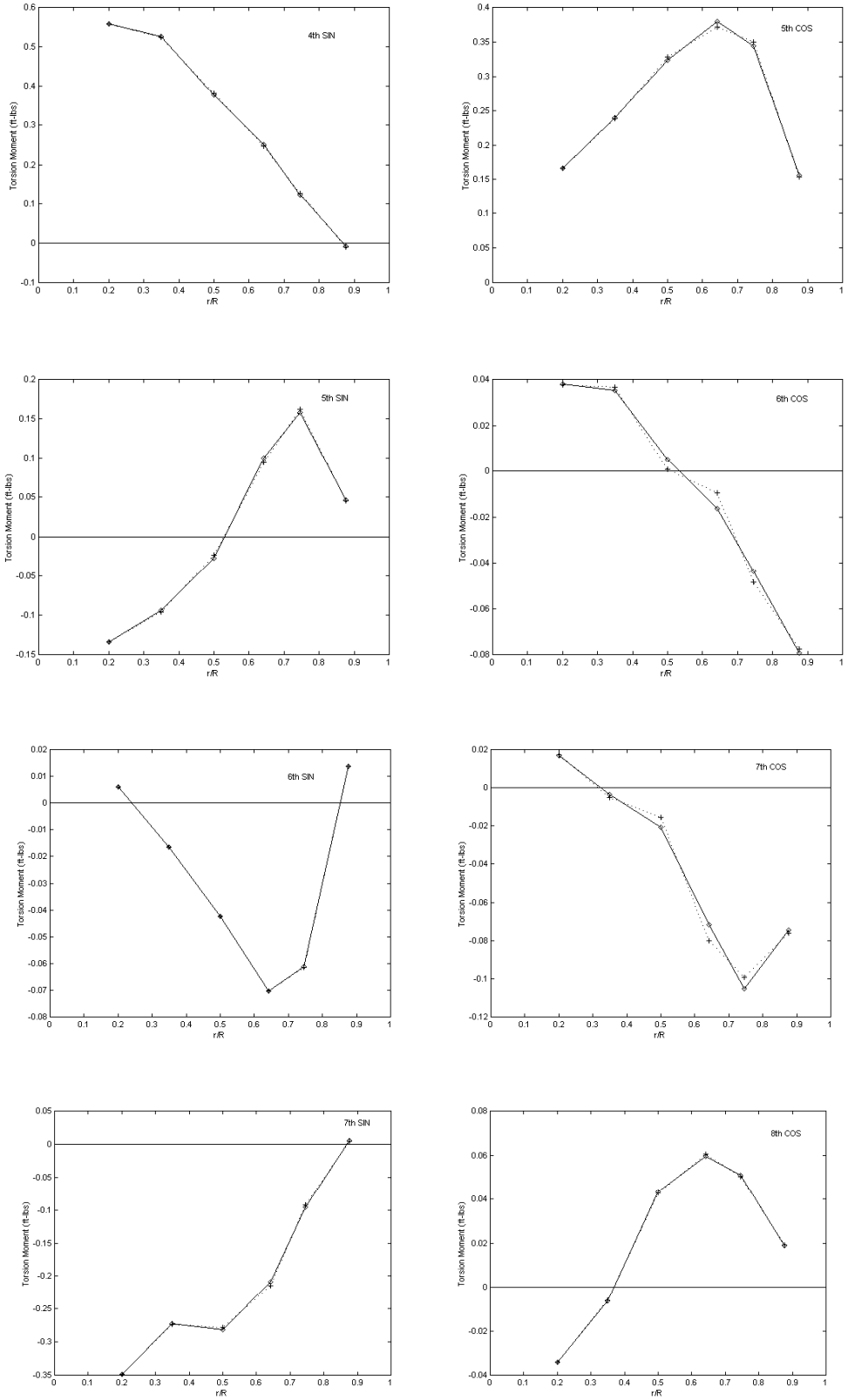

Figure 67. Five-Mode SPA versus Measured Torsion Moments for 4th Sine to 8th Cosine.

UH-60A Model Rotor, Measured = Dotted Line, SPA = Solid Line

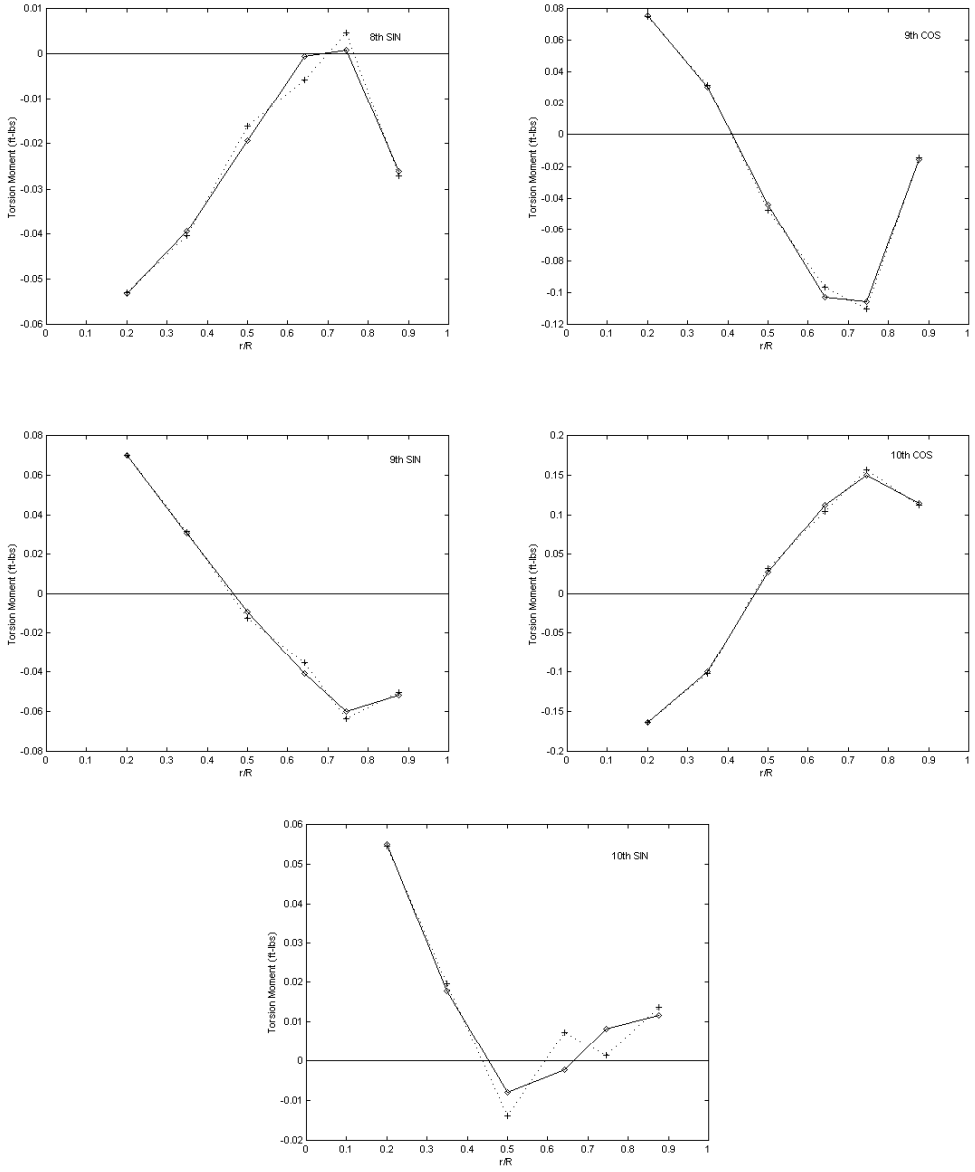

Figure 68. Five-Mode SPA versus Measured Torsion Moments for 8th Sine to 10th Sine.

UH-60A Model Rotor, DNW Run 13.20, $\mu = 0.301$

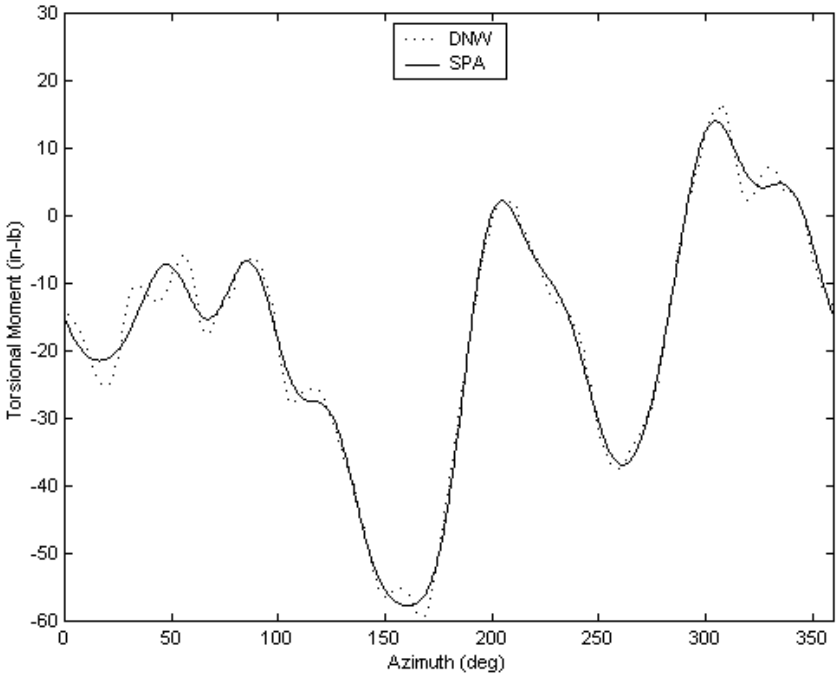

Figure 69. Five-Mode SPA versus Measured Torsion Moment Time History at x = 0.2.

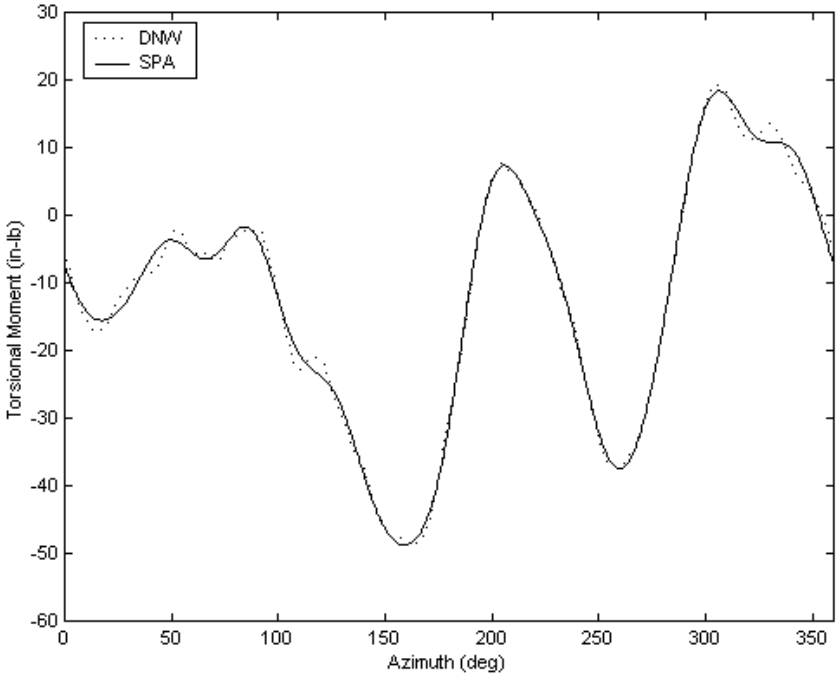

Figure 70. Five-Mode SPA versus Measured Torsion Moment Time History at x = 0.35.

UH-60A Model Rotor, DNW Run 13.20, $\mu = 0.301$

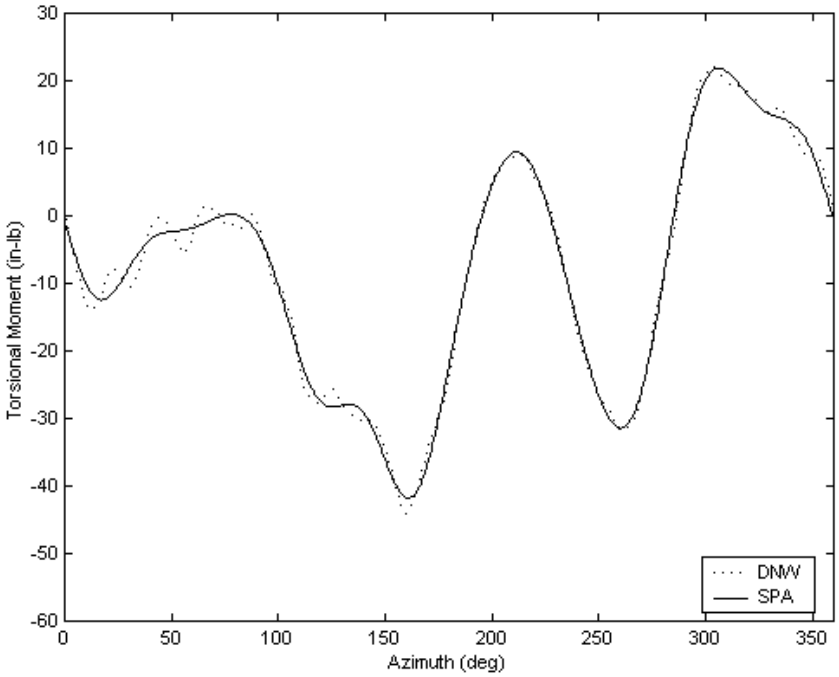

Figure 71. Five-Mode SPA versus Measured Torsion Moment Time History at x = 0.5.

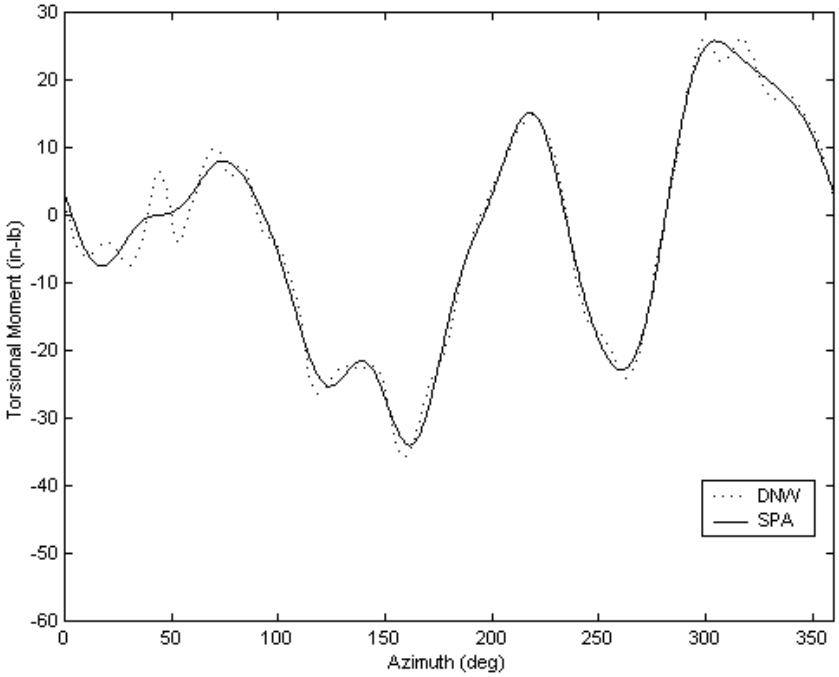

Figure 72. Five-Mode SPA versus Measured Torsion Moment Time History at x = 0.642.

UH-60A Model Rotor, DNW Run 13.20, $\mu = 0.301$

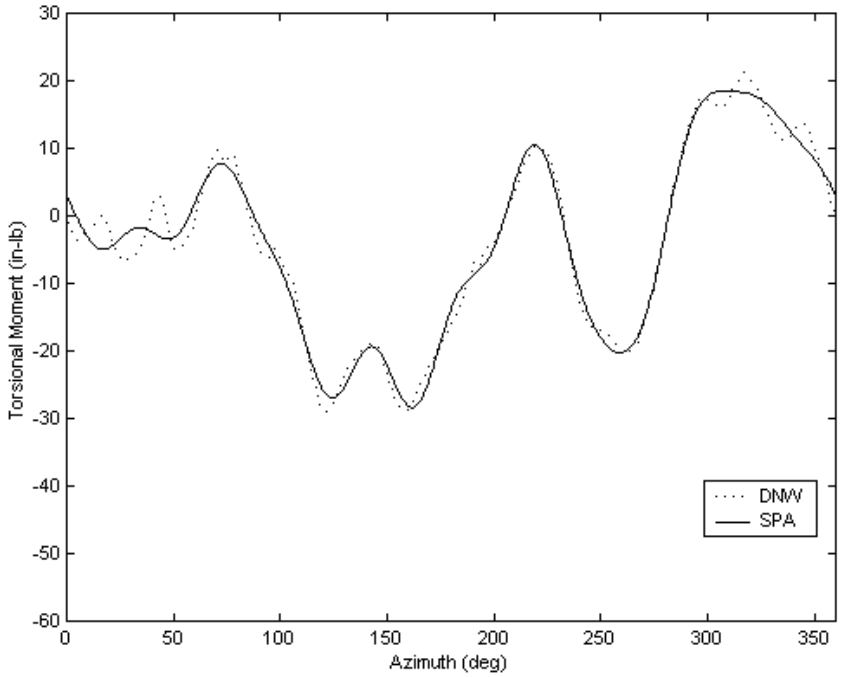

Figure 73. Five-Mode SPA versus Measured Torsion Moment Time History at x = 0.745.

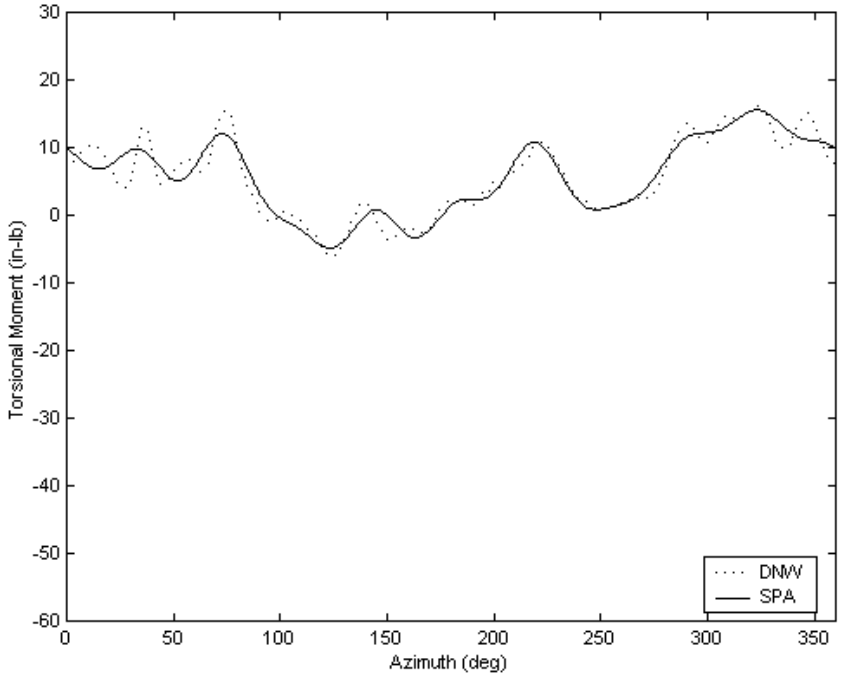

Figure 74. Five-Mode SPA versus Measured Torsion Moment Time History at x = 0.875.

UH-60A Model Rotor, DNW Run 13.20, $\mu = 0.301$

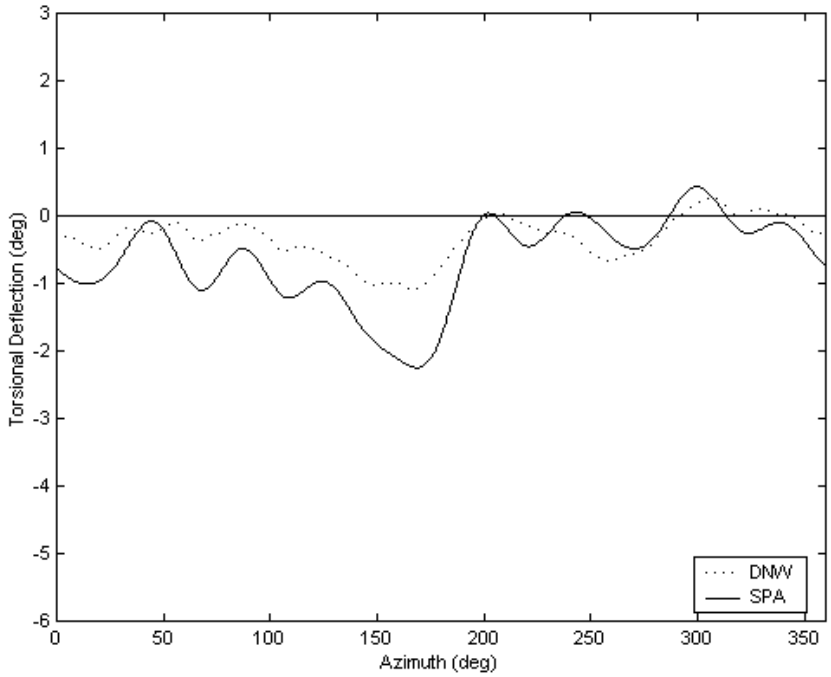

Figure 75. Five-Mode SPA versus DNW Calculated Deformation Time History at x = 0.225.

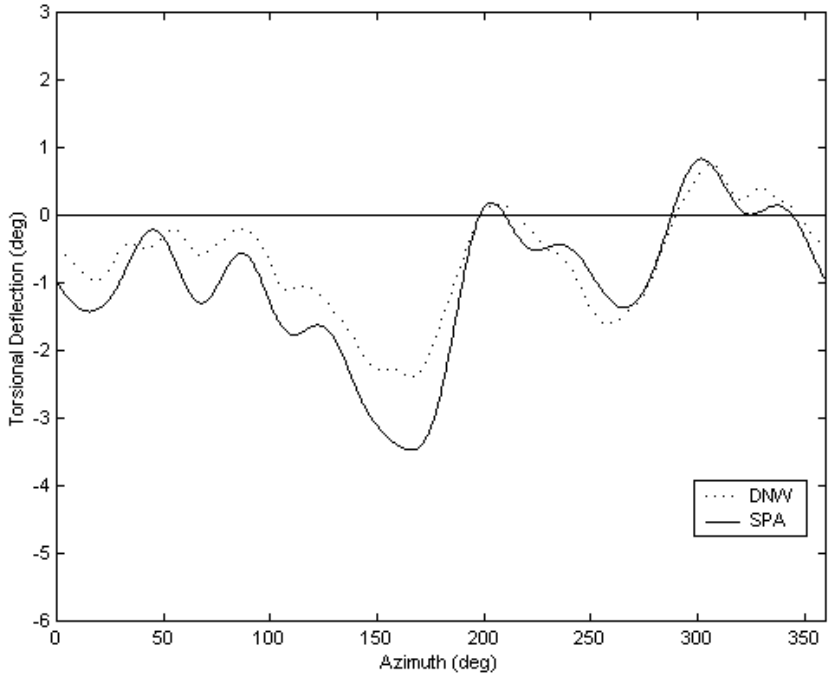

Figure 76. Five-Mode SPA versus DNW Calculated Deformation Time History at x = 0.4.

UH-60A Model Rotor, DNW Run 13.20, $\mu = 0.301$

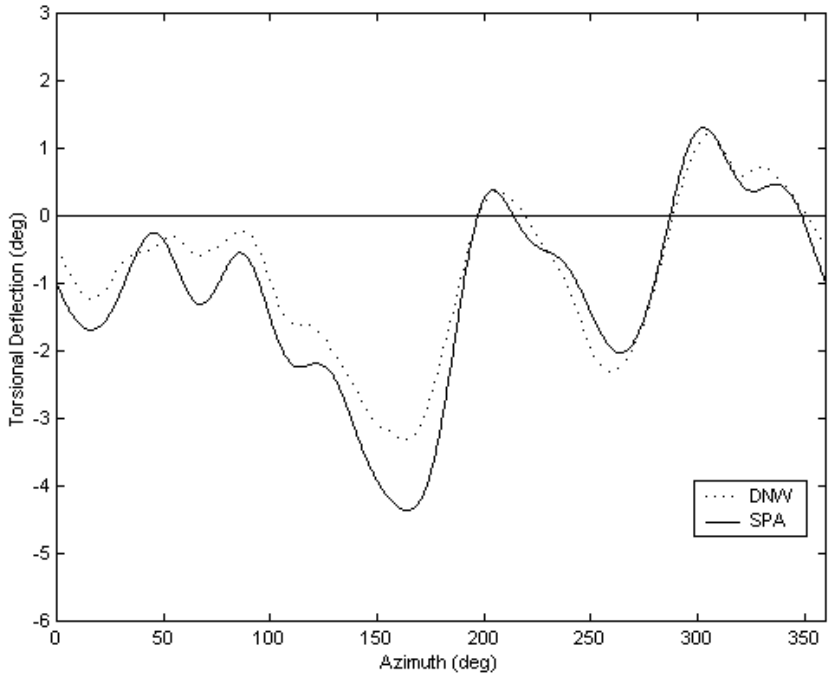

Figure 77. Five-Mode SPA versus DNW Calculated Deformation Time History at x = 0.55.

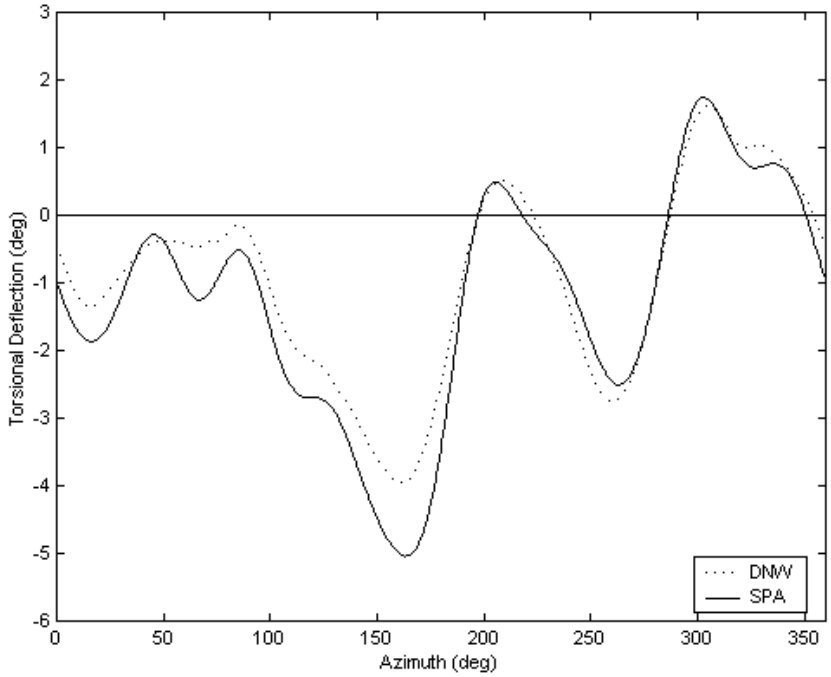

Figure 78. Five-Mode SPA versus DNW Calculated Deformation Time History at x = 0.675.

UH-60A Model Rotor, DNW Run 13.20, $\mu = 0.301$

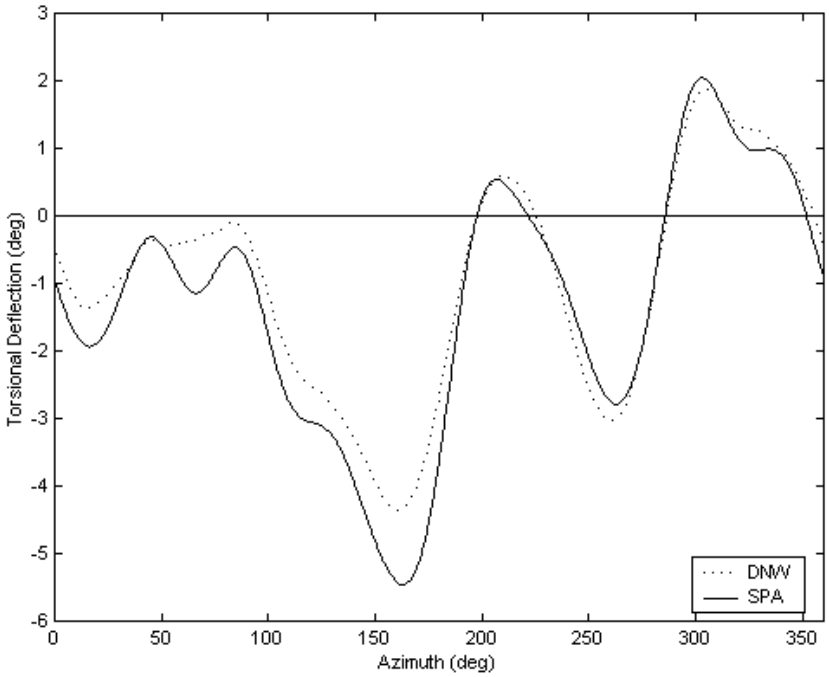

Figure 79. Five-Mode SPA versus DNW Calculated Deformation Time History at x = 0.775.

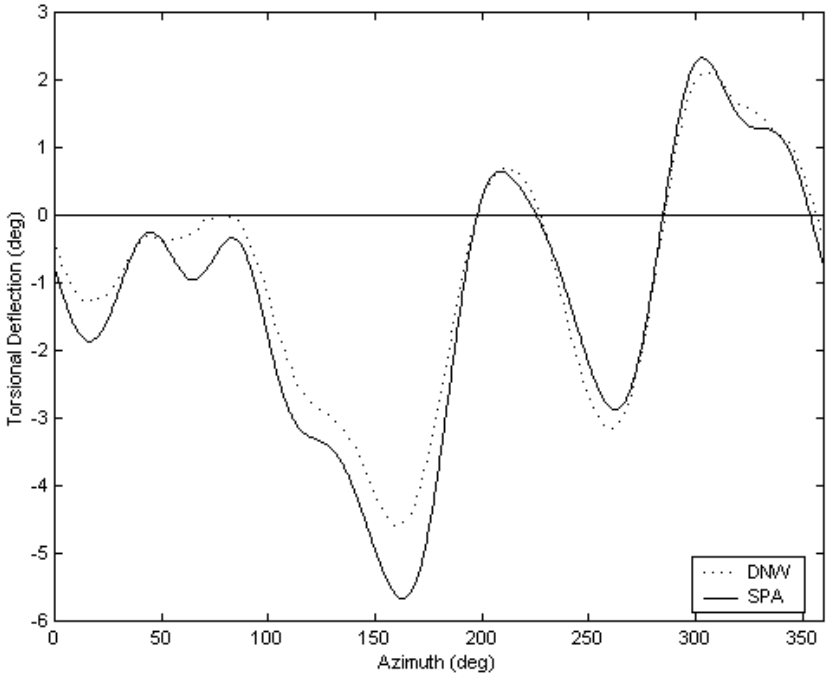

Figure 80. Five-Mode SPA versus DNW Calculated Deformation Time History at x = 0.865.

UH-60A Model Rotor, DNW Run 13.20, $\mu = 0.301$

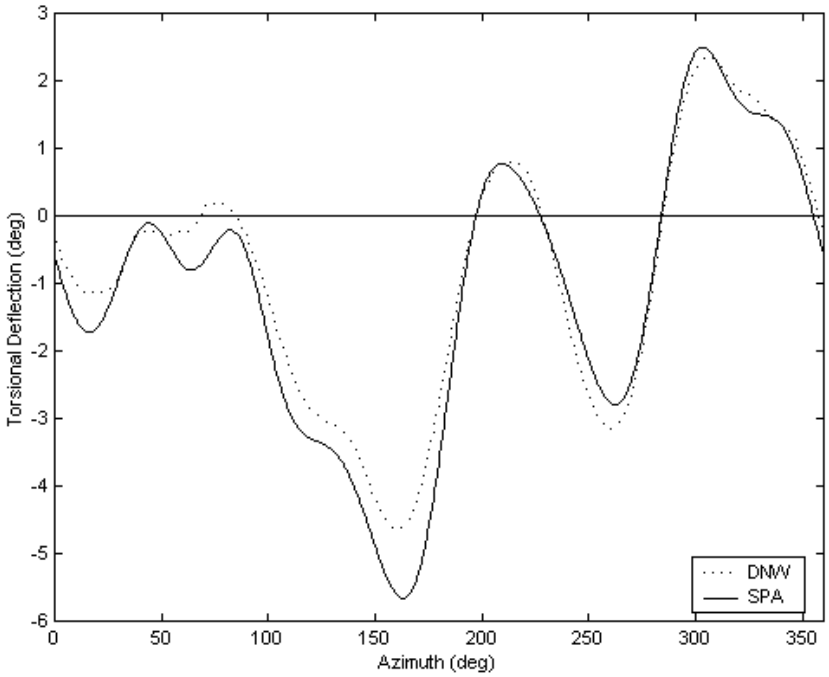

Figure 81. Five-Mode SPA versus DNW Calculated Deformation Time History at x = 0.92.

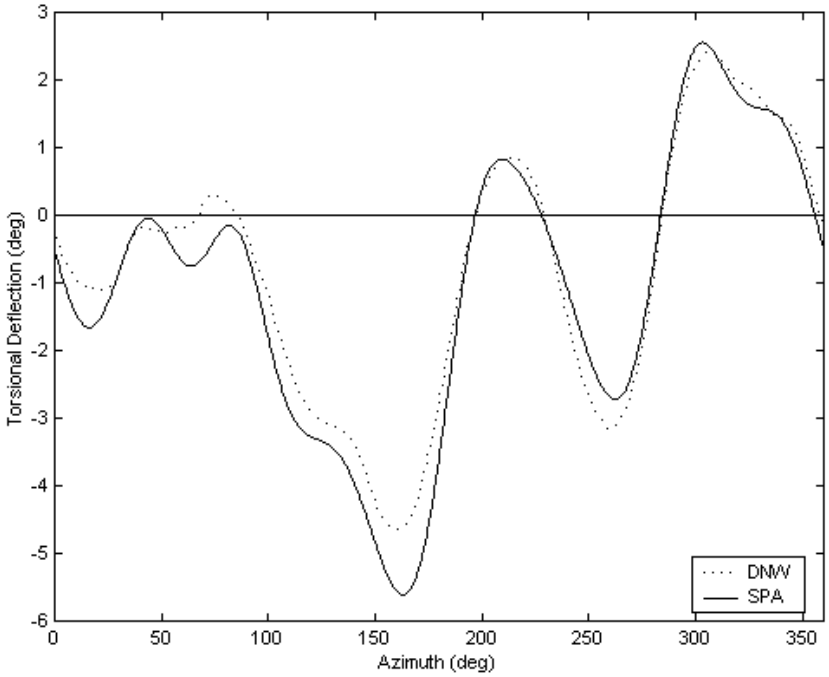

Figure 82. Five-Mode SPA versus DNW Calculated Deformation Time History at x = 0.945.

UH-60A Model Rotor, DNW Run 13.20, $\mu = 0.301$

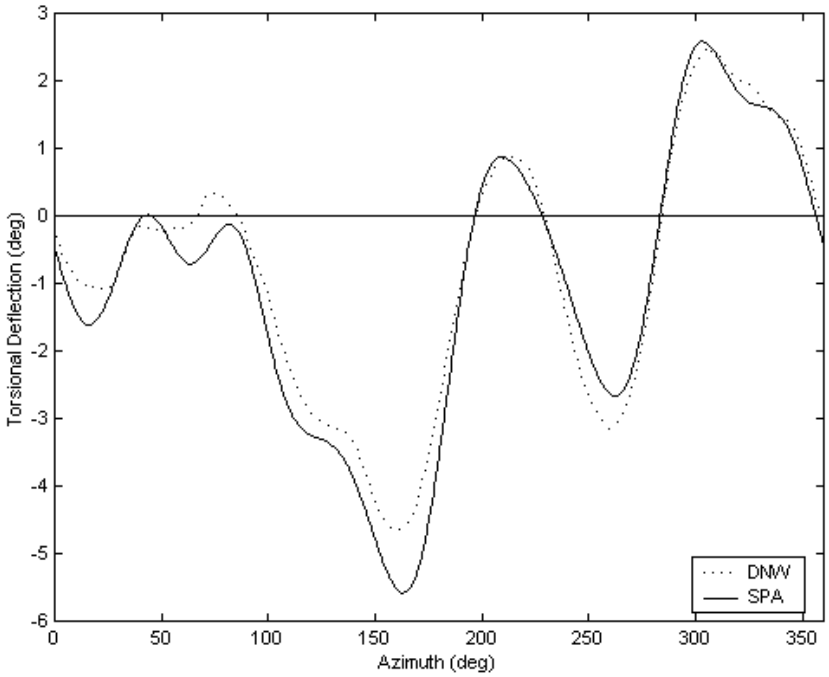

Figure 83. Five-Mode SPA versus DNW Calculated Deformation Time History at x = 0.965.

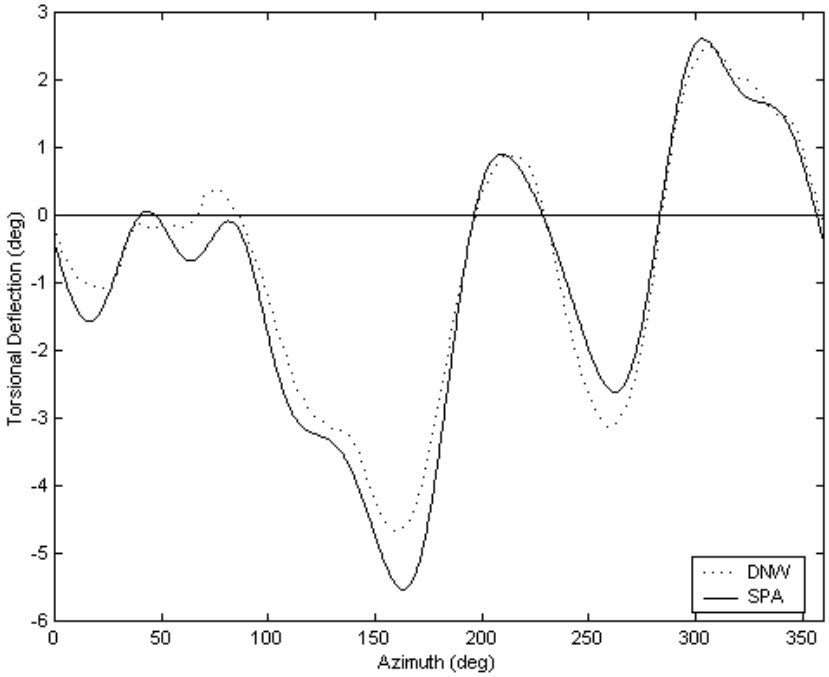

Figure 84. Five-Mode SPA versus DNW Calculated Deformation Time History at x = 0.99.

UH-60A Model Rotor, DNW Run 13.20, $\mu = 0.301$

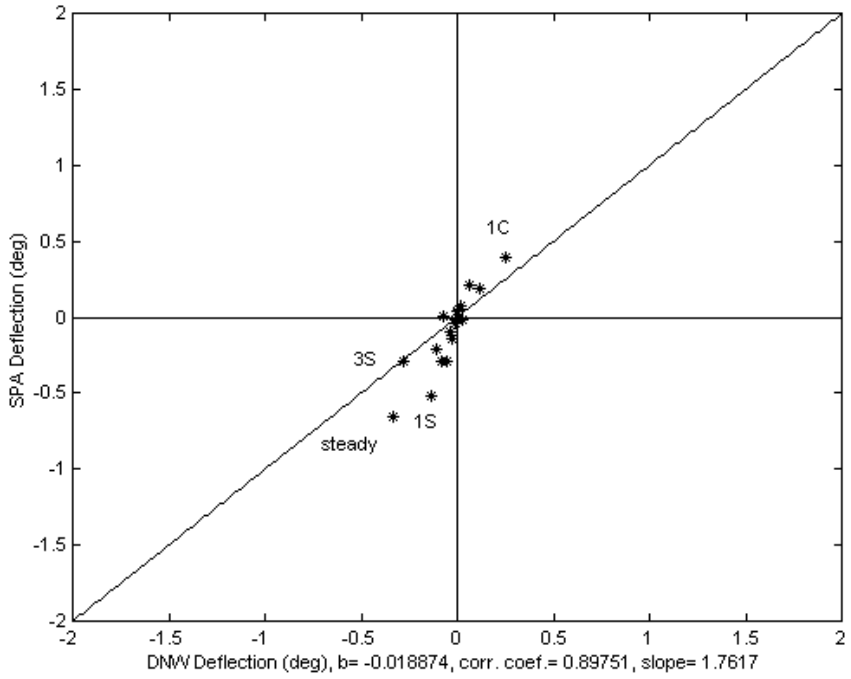

Figure 85. Linear Regression Plot of Five-Mode SPA versus Measured Torsional Deformation by Harmonic at x = 0.225.

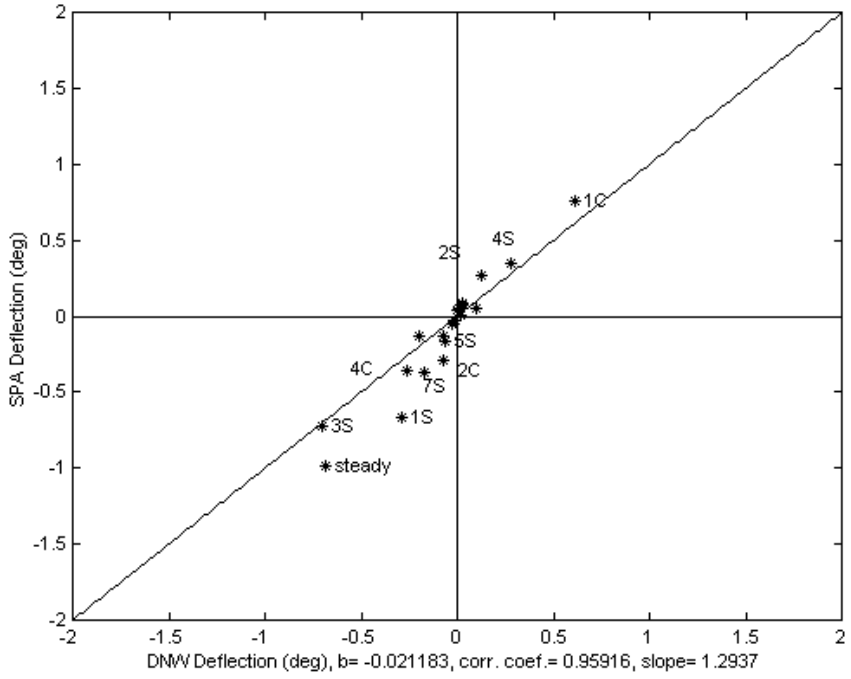

Figure 86. Linear Regression Plot of Five-Mode SPA versus Measured Torsional Deformation by Harmonic at x = 0.4.

UH-60A Model Rotor, DNW Run 13.20, $\mu = 0.301$

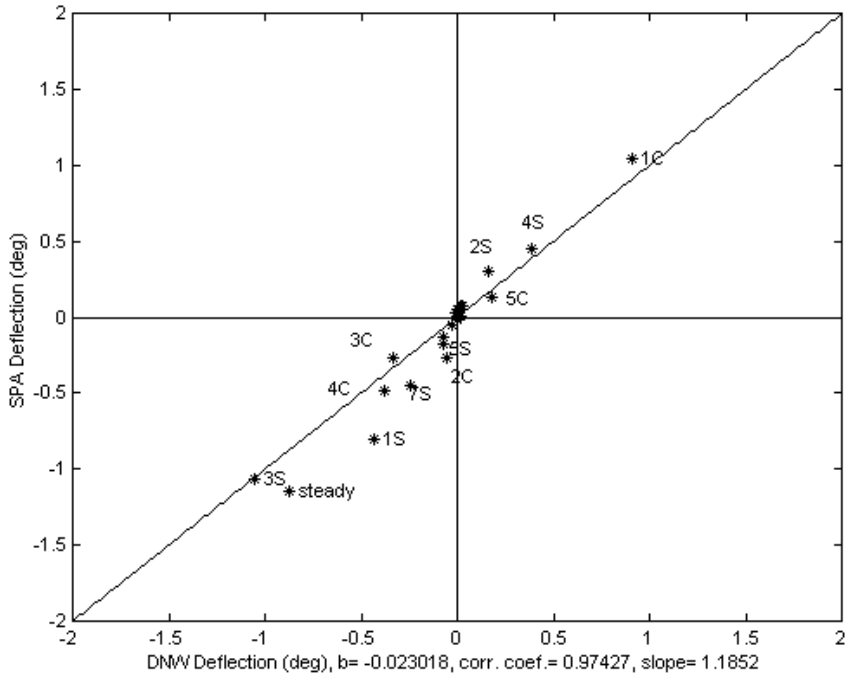

Figure 87. Linear Regression Plot of Five-Mode SPA versus Measured Torsional Deformation by Harmonic at x = 0.55.

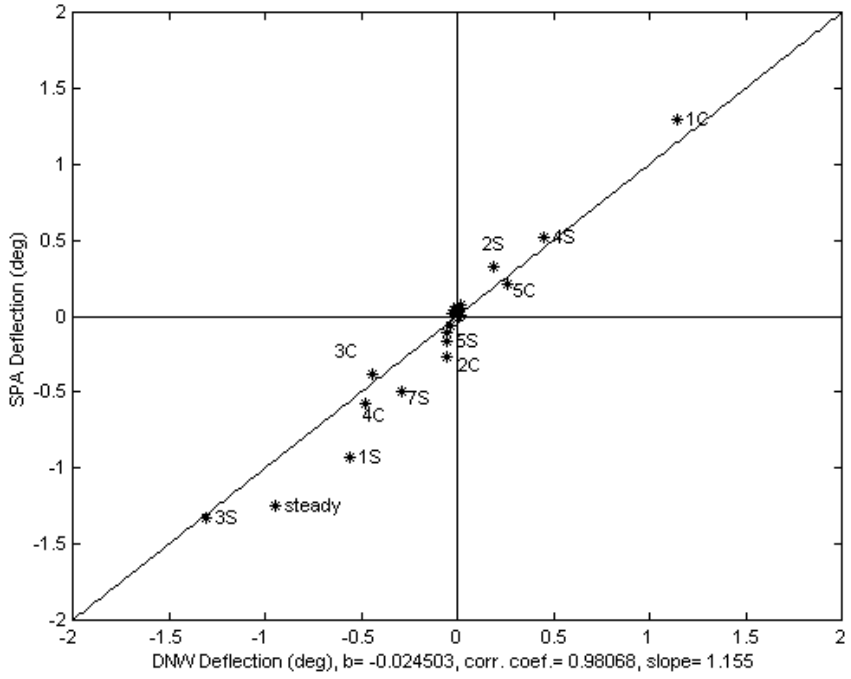

Figure 88. Linear Regression Plot of Five-Mode SPA versus Measured Torsional Deformation by Harmonic at x = 0.675.

UH-60A Model Rotor, DNW Run 13.20, $\mu = 0.301$

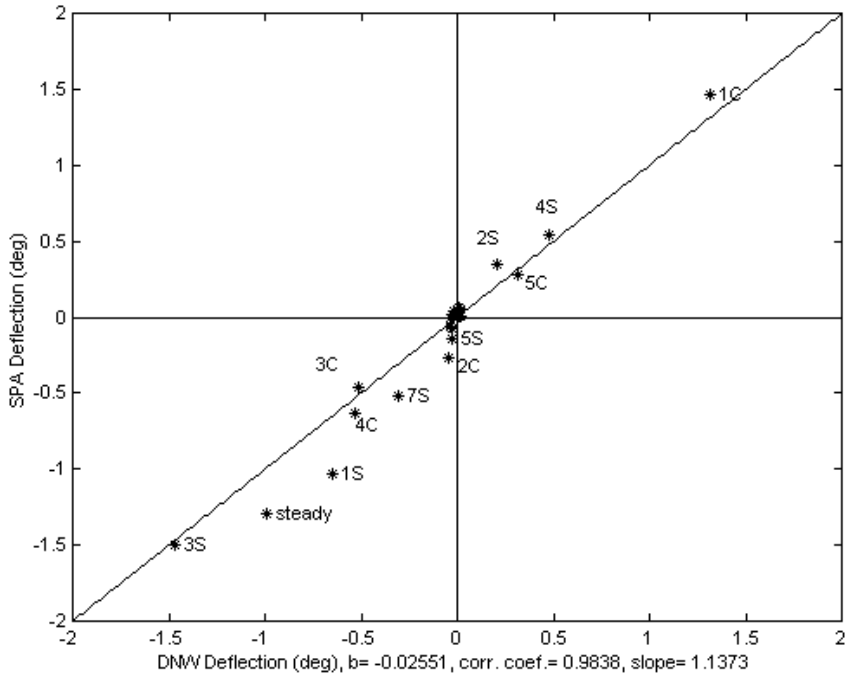

Figure 89. Linear Regression Plot of Five-Mode SPA versus Measured Torsional Deformation by Harmonic at x = 0.775.

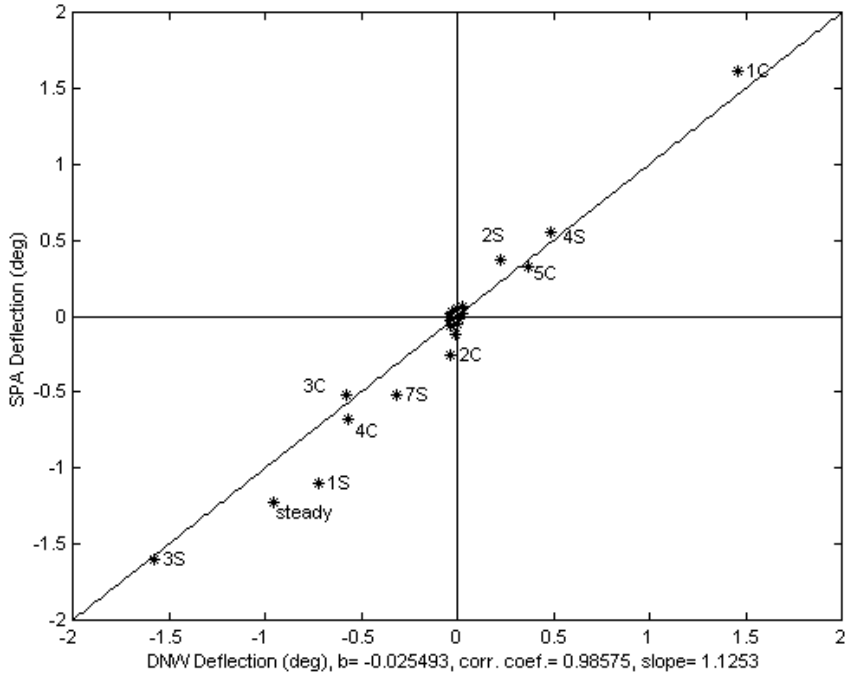

Figure 90. Linear Regression Plot of Five-Mode SPA versus Measured Torsional Deformation by Harmonic at x = 0.865.

UH-60A Model Rotor, DNW Run 13.20, $\mu = 0.301$

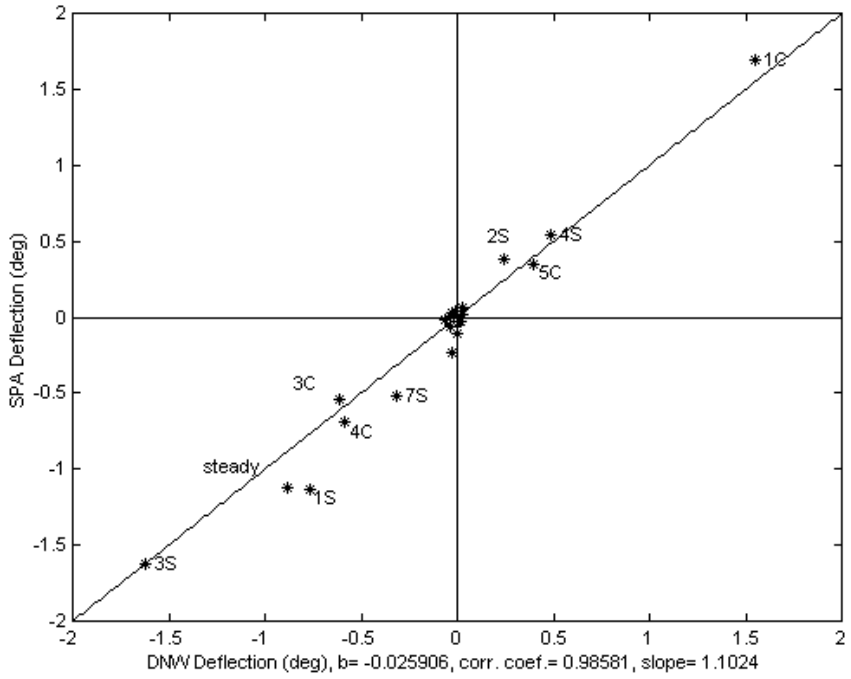

Figure 91. Linear Regression Plot of Five-Mode SPA versus Measured Torsional Deformation by Harmonic at x = 0.92.

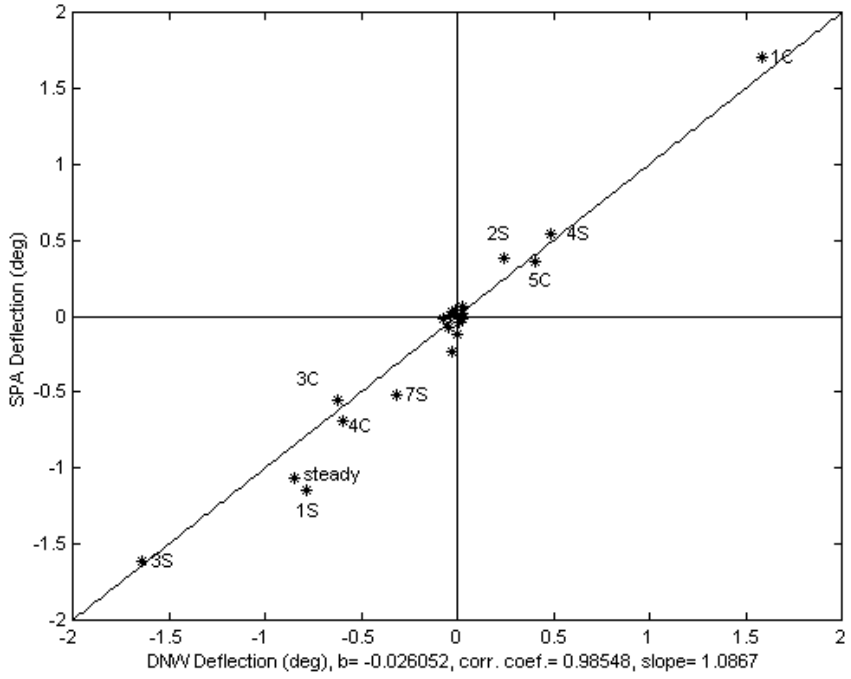

Figure 92. Linear Regression Plot of Five-Mode SPA versus Measured Torsional Deformation by Harmonic at x = 0.945.

UH-60A Model Rotor, DNW Run 13.20, $\mu = 0.301$

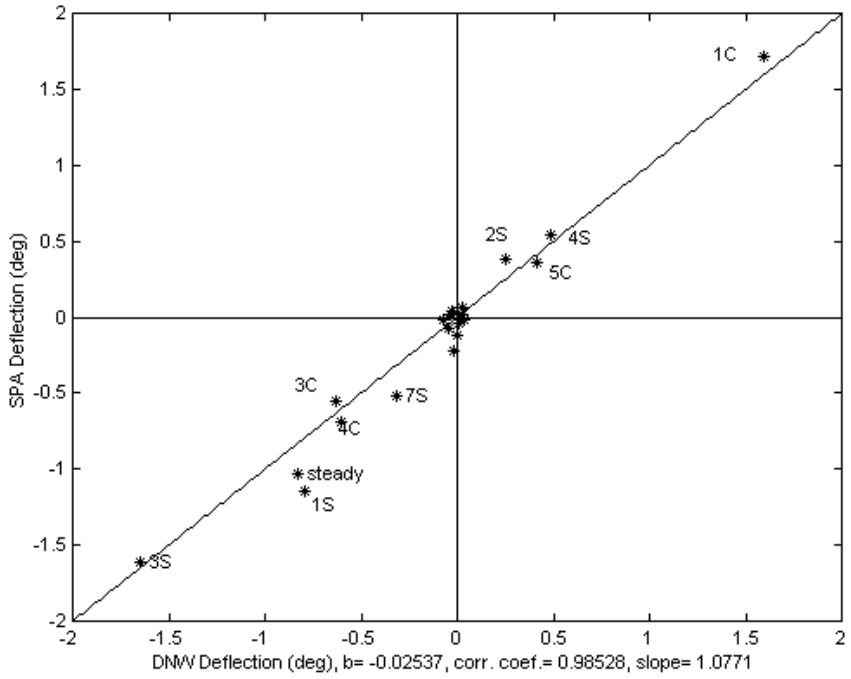

Figure 93. Linear Regression Plot of Five-Mode SPA versus Measured Torsional Deformation by Harmonic at x = 0.965.

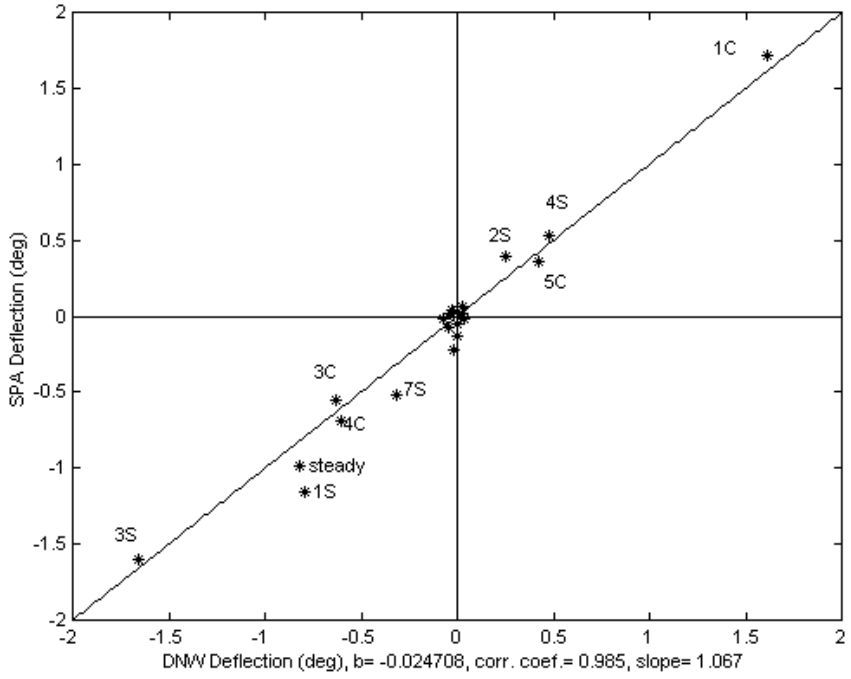

Figure 94. Linear Regression Plot of Five-Mode SPA versus Measured Torsional Deformation by Harmonic at x = 0.99.

UH-60A Model Rotor, DNW Run 13.20, $\mu = 0.301$

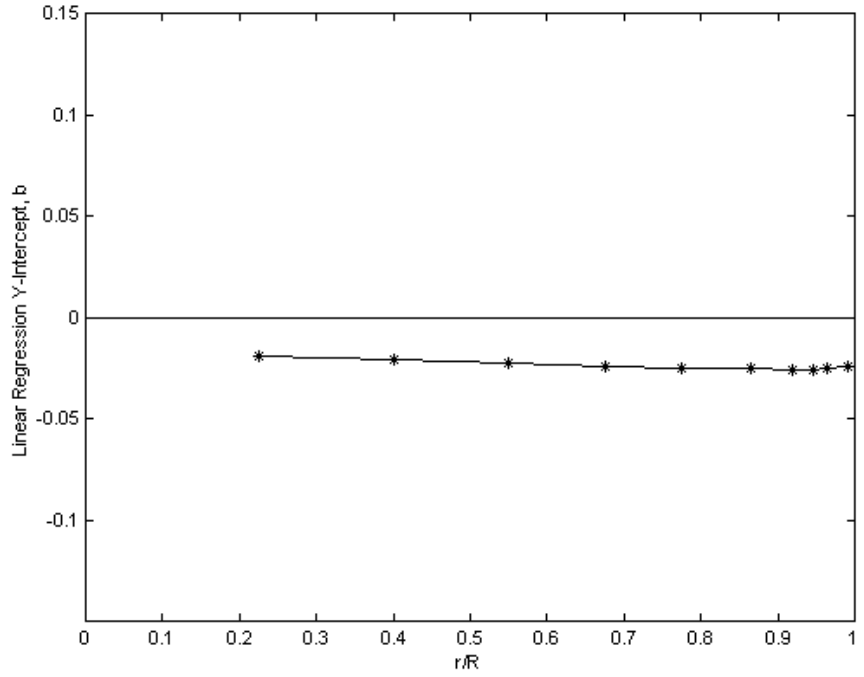

Figure 95. Linear Regression Y-intercept versus Span.

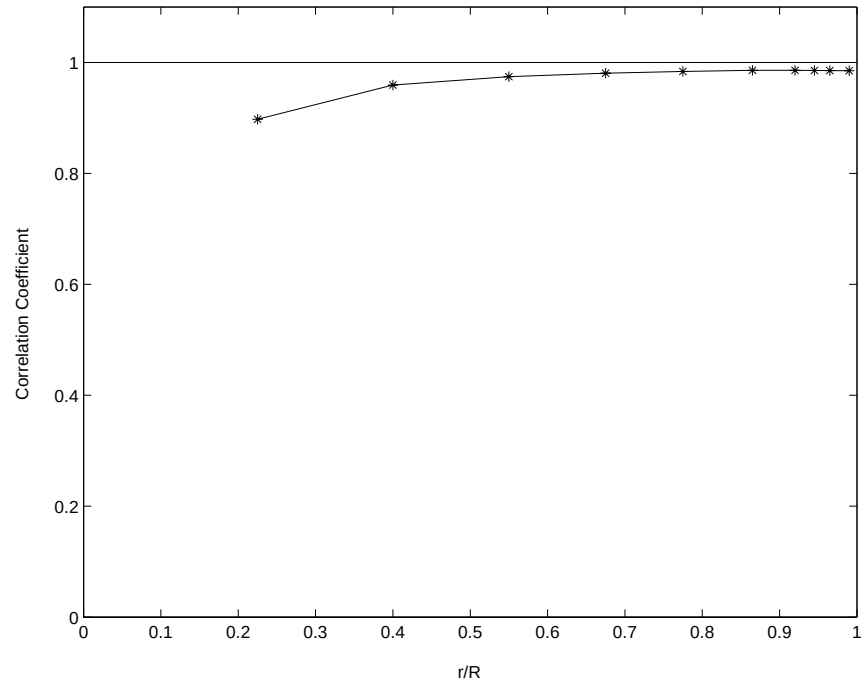

Figure 96. Linear Regression Correlation Coefficient versus Span.

UH-60A Model Rotor, DNW Run 13.20, $\mu = 0.301$

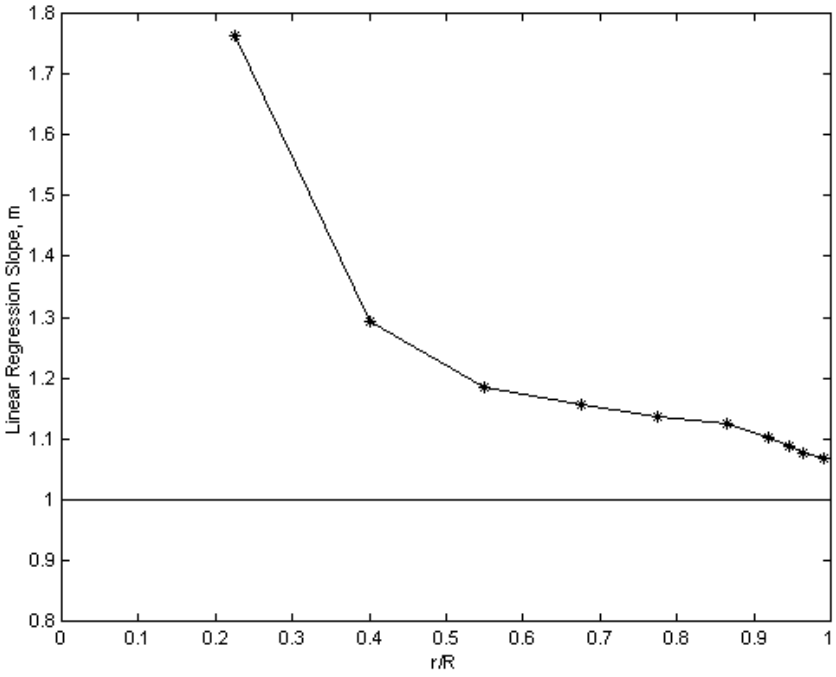

Figure 97. Linear Regression Slope versus Span.

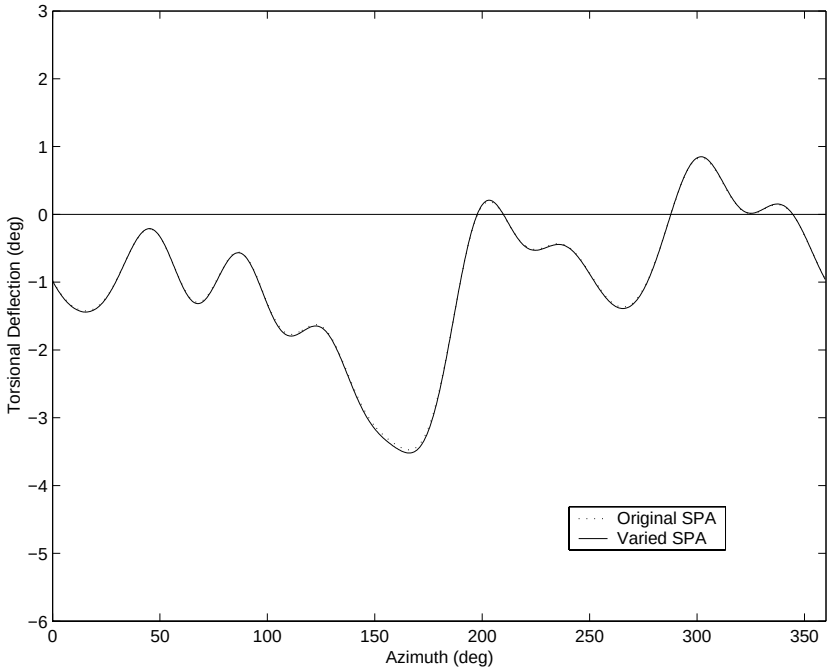

Figure 98. Varied Structural Property versus Original Five-Mode SPA at x=0.400.

UH-60A Model Rotor, DNW Run 13.20, $\mu = 0.301$

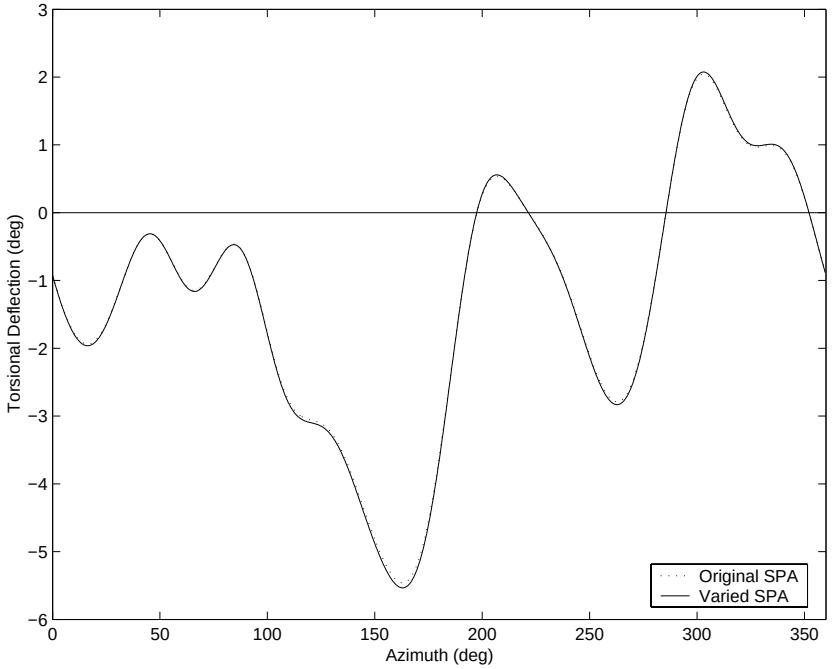

Figure 99. Varied Structural Property versus Original Five-Mode SPA at x=0.775.

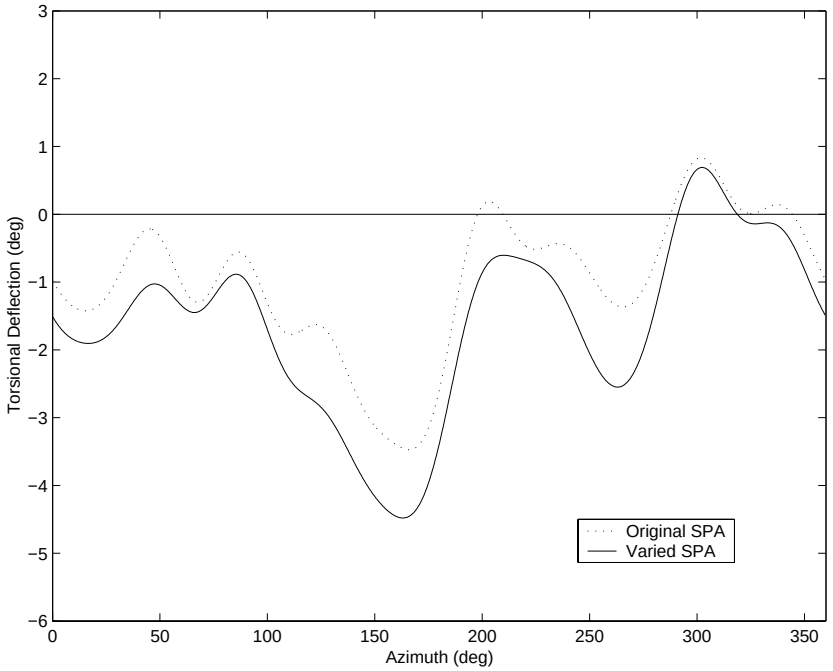

Figure 100. Eliminated Strain Gage Four-Mode versus Original Five-Mode SPA at x=0.400.

UH-60A Model Rotor, DNW Run 13.20, $\mu = 0.301$

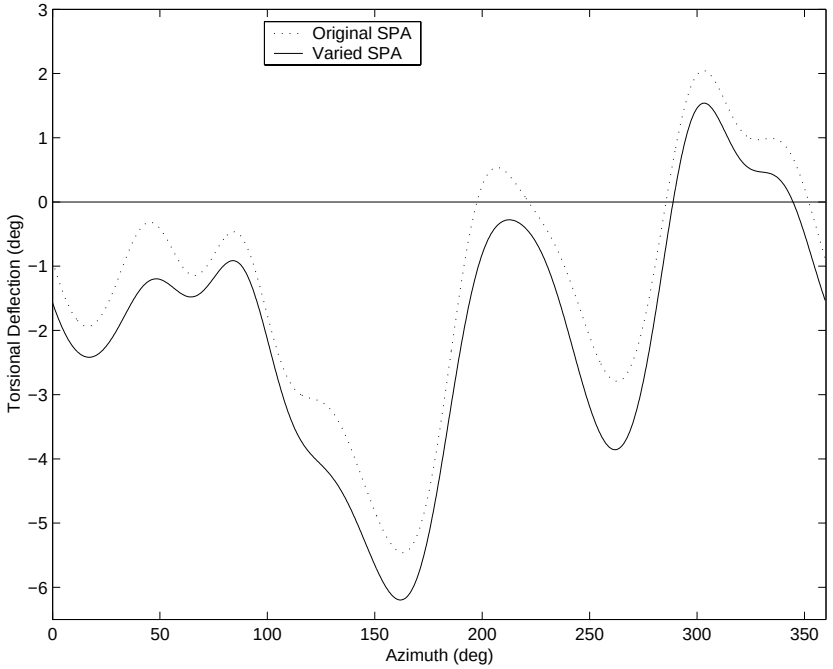

Figure 101. Eliminated Strain Gage Four-Mode versus Original Five-Mode SPA at x=0.775.

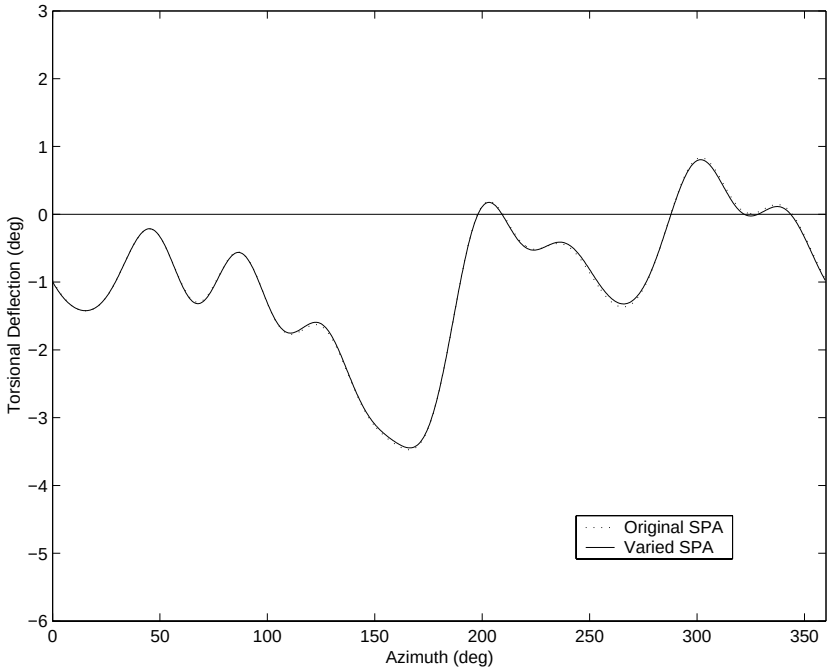

Figure 102. Varied Measurement versus Original Five-Mode SPA at x=0.400.

UH-60A Model Rotor, DNW Run 13.20, $\mu = 0.301$

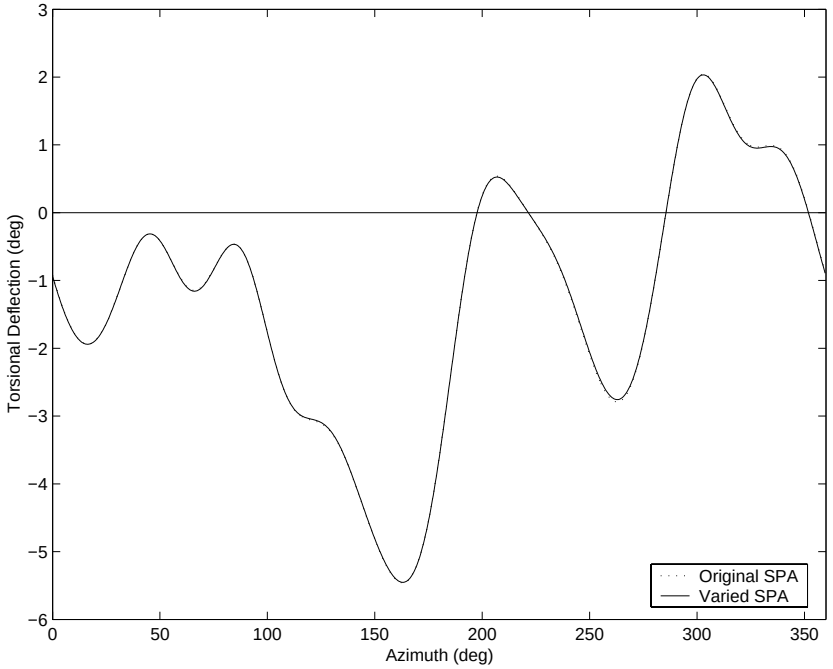

Figure 103. Varied Measurement versus Original Five-Mode SPA at x=0.775.

LIST OF REFERENCES

1. Johnson, Wayne, *Helicopter Theory*, pp. 23-468, Princeton University Press, 1980.

2. Bielawa, Richard L., *Rotary Wing Structural Dynamics and Aeroelasticity*, pp. 76-105, American Institute of Aeronautics and Astronautics, Inc., 1992.

3. NASA Technical Memorandum 100020, USAAVSCOM Technical Report 87-A-8, *Estimation of Blade Airloads from Rotor Blade Bending Moments*, by William G. Bousman, pp. 1-20, August 1987.

4. E. Mercker, K. Pengel, R. Kube, B. v.d.. Wall, A. Boutier, and F. Micheli, "On the Blade Deformation Measured at a Scaled Helicopter Rotor", *Proc. of American Helicopter Society 2nd International Aeromechanics Specialists Meeting*, Bridgeport, CT, 11-13 October 1995.

5. Meirovitch, Leonard., *Elements of Vibration Analysis*, pp. 156-256, McGraw Hill, Inc, 1975.

6. D.R. Gaukroger and C.J.W. Hassal, "Measurement of Vibratory Displacements of a Rotating Blade", *Vertica*, Vol. 2, pp. 111-114, January 1978.

7. Nicolas Tourjansky and Edmond Szechenyi, "The Measurement of Blade Deflections", *Proc. of Eighteenth European Rotorcraft Forum, Paper No. 6*, Avignon, France, pp.1-12, 15-18 September 1992.

8. Schott, James R., *Matrix Analysis for Statistics*, pp. 24-51, John Wiley & Sons, Inc., 1997.

9. E.Roberts Wood and W. Gerstenberger, "Analysis of Helicopter Aeroelastic Characteristics in High-Speed Flight", *AIAA Journal*, Vol. 1, No. 10, pp. 2366-2381, October 1963.

10. Bramwell, A.R.S., *Helicopter Dynamics*, pp.290-326, Edward Arnold Publishers Ltd, 1976.

11. Thomson, W.T. and Dahleh, M.D., *Theory of Vibration with Applications,* 5th ed., pp. 269-499, Prentice Hall, 1998.

12. Scanlan, R. and Rosenbaum, R., *Introduction to the Study of Aircraft Vibration and Flutter*, pp. 133-163, The MacMillan Company, 1951.

13. NASA Technical Note D-7818, *Nonlinear Equations of Motion for the Elastic Bending and Torsion of Twisted Nonuniform Rotor Blades*, by D.H. Hodges and E.H. Dowell, pp. 1-44, December 1974.

14. United Technologies Research Center Report R91-153577-1, *Pressure-Instrumented Model UH-60A Black Hawk Rotor Test at DNW, Volume I: Description of Experiment*, by Peter F. Lorber, pp. 1-82, February 1991.

15. NASA Technical Memorandum 4239, *Modal Analysis of UH-60A Instrumented Rotor Blades*, by K.S. Hamade and R.M. Kufeld, November 1990.

16. Yeo, H., Spreadsheet of Full-Scale, UH-60A Rotor Blade Structural Properties, Army/NASA Rotorcraft Division, Moffett Field, California, 2001 (unpublished).

17. Johnson, Wayne, Spreadsheet of model-scale, UH-60A, Rotor Blade Structural Properties, Army/NASA Rotorcraft Division, Moffett Field, California, 2001 (unpublished).

18. E. Roberts Wood and K.D. Hilzinger, "A Method for Determining the Fully Coupled Aeroelastic Response of Helicopter Rotor Blades", *Proc. of American Helicopter Society 19th Annual National Forum*, Washington, DC, May 1963.

INITIAL DISTRIBUTION LIST

1. Defense Technical Information Center
   Ft. Belvoir, Virginia

2. Dudley Knox Library
   Naval Postgraduate School
   Monterey, California

3. Dr. E. Roberts Wood
   Naval Postgraduate School
   Monterey, California

4. William G. Bousman
   Aeromechanics Branch, Army/NASA Rotorcraft Division
   Moffett Field, California

5. Dr. Joon W. Lim
   Aeromechanics Branch, Army/NASA Rotorcraft Division
   Moffett Field, California

6. Dr. William Warmbrodt
   Aeromechanics Branch Chief, Army/NASA Rotorcraft Division
   Moffett Field, California

7. Andrew W. Kerr
   Director AFDD AMCOM, and Director NRTC
   Moffet Field, California

8. Dr. Michael P. Scully
   U.S. Army, Chief Design Engineer
   Moffett Field, California

9. Dr. Peter F. Lorber
   United Technologies Research Center
   East Hartford, Connecticut

10. Robert K. Goodman
    Sikorsky Aircraft Corporation
    Stratford, Connecticut

11. Wayne R. Mantay
    U.S. Army Joint Research Projects Office
    Langley Research Center, Virginia

12. Louis J. Silverthorn
    The Boeing Company
    Mesa, Arizona

13. Dr. Friedrich Karl Straub
    The Boeing Company
    Mesa, Arizona

14. Gary Anderson
    U.S. Army Research Office
    Research Triangle Park, North Carolina

15. Edward E. Austin
    U.S. Army, AATD
    Fort Eustis, Virginia

16. Raymond G. Kvaternik
    NASA Langley Research Center
    Hampton, Virginia